AD-A165 250 A HIGH-RESOLUTION CLUSTER OF OCEANOGRAPHIC INSTRUMENTS FOR BOUNDARY LAYER MEASUREMENTS UNDER ICE(U) FLOW INDUSTRIES INC KENT WA H LIU ET AL. NOV 85 1/2

UNCLASSIFIED TR-352/11-85 N00014-83-C-0764 F/G 8/10 NL

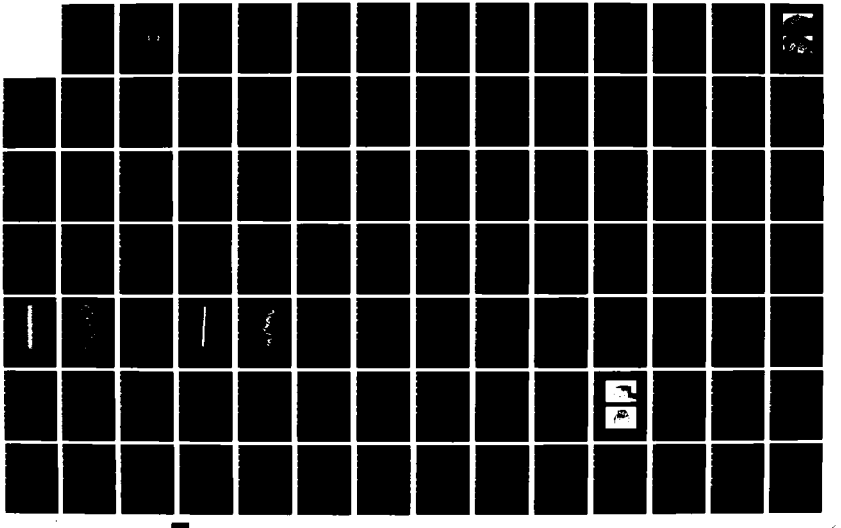

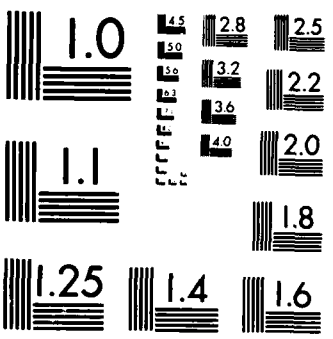

SBE 003

(12)

Report TR-352/11-85

AD-A165 250

A HIGH-RESOLUTION CLUSTER OF OCEANOGRAPHIC INSTRUMENTS FOR BOUNDARY LAYER MEASUREMENTS UNDER ICE

H.-T. Liu, J.J. Kolle and P.D. Bondurant

Flow Industries, Inc.
Research and Technology
21414 - 68th Avenue South
Kent, Washington 98032

November 1985

Phase II Final Report

APPROVED FOR PUBLIC RELEASE
DISTRIBUTION UNLIMITED

Prepared for:

OFFICE OF NAVAL RESEARCH
800 North Quincy Street
Arlington, Virginia 22217

REPORT DOCUMENTATION PAGE

READ INSTRUCTIONS BEFORE COMPLETING FORM

1. REPORT NUMBER	2. GOVT ACCESSION NO. AD-A165250 / 3. RECIPIENT'S CATALOG NUMBER
4. TITLE (and Subtitle) A High-Resolution Cluster of Oceanographic Instruments for Boundary Layer Measurements Under Ice	5. TYPE OF REPORT & PERIOD COVERED Phase II Final Report 26 Sept 1983 - 30 Nov 1985
	6. PERFORMING ORG. REPORT NUMBER Flow Report No. 352
7. AUTHOR(s) H.-T. Liu, J. J. Kolle and P. D. Bondurant	8. CONTRACT OR GRANT NUMBER(s) N00014-83-C-0764
9. PERFORMING ORGANIZATION NAME AND ADDRESS Flow Industries, Inc. 21414 68th Avenue South Kent, Washington 98032	10. PROGRAM ELEMENT, PROJECT, TASK AREA & WORK UNIT NUMBERS
11. CONTROLLING OFFICE NAME AND ADDRESS Office of Naval Research 800 North Quincy Street Arlington, Virginia 22217	12. REPORT DATE November 1985
	13. NUMBER OF PAGES 98
14. MONITORING AGENCY NAME & ADDRESS(if different from Controlling Office)	15. SECURITY CLASS. (of this report) Unclassified
	15a. DECLASSIFICATION/DOWNGRADING SCHEDULE

16. DISTRIBUTION STATEMENT (of this Report)

Approved for public release; Distribution unlimited.

17. DISTRIBUTION STATEMENT (of the abstract entered in Block 20, if different from Report)

Approved for public release; Distribution unlimited.

18. SUPPLEMENTARY NOTES

19. KEY WORDS (Continue on reverse side if necessary and identify by block number)

coherence length	laser Doppler velocimeter	oceanic boundary layer
diode laser	marginal ice zones	
Doppler burst	spatial resolution	
Doppler frequency	spectral bandwidth	
frequency response	turbulent flux	

20. ABSTRACT (Continue on reverse side if necessary and identify by block number)

- Three high-resolution clusters (HRCs) of oceanographic instruments, each consisting of three diode laser Doppler velocimeters (DLDVs), a high-frequency thermistor probe and a dual-electrode conductivity probe, have been developed for measurements of turbulent momentum, heat and mass fluxes in the oceanic boundary layer under ice. The spatial resolution was designed to be 2 cm or better. The DLDVs, which are the essential components of the HRCs, were first developed and successfully tested in the laboratory, then they were deployed

20. (cont.)

during two field experiments. Two experimental units were deployed during the 1984 Marginal Ice Zone Experiment (MIZEX 84), and two prototype velocity-temperature-conductivity clusters were deployed during the 1985 Arctic Internal Wave Experiment (AIWEX 85). During MIZEX 84, velocity components were measured simultaneously with the DLDV and ducted current meters. Good agreement was generally observed. The AIWEX 85 results also included temperature and conductivity measurements. Variations in temperature and conductivity at depths of 2 and 4 m were only observed with one sensor to exceed 0.01°C and 10 umho/cm, respectively, for a time scale up to one hour. This indicates that the boundary layer under the ice floe was essentially well-mixed, which is consistent with other observations during the same time period (April and May 1985). Both field experiments showed adequacy of scattering particles for use with the DLDV. The spatial resolution of the DLDV, which was found to be proportional to the sampling rate, achieved the target value of 2 cm, at least one order of magnitude better than that attainable by mechanical current meters. The field worthiness of the DLDV, in terms of its portability, robustness and performance is proven through the two field experiments.

TABLE OF CONTENTS

LIST OF ILLUSTRATIONS

LIST OF TABLES

Delete the proprietary statement on Page 80
of this report.
Per Dr. Robert O'Brochta, ONR/Code 1125AR

ACKNOWLEDGEMENTS

The development of the DLDV as an ocean sensor was initiated by Dr. John Carl Schedvin, who passed away after completion of the Phase I feasibility investigation. The authors would like to thank Mr. D. Schmidt for developing the hardware and implementing the software for the DLDV processor, Mr. P. Tacheron for assembling and testing the DLDV modules, and Mr. C. Lentz for assembling the DLDV processor. The conductivity/temperature circuitry was designed by Mr. P. Stockton of Datacon Electronics. Logistical support was supplied by the Polar Science Center, University of Washington.

1. INTRODUCTION

The feasibility of developing a diode laser Doppler velocimeter (DLDV) for oceanographic measurements of current and turbulence has been demonstrated by Flow Industries, Inc. (FLOW) in a DOD SBIR Phase I investigation sponsored by the Office of Naval Research (see Phase I final report, Schedvin and Liu, 1984 -- referred to as [I] hereafter). The Phase II work, which is documented in this report, was directed toward the development of a complete DLDV sensor system that could be easily adapted to a number of field measurement applications. This required the development of both single-component and multi-component DLDV sensors and the development of a flexible data analysis electronics system that can be used under a variety of flow conditions. A direct product of the Phase II effort is an oceanic boundary layer measurement system using high-resolution sensor clusters (HRCs). The DLDV sensors developed for the measurement system serve as prototypes of the commercial sensors to be manufactured and marketed in Phase III.

Part of the Phase II work also involved supporting the development and field deployment of moderate-resolution clusters (MRCs), each consisting of three small, partially ducted current meters and a fast-response temperature and conductivity sensor (McPhee and Smith, 1976). The spatial resolution of the MRC is limited to about 10 to 30 cm by the response of the current meters and colocation of the sensors. A detailed description of the MRC, the field deployment and results is given elsewhere (McPhee, 1984, 1985a).

The Phase II effort focused mainly on the further development of the DLDV sensor. The Phase I results [I] indicated the feasibility of an underwater DLDV sensor. However, a number of developmental steps were still needed to produce an instrument of commercial interest for oceanographic measurements. The two primary objectives of the Phase II work are described below.

(1) Development of a compact, reliable DLDV sensor with optional flow direction sensing.

This objective represented the main developmental effort of Phase II. Primary tasks were the development of Doppler signal analysis electronics and the selection and implementation of the optimal method of flow direction sensing. Other tasks included the optimization of the laser diode optical configuration, the photodetector, scattered light pickup,

and underwater packaging for low flow disturbance and ease of maintenance. The result is a high-resolution, low-power, compact velocity sensor with many oceanographic applications.

(2) Development of a high-resolution turbulent flux measurement cluster for oceanic boundary layer measurements.

The high-resolution clusters use the DLDV sensors to provide a three-component velocity measurement and include fast-response temperature and conductivity sensors. A modular approach utilizing the single-component DLDV sensor and associated analysis electronics was adopted. A standard digital interface bus is used for all instruments, with microprocessor control of sampling and data storage. This allows great flexibility in the auxiliary sensor and the configuration of the DLDV sensors.

Our goal was to achieve a spatial resolution of about 2 cm for the HRCs, 10 times greater than that of the MRCs. This represents a significant advance in oceanographic instrumentation for boundary layer measurements toward complete resolution of the turbulent fluxes. While field sensors with such a high resolution are lacking, the turbulent fluxes of momentum, heat and mass at this fine-scale (and high-frequency) range may prove to contribute significantly to the total fluxes in the oceanic boundary layer under ice, such as has been observed in the atmospheric boundary layer (Lumley and Panofsky, 1964).

The modular instrument design with flexible digital interfacing and control will provide a versatile oceanographic sensor. While the initial commercial prototypes are intended for oceanic boundary layer measurements, the instruments could also be used on towed or self-propelled platforms and on vertically profiling packages.

Field testing was an important part of the Phase II effort and had two primary goals. First, the field tests provided an assessment of the reliability of the DLDV sensors and allowed evaluation of sensor performance with oceanic scatterer concentrations. This information was used to improve the design of the sensor and the Doppler signal analysis electronics. Second, the field tests provided the environment for examining the capabilities of the moderate- and high-resolution clusters for conducting turbulence flux

measurements in the oceanic boundary layer under ice, as well as providing important data sets for Arctic Ocean boundary layer studies.

This report documents the research and development conducted in the Phase II investigation that led to the completion of two experimental DLDV underwater units deployed during MIZEX 84 and subsequently the completion of three prototype velocity-temperature-conductivity (V-T-C) HRCs deployed during AIWEX 85. Documentation of the two field experiments, MIZEX 84 and AIWEX 85, and some of the field results are also included. Section 2 describes the individual instruments and equipment that make up the HRC. In Section 3, we present the performance characteristics of the HRC sensors. The software for data acquisition and analysis is given in Section 4. Section 5 documents the field experiments and the results analyzed to date. Finally, a summary to assess the performance of the HRC in the Arctic environment and recommendations for future work are presented in Sections 6 and 7, respectively.

2. INSTRUMENTATION OF THE HIGH-RESOLUTION CLUSTER

The high-resolution cluster consists of three DLDV underwater units, a high-frequency thermistor probe and a dual-electrode conductivity probe mounted on an octagonal holder made of stainless-steel tubes and parts. Most of the research and development concentrated on the DLDV units. During the Phase I feasibility demonstration, we constructed and tested a bench test model of the DLDV [I]. Then, in Phase II, we built two experimental DLDV units and deployed them during MIZEX 84 to demonstrate their field applicability. Both a counter and a frequency tracker were used as the Doppler signal processors in an attempt to determine the optimal processor for our intended field measurements. Based on the findings obtained in the laboratory tests and MIZEX 84, we redesigned and assembled nine prototype DLDVs and integrated them into three HRCs, which were deployed subsequently during AIWEX 85. Figures 1 and 2 show a schematic and photographs of the HRC.

The thermistor probes and conductivity probes selected for the HRCs have been used in oceanographic measurements. Their performance characteristics have been reported in the literature (Meagher et al., 1982). Several new features were incorporated into the circuit design to be compatible with our measurement strategy.

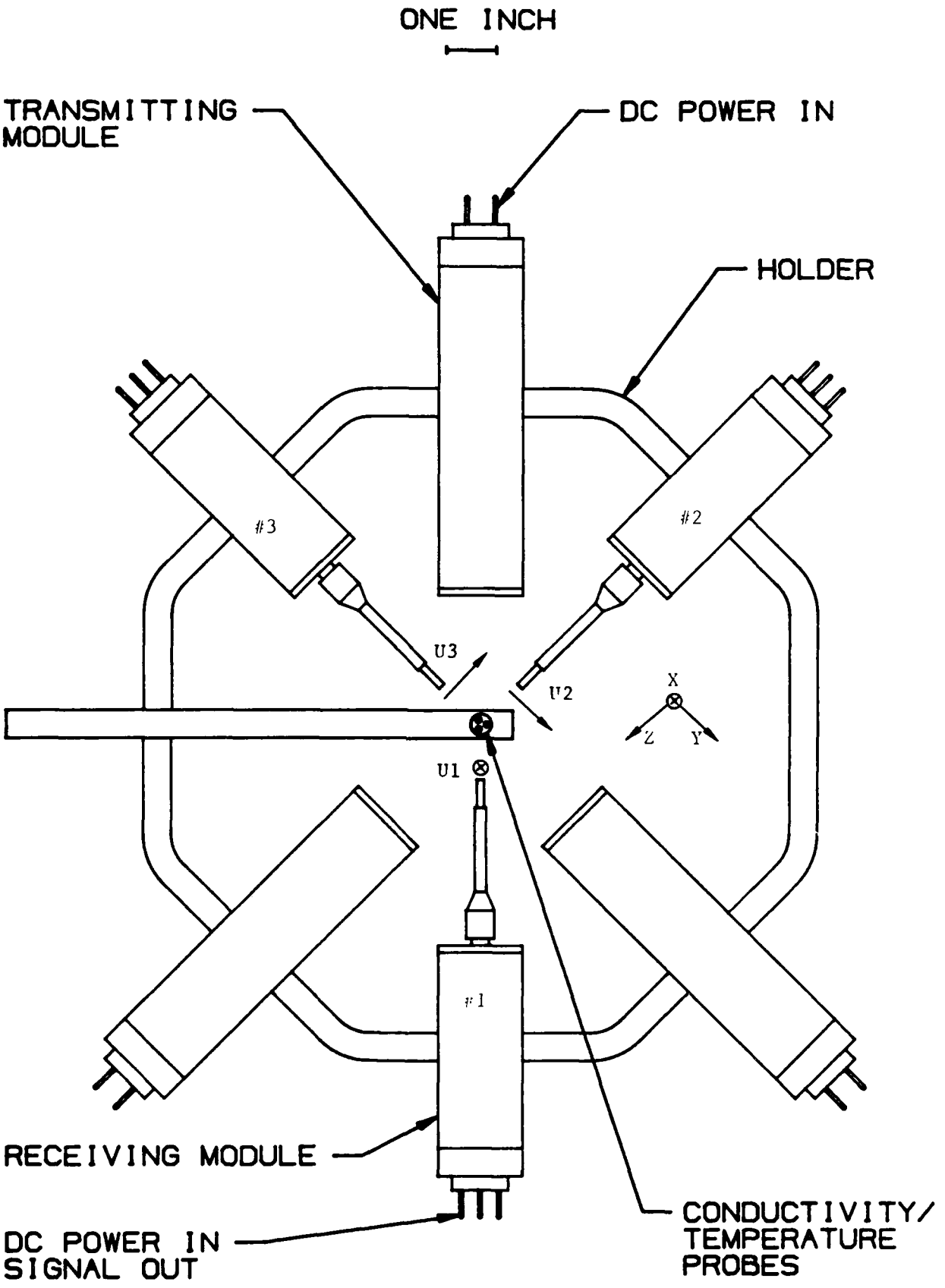

Figure 1. Schematic of the HRC Consisting of a Three-Axis DLDV System and a Temperature/Conductivity Probe Pair - Note the right-handed coordinate system with mean flow into page.

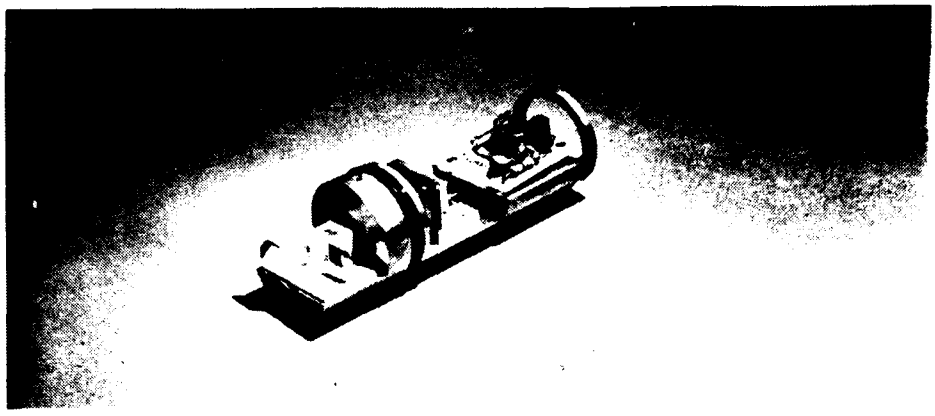

a. Basic Building Block of the Transmitting Module

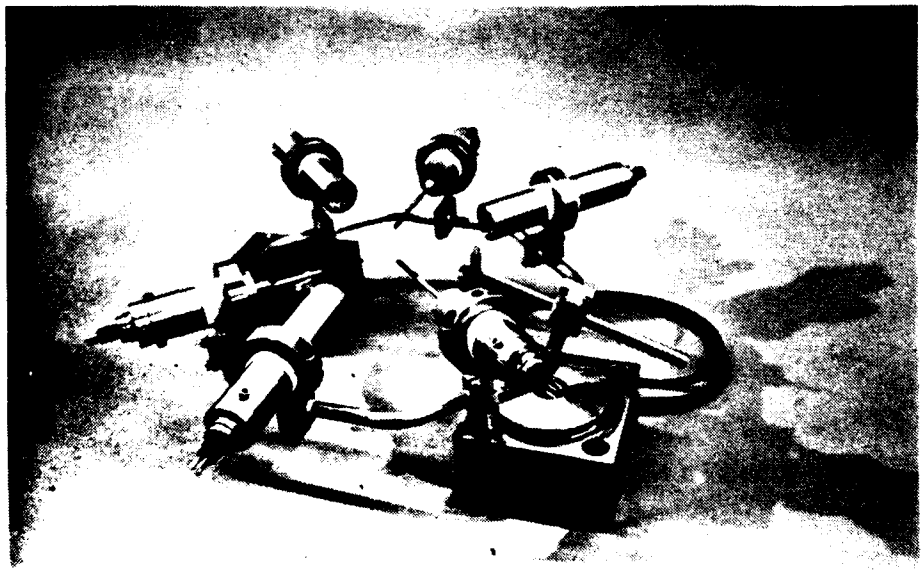

b. Layout of the HRC Sensors

Figure 2. Photographs of the High-Resolution Cluster

The sensors on each HRC were connected to a processor developed and assembled by FLOW, which provides power to drive the sensors, provides signal amplification, filtering and preprocessing, and interfaces the signal outputs with the host computer.

In this section, we describe in detail the individual sensors. First we discuss the DLDV modules, then the temperature/conductivity probe pair, and finally the HRC processors.

2.1 DLDV Modules

The concept of the DLDV and the design considerations are given in detail in [I]. In this report, we describe the actual design and assembly of the prototype units. The DLDV consists of a transmitting module and a receiving module. A schematic of the two modules set up for velocity measurements together with detailed drawings is shown in Figure 3 (also see Figure 14 of [I]).

2.1.1 Transmitting Module

As shown in Figure 3, the transmitting module includes the electro-optical (EO) components to form a diode laser, to split the laser beam and to configure the beams into the fringe mode of arrangement for use with laser velocimetry. The EO components are mounted on an aluminum chassis, which is in turn placed in an underwater housing made of a stainless-steel tube (15.2 cm long and 3.8 cm OD). The diode laser consists of a 5-mW laser diode (Hitachi HL7801G) mounted on a three-dimensional miniature stage, a collimator (Fischer 40x objective), a beam splitter and a focal lens (8.5 focal length in air). The nominal wavelength of the diode laser is 793 nm, which is in the deep red regime [not visible unless viewed with a fluorescent screen (Optical Engineering)].

The beam splitter is formed by gluing five 1-cm prisms manufactured by Melles Griot. Two of the prisms are preassembled by the manufacturer (Melles Griot) to form a cube beam splitter coated for laser diode applications. The rest of the prisms are glued to the cube beam splitter using an optical adhesive that is cured with an UV light. A special jig mounted on an optical table is used to align the prisms, and the alignment is monitored using a 5-mW He-Ne laser during the entire curing period. The error in parallelism of the two split beams is maintained to be within $\pm$ 5 millidegrees in both planes. The prisms and the focal lens are coated with a HEBBAR anti-reflection coating (Melles Griot) to reduce reflection and to enhance optical transmission.

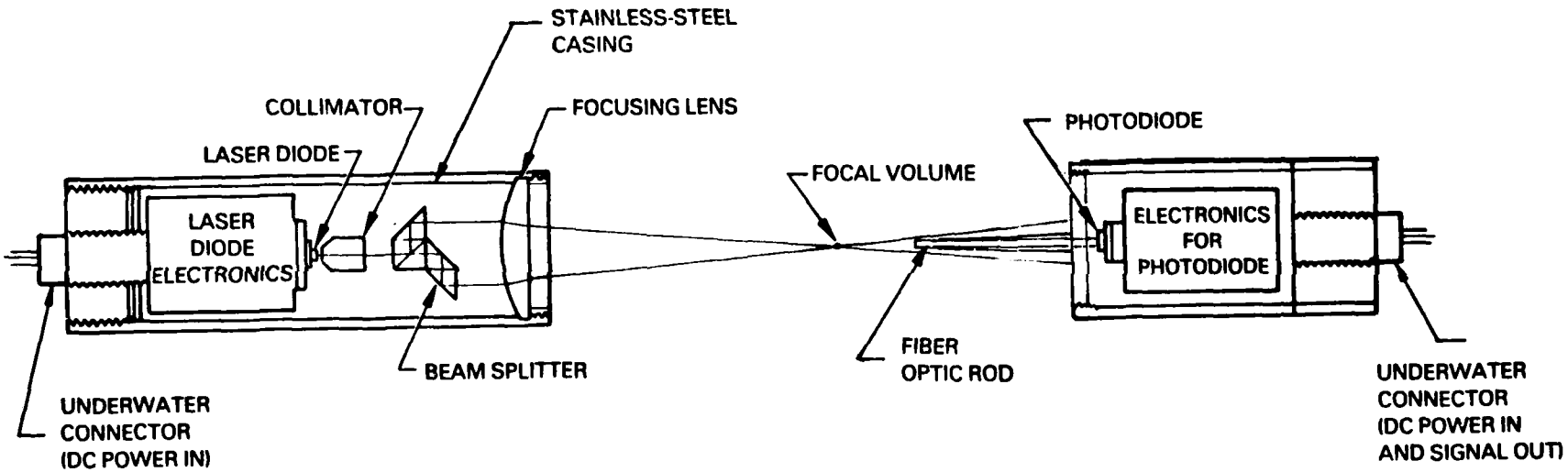

Figure 3. Design of the DLDV Transmitting/Receiving Modules

To maintain a constant laser power output and to protect the laser diode from large electrical surges or spikes present in the power source, a special circuit (Figure 4) was designed and inserted between the diode and the DC power supply. The desired forward current may be set using a 10-turn pot. A feedback loop using the output from a built-in photodiode, which monitors the laser power output, controls the forward current to maintain a constant laser power output. For example, when the surrounding temperature drops, the diode laser becomes more efficient. The feedback loop automatically reduces the forward current to maintain a constant laser power.

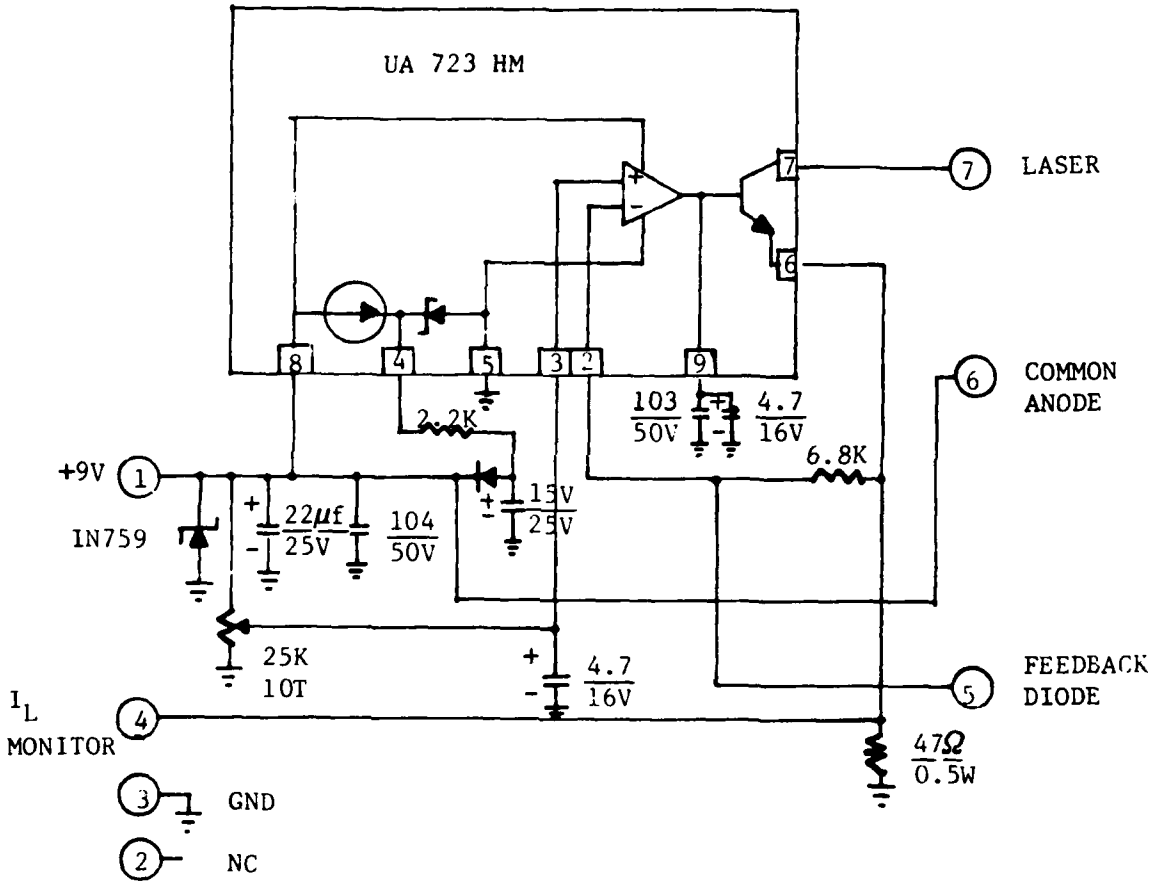

Figure 4. Feedback Circuitry for Control of the Laser Power Output

2.1.2 Receiving Module

The receiving module consists of the EO components for collecting and sensing the scattered light from tracer particles passing through the focal volume of the laser beams. A detailed schematic of the module is shown in

Figure 3. The module is enclosed in an underwater housing made of a stainless-steel tube (10.2 cm long and 3.8 cm OD). A 3-mm-diameter fused fiber optic rod is used as the collector of scattered light. The advantage of using a fiber optic rod is twofold: it avoids the necessity for precision alignment, and it reduces light attenuation by bringing the rod end reasonably close (2 to 3 cm) to the focal volume without introducing significant flow disturbance. Scattered light falling on the rod end is internally reflected by the individual fibers (about 70,000 in the rod used) and routed to the photodiode (Devar Inc., Type 539-01-5, with a 5-mm^2 sensing area). The driver of the photodiode is mounted on a printed circuit board next to the diode. In addition to driving the photodiode, the circuit provides the functions of low-pass filtering and amplification (up to a gain of 20) of the signals. The output signals and the DC power ($\pm$ 15 volts) are transmitted to and from the surface through the main underwater cable with a pigtail (branched out from a junction box) plugged into a five-pin connector at the end of the module.

2.2 Temperature/Conductivity Probe Pair

Figure 5 shows a drawing of the temperature/conductivity probe pair used on the HRC cluster. It consists of a thermistor probe (FASTIP, Model FP07, Thermometrics, Inc.) and a dual-electrode conductivity probe glued together with the three tips 3 mm apart and forming a triangle. The thermistor is housed at the tip of a shock-resistant glass tube. The small bead thermistor

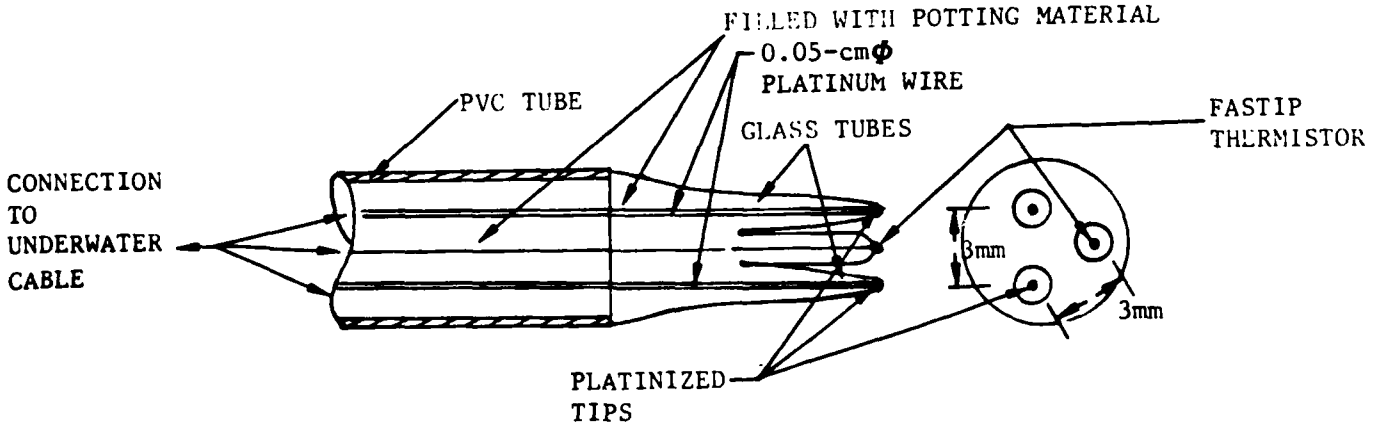

Figure 5. Schematic of Temperature/Conductivity Probe Pair

has an extremely thin glass coating. Its response time is 7 ms in water as measured in a plunging test. The nominal resistance of the thermistors is 10 kohm at 25°C. The conductivity probe consists of two thin platinum wires (0.05 cm in diameter) each sealed in a thin glass tube with the tip exposed and platinized with a platinum black solution manufactured by Yellow Spring Instrument Co. The probe is similar to that reported by Meagher et al. (1982) with the wires 2.5 times smaller in diameter than their probes.

The selection of the dual-electrode probe rather than the larger conductivity cells, such as those of the Neil Brown or Sea-Bird cells, is due primarily to the compatibility of the DLDV sensors in terms of physical size, configuration, and dynamic response. Our goal is to achieve an overall spatial resolution of 1 to 2 cm^3 for the V-T-C high-resolution cluster. According to Meagher et al. (1982), the dynamic response of a dual-electrode probe (0.05-inch-diameter platinum wires) is about 100 cpm (cycles/meter) at the 3-dB point. Our probe should have better response because the size of the wire is about 2.5 times smaller than theirs. The trade-off in using the dual-electrode probe is some sacrifice of calibration stability. Meagher et al. (1982) measured a drift rate of this type of probe to be approximately 0.01 S/m (siemens/meter; 1 S/m = 0.1 μmho/cm). Such a slow drift has little effect on the density flux measurements because the differential rather than the absolute conductivity is of interest to us.

It is interesting to point out that the dual-electrode probes are less prone to noncatastrophic fouling than the large, more stable conductivity cells. Experience with three types of probes towed in the seasonal thermocline of the Sargasso Sea shows that the 1.5-cm Neil Brown cell, the Neil Brown planar cell, and the dual-electrode probes were fouled 35%, 42%, and 8% of the time, respectively (Meagher et al., 1982).

2.3 HRC Processors

The function of the processor is to provide DC and AC power to drive the various electronic active elements of the DLDV and temperature/conductivity sensors and to receive and condition (filtering, amplification and DC voltage offsetting) the raw signals output from these sensors. The conditioned, analog data are then converted into digital form to be recorded with a COMPAQ computer using a 12-bit D/A converter. Appendix A is a set of operating instructions for the software controlling the HRC processors.

2.3.1 DLDV Processor

An important part of the Phase II effort was the development of flexible data analysis electronics for the Doppler signal. Standard approaches to Doppler signal analysis are the use of period counters and frequency trackers. Because the output power of laser diodes is fairly low, small sampling volumes are necessary for adequate scattered light intensity. This requirement, combined with the low to moderate scatterer densities expected in the open ocean and in particular in the Arctic, indicates that a counter processor is probably the best choice for the Doppler signal analysis electronics (Krumholz and Murphy, 1974). During MIZEX 84, we used both a tracker and a counter to process the Doppler signals. The superiority of the counter to the tracker was confirmed from the MIZEX 84 results (see Section 5.1). Therefore, we decided to adopt the counter approach.

The approach used in a counter processor is to first band-pass filter the photodetector output to remove the pedestal signal. This is a low-frequency component that is associated with the variation in the average scattered light intensity as a particle moves through the sampling volume. The remaining Doppler frequency burst (Figure 6) is then fed to a period counter processor. This processor determines the time interval for a number of zero crossings of the Doppler signal. The time interval is obtained by counting a high-frequency clock. Also, valid zero crossings are determined by simultaneously checking to see that the Doppler signal crosses an appropriate threshold (either above or below 0 volts) after each zero crossing (see Figure 6). Typically, the time for a number of zero crossings, say 8, is compared to the time for the first 5 zero crossings. If these times do not indicate the same frequency within some allowable error, e.g., 2%, then the Doppler burst is rejected for further processing.

A block diagram of the dual-counter Doppler signal analysis system is shown in Figure 7. The input stage is a bank of analog filters. The band-pass and rolloff of the analog filters were chosen to assure the pedestal would be removed. The output of each filter feeds a dual-counter section where each counter counts a high-frequency clock gated by a selectable number of Doppler counts (3, 5, 8, or 13 counts). The outputs of the dual counters are fed to the microprocessor, which reads each of the dual-counter channels and determines the highest frequency Doppler channel that has valid data. A valid channel is one that has had at least 8 counts (if strapped for a 5/8 comparison) and that has a count ratio between the two counters within a software

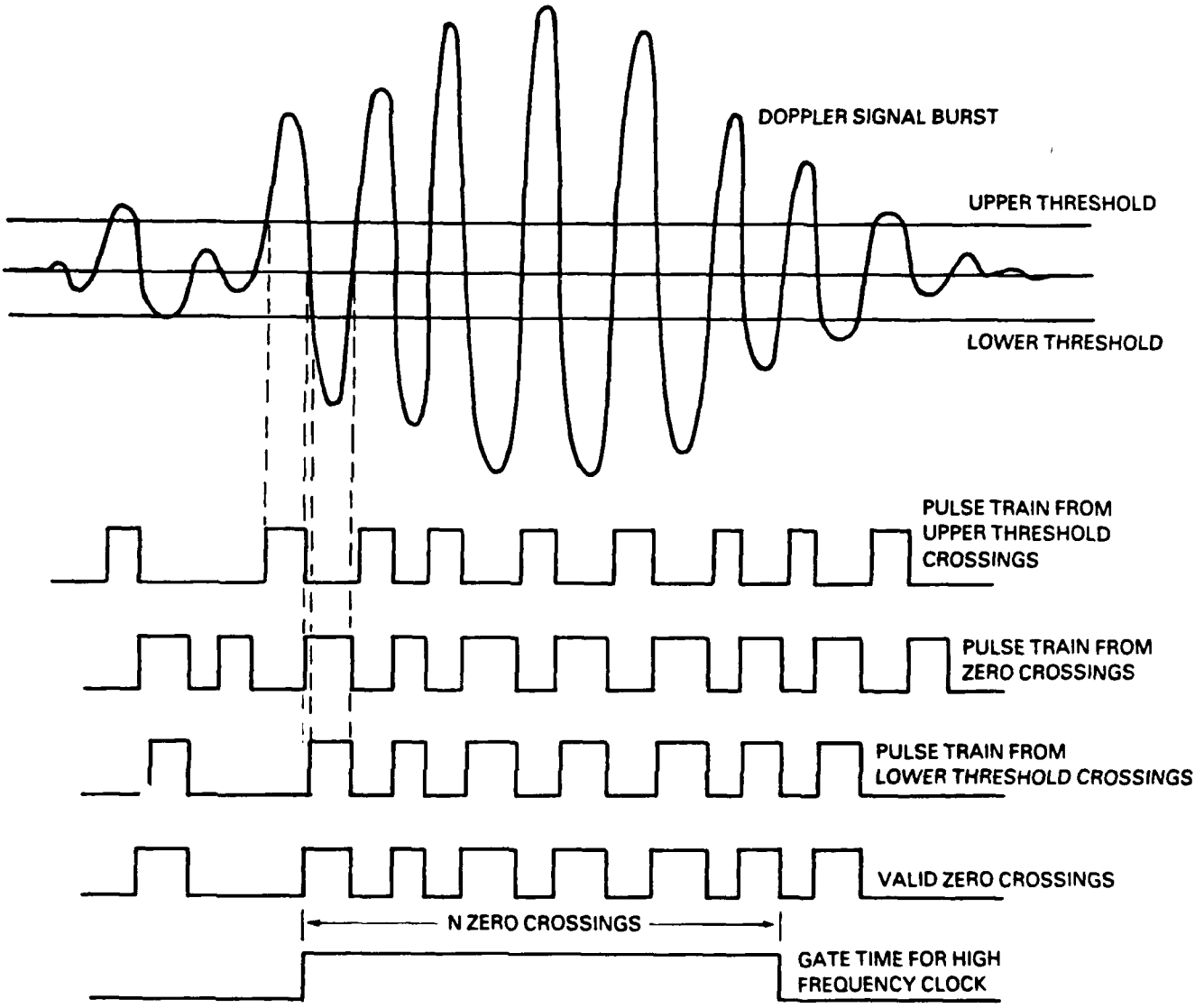

Figure 6. Counter-Period Timing System for Doppler Signal Analysis - Upper and lower thresholds are used to identify valid zero crossing. A high-frequency clock is counted for N valid zero crossings (gate time).

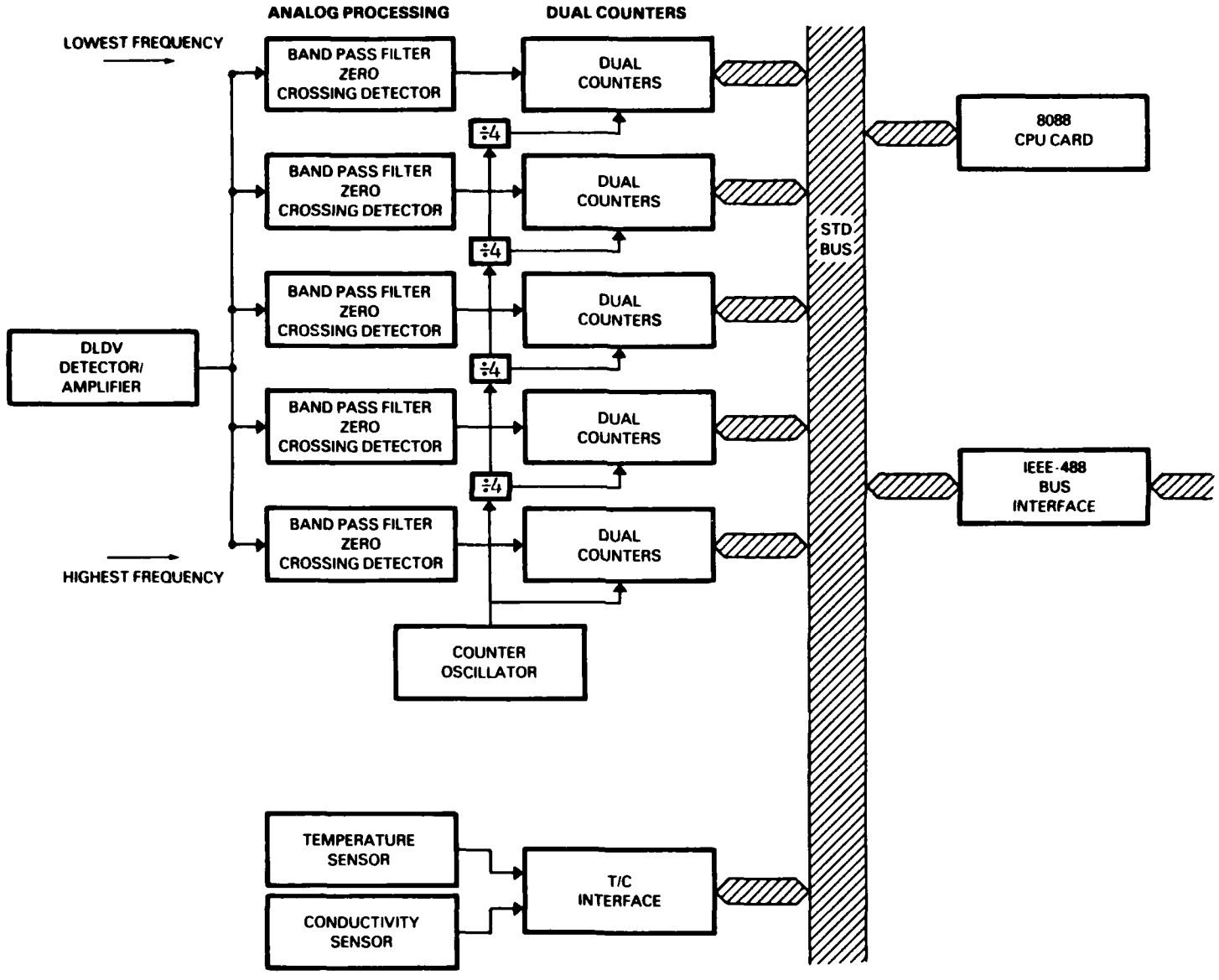

Figure 7. Block Diagram of Doppler Signal Processing Electronics for Dual Counter Design - Diagram shown for one velocity axis. Additional analog circuits and counters used for further axes with the same CPU and operator interface.

selectable percentage of the 5/8 ratio. All of the Doppler channels are sampled for valid data and sent via IEEE-488 at the sample frequency selected by the operator via the host computer (COMPAQ).

System design

The first step was to produce an overall system design for an HRC including a three-component DLDV and temperature and conductivity sensors. A detailed block diagram of the system was completed that identified off-the-shelf components that could be used. The data processing electronics was based on the industry standard STD bus (8 bit). This allowed the use of off-the-shelf microprocessor boards, remote computer interfaces and interfaces to the temperature and conductivity sensor digital inputs. To retain compatibility with FLOW's microprocessor development system and the STD bus, an 8088-based microprocessor was used.

Prototype hardware design

This is part of the circuitry that separates the pedestal from the Doppler signal. Computer simulation was used to select the required bandwidth and rolloff for the analog front end. The computer was used to generate a worst case Doppler burst, and the simulation was used to select the bandwidth and rolloff necessary to remove the pedestal and still keep circuit complexity to a minimum. A rolloff of 24 dB/octave on both ends of the band-pass is sufficient to remove the pedestal. The frequency ranges (band-pass) selected are shown in Table 1. There are six counter boards per cluster (two per axis)

Table 1. Frequency Ranges for Counter Channels

Channel	Frequency Range
1	250.0 Hz to 1.0 kHz
2	1.0 kHz to 4.0 kHz
3	4.0 kHz to 16.0 kHz
4	16.0 kHz to 64.0 kHz
5	64.0 kHz to 250.0 kHz
6*	250.0 kHz to 1.0 MHz

*Not used for this experiment.

with three dual-counter channels per board. This gives six frequency ranges per axis. A diagram of the counter circuit is given in Appendix B.

Each counter channel was strapped to generate a 5/8 count ratio. The count clock is set for approximately 20 times the maximum frequency for a given range. This gives plenty of frequency resolution over an 8 Doppler count window. Each of the counter boards fits into the STD bus card cage, along with the microprocessor boards and the temperature and conductivity interface.

Each set of two counter boards is driven by a board mounted outside the STD bus rack containing the analog signal processing electronics (there are three analog boards per cluster). This board consists of a differential input stage driven by the velocimeter head for that particular axis. This is followed by the six sets of filter stages (one for each of the six velocity ranges) and six comparator and gating stages, which convert the analog Doppler bursts into digital bursts. These digital bursts are then sent differentially to the two counter cards in the STD bus. There are two adjustments on each of the six channels: one sets the amplification of the analog signal processing electronics, and one sets the comparator threshold level. A 9-volt regulator is also on each analog board for driving the laser diode (see Appendix B).

Prototype software design

Simultaneously with the hardware design, a software package was developed. The majority of the software was written in C, with a little in assembly language. This speeds the development time and makes the software easier to follow for documentation purposes and easier to upgrade for future modifications. The software performs the tasks of reading, validating, and interpreting the raw Doppler signal data from the dual counters. The software is capable of averaging over several readings, keeping track of particle count rates, and transmitting the data to an auxiliary processor/microcomputer for data storage and analysis.

2.3.2 Circuitry for Temperature/Conductivity Sensors

The unit is a single circuit board designed to be STD bus compatible. The prototype board performs three basic functions:

(1) To convert temperature to a voltage acceptable to the analog interface board.

(2) To convert the conductivity of ocean water to a voltage acceptable to the analog interface board.

(3) To provide programmable control of both temperature and conductivity to enable computer control of gain and offset for both temperature and conductivity. This capability provides very high resolution over a wide dynamic range.

A detailed design of the circuit board is given in Appendix C. In essence, the temperature circuit is a simple, balanced resistance divider where the temperature-sensitive element is connected to a precision load resistor (R1). Voltage to this divider is provided by a precision voltage reference source. The divider resistor values have been chosen to provide maximum sensitivity at the anticipated temperature range of -4 to +15°C. The balanced temperature sensor input is preamplified through a very low-noise, low-drift precision difference voltage follower. The signal is then low-pass filtered at either 3.8, 6.3, or 12.5 Hz. The signal is then a voltage representing temperature and is controllable by the computer through a selectable gain amplifier and off-settable by a 16-bit digital-to-voltage converter. The possible gains are x1, x10, x100, and x1000. Prior to the gain control, the signal is off-settable from 0 VDC to +10.0000 VDC in increments of 0.000153 VDC.

Conductivity is determined by the root-mean-square (rms) value of an alternating current (Isig) flowing through the sample solution being tested. The conductivity is equal to the probe current (Isig) divided by the probe voltage (Vsig). The circuit measures both Isig and Vsig and divides Isig by Vsig to obtain a voltage proportional to the conductivity independent of fluctuations in Vsig (within limits). This voltage is then processed through exactly the same circuitry as the temperature so that the control circuitry has a matched frequency response and phase shift.

Note that the rms DC converters in the conductivity circuit may produce a small correlation error of the temperature versus the conductivity. They also limit the frequency response, but compared to the low-pass filters should be negligible.

2.3.3 Miscellaneous Hardware

The underwater HRCs are connected to the processor through an underwater cable. At the lower end of the cable, a set of pigtails is potted to a junction box. At the end of the pigtails, different types of underwater connectors are plugged into individual sensors on the HRC. A total of three underwater cables are being fabricated. These cables are 15, 20 and 65 m long, respectively. The different cable lengths will provide flexibility for measurements at different depths under an ice floe.

3. PERFORMANCE CHARACTERISTICS OF THE HRC SENSORS

Several series of laboratory tests were conducted during Phase I and Phase II to determine the performance characteristics of the sensors used on the HRCs. The tests conducted in Phase I are reported in detail in [I]. In this section, we describe the Phase II tests and results. From these results, we define the performance characteristics of the sensors.

3.1 Diode Laser Doppler Velocimeter

3.1.1 Prototype DLDV

For a dual-beam system using the fringe model [I], the calibration of the LDV depends on the wavelength of the laser, λ, and the half angle of the beam crossing, ϕ, or

$$f_D = \frac{2\, u_x \sin \phi}{\lambda} \tag{1}$$

where f_D is the Doppler frequency and u_x is the velocity component perpendicular to the bisector of the two illuminating beams. Replacing $\lambda/(2 \sin \phi) = d_f$, we have

$$\frac{f_D}{u_x} = \frac{1}{d_f} \quad [\text{Hz}/(\text{cm/s})] \tag{2}$$

where d_f is the fringe spacing.

These two equations indicate that the calibration of the DLDV is linear and its sensitivity in hertz per centimeters/second is inversely proportional to the fringe spacing. For a DLDV with a known geometrical arrangement of the

crossing beams, the calibration will stay the same until the laser diode is replaced. For a given diode, the peak wavelength (about 790 nm for a Hitachi HL7801G diode) increases slightly with the output power and, therefore, with the device (but not the ambient) temperature.* The typical average temperature coefficient of the peak wavelength is 0.2 to 0.3 nm/°C. In the extreme situation of a 10°C drop in the device temperature in response to a 20°C ambient temperature drop, the peak wavelength decreases less than 0.4%. This corresponds to an increase of 0.4% in the sensitivity, which may be corrected for if the device temperature is known. In practice, such a small correction is generally well within the experimental error (typically $\pm$ 5 to 10%) for field experiments.

A series of tow-tank experiments was conducted at FLOW prior to MIZEX 84 to confirm Equation (2). One of the DLDV units tested had an HL7801G diode (No. 0005) with a peak wavelength of 793 nm at 3 mW. The half angle measured in water, ϕ_w, was 3.5°. The fringe spacing was therefore

$$d_f = \lambda_a/2 \sin \phi_a = \lambda_a/2\, n_w \sin \phi_w = 4.87\ \mu m \qquad (3)$$

where $n_w = 1.333$ is the index of refraction of water. The corresponding sensitivity, according to Equation (2), was estimated to be 2052 Hz/(cm/s). Figure 8 shows the results of the calibration. The ordinate and abscissa are, respectively, the velocity of the tow carriage on which the DLDV was mounted, U_T, and that measured with the DLDV, U_m. As can be seen in the figure, the data points are within $\pm$ 3% of the 45° line. Similar results were obtained with another DLDV unit in which an LDL SCW21 diode (831 nm at 7 mW) was installed. Both units were used during MIZEX 84.

Additional tow-tank tests were conducted to test the three 3-axis clusters prior to AIWEX 85. For all nine units, the nominal wavelength of the diodes was 790 $\pm$ 5 nm, and the nominal half angle between the beams was 6.71° in air. The fringe spacing was therefore 3.38 μm and the sensitivity was 2960 Hz/(cm/s).

During the tow tests, we had to add powdered milk into the tank in which the water was filtered through a 10-μm filter. There were simply not enough particles left in the filtered water for the DLDV to work satisfactorily.

---

*Sources quoted from "Optical Semiconductor Devices Data Book" issued by Hitachi America, Ltd., Documentation No. S13.

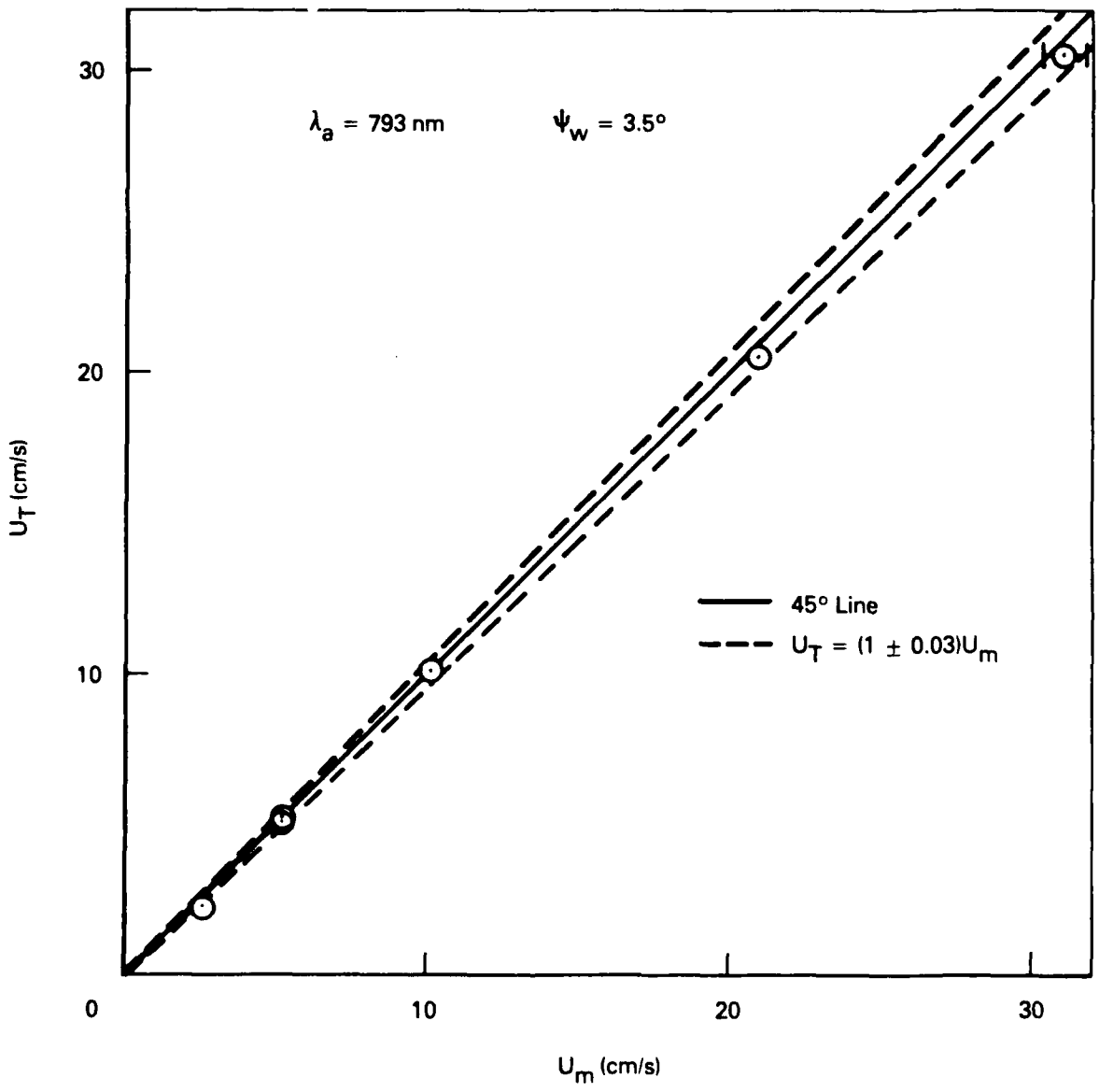

Figure 8. Typical Calibration Data for the DLDV Using an HL7801G Diode Laser

3.1.2 Configuration for Three-Axis HRC System

As shown in Figure 1, three single-axis DLDVs are mounted on an octagonal frame that is held vertically. The transmitter receiver pairs are identified as #1, #2 and #3. U1 measures the velocity component perpendicular to the plane of the frame, while U2 and U3 measure the velocity components in the plane of the frame inclined at 45° to the vertical. The frame is rotated in the horizontal plane so that the current flows into the frame at an angle of 30 to 45° to the right of the frame axis. This ensures that all three DLDV pairs observe a substantial mean flow component. The orientation of all three DLDV pairs is shown in Figure 1.

3.2 Temperature and Conductivity Probes

The FASTIP thermistor by Thermometrics (Series FP07) has a very thin tip (0.18 mm overall diameter) in which the thermistor bead is housed. As a result, it has a frequency response of 21 Hz, which is about a factor of 2 higher than those sealed in a glass tube without a thin tip (Lueck et al., 1978; Gregg and Meagher, 1980). The thermistor circuit was designed to have the maximum sensitivity at temperatures around 0°C (see Appendix C). At a gain of 1, the sensitivity was typically 5 to 6 mV/°C. Due to the relatively low sensitivity, any small electronic drift (not the sensitivity) would result in a noticeable shift in the measured absolute temperature. Therefore, this particular design was not suitable for absolute temperature measurement. However, the absolute temperature may be inferred from nearby conventional temperature gauges deployed simultaneously. The rms noise level, which was predominantly 60 Hz, was measured to be about 0.7 mV at a gain of 100 and with the low-pass filter set at 100 Hz. The noise level decreased significantly when the low-pass filter was subsequently set at or below 12.5 Hz. Therefore, the thermistor gauge is capable of resolving minute temperature changes of about 0.001°C. The sensitivity of the thermistor varies with the temperature but may be considered constant within a narrow temperature range of 2 to 3°C. The actual resolution of the gauge is about 0.002°C at a gain of 100 and a 12-bit A/D conversion (10 V full scale).

As described in Section 2.2, the dual-electrode conductivity probes have been subjected to field tests and found to be satisfactory for measurements of conductivity differentials (Meagher et al., 1982). To ensure sufficient spatial resolution (1 to 2 cm), we reduced the diameter of the platinum wires

2.5 times from 1.3 mm to 0.5 mm at the sacrifice of some sensitivity and, probably, stability. The frequency response of the dual-electrode probe is expected to reach hundreds of hertz (Dugan and Okawa, 1982). To avoid salinity "spiking" (Dantzler, 1974; Roden and Irish, 1975), however, the circuit has the same low-pass filter as that of the thermistor probe, i.e., 12.5 Hz or lower.

The circuitry of the dual-electrode probe was designed to have voltage output linearly proportional to conductivity. Calibration of the conductivity gauge was made by using four jars of salt solution with different brine concentrations (ρ = 1.0, 1.01, 1.02, and 1.025 gr/cm^3). The jars were kept in a constant temperature bath at 20°C. The conductivity was measured with a Beckman conductivity gauge (Model RC-16C) using a standard cell with a cell constant of 1.0 cm^{-1}. Figure 9 shows three repeated sets of calibration data. The nominal sensitivity is about 15 mmho/cm/V at a gain of 1. This sensitivity deteriorates slowly with time in submersion due to fouling of the platinum black coating. Typically, the sensitivity decreases 2 to 5% after 2 to 3 days of submersion in the calibration jars. To revive a desensitized probe, one may simply dip it in a 10% HCl solution for 2 to 3 minutes (a standard practice recommended by Beckman for their conductivity cells). One may also replatinized the probe, but that would change the sensitivity noticeably depending on the condition of the replatinized tip surfaces, which cannot be controlled accurately.

At a gain of 100 and with the low-pass filter set at 100 Hz, the rms noise level was measured to be about 26 mV. This noise level again decreased noticeably after the low-pass filter was set at or below 12.5 Hz. At a gain of 100, the dual-conductivity probe is capable of resolving minute conductivity changes of 1 µmho/cm. The actual resolution is about 2 µmho/cm at a gain of 100 and a 12-bit A/D conversion (10 V full scale).

4. SOFTWARE FOR DATA ACQUISITION AND ANALYSIS

4.1 Data Acquisition Software

The V-T-C HRC is an intelligent instrument that includes a GPIB interface for transfer of data to a host computer. We designed the software to maximize use of the interface so that all system parameters were under direct program control. Temperature and conductivity probe calibration coefficients are downloaded to the cluster prior to the experiment. The user, through the host

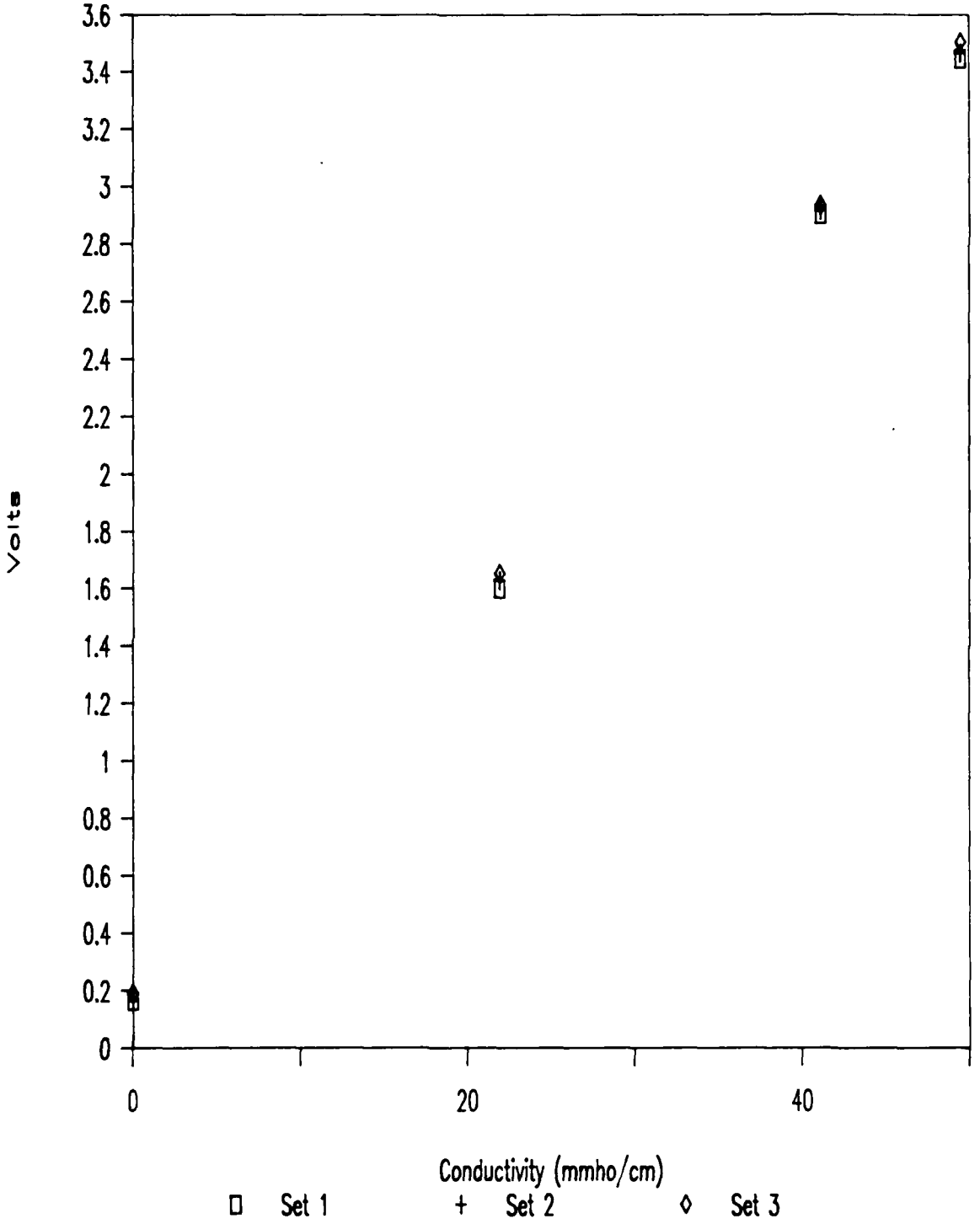

Figure 9. Calibration Data for Conductivity Probes

computer cluster communications program, may also specify a sampling rate from 3 to 25 Hz. When a trigger command is sent to the HRC, sampling of the three DLDV velocity channels and the high-resolution temperature and conductivity channels begins. After each sampling time, the values of the three velocity components, temperature and conductivity are transferred over the GPIB to the host computer for storage on a hard disk.

Several independent clusters may be connected in parallel on the GPIB bus, so that a single host computer may simultaneously accept data from all clusters. The computer software was designed to be very flexible in order to allow users to configure the system to their requirements.

The system is controlled by an 8088-based microprocessor on an STD bus card. An 8087 numeric data processor also resides on the card to carry out fast floating-point calibration operations. The operating instructions for the data acquisition software are given in Appendix A.

4.2 Data Analysis Software

The raw data files were too large to store on floppy disk, so a program called CULL was written to read them and do some primary processing. The raw data from different processors were stored in an interleaved fashion on a single file. The CULL program first separates the data according to cluster and then determines the time at which each data point was taken. Null data are eliminated, and Doppler frequencies are transformed into velocities.

A number of problems were encountered with spurious data points in the files resulting from inadequate filtering and discrimination by the processor. The CULL routine thus has a provision for a minimum acceptable velocity from each channel. In addition, a persistence check is made. Sequential data points are assumed to be invalid if they are outside a fixed range about the last valid data point. This persistence was generally set at 2 to 3 times the variance of the velocity. As time went on (during AIWEX 85) and the processors were better adjusted and the proper filterbands disabled, the problem with spurious data points abated.

The files created by CULL were on the order of 300 kilobytes long so that they could be stored on floppy disk. These files were also short enough that it was possible to read through them using a text editor to check for spurious data, data rate and overall system behavior. Some of the files were too long to be edited and were lost when this was attempted.

The CULL routine counts the number of valid data points on each channel and writes this information at the top of the output file. In addition, it was necessary to reinput the temperature/conductivity probe parameters because the binary files were written with tabs, which are not readable in Fortran. CULL requires approximately one hour of processing time on an average-sized file.

Two programs were written to provide initial analysis of the data. These provide Reynolds stress, turbulent fluxes of heat and salinity, variances of velocity, temperature and conductivity and the one-dimensional wavenumber spectra of velocity fluctuations.

The first program is called TURB. This program separates the velocity into a mean and a fluctuating part,

$$u_i = U_i + u_i', \tag{4}$$

and then calculates the variance-covariance tensor of the three-component fluctuating velocity field,

$$\sigma = \begin{bmatrix} \sigma_{11} & \sigma_{12} & \sigma_{13} \\ \sigma_{21} & \sigma_{22} & \sigma_{23} \\ \sigma_{31} & \sigma_{32} & \sigma_{33} \end{bmatrix} \tag{5}$$

where

$$\sigma_{ij} = \overline{u_i' u_j'} \quad . \tag{6}$$

The overbar indicates averaging over the observed values of velocity. The diagonal elements of the tensor are the variances of the three observed velocity components, while the off-diagonal terms are covariances. The covariance terms describe the shear stress in the flow. These must be rotated into a reference frame with one axis vertical, one in the horizontal plane aligned with the mean flow and the last orthogonal to these two. This is accomplished with two rotation matrices. The first provides a reference frame rotation of 45° in a counterclockwise direction about the horizontal axis of the cluster so that the U3 coordinate axis is vertical and pointing down. This rotation matrix is

$$R_1 = \begin{bmatrix} 1 & 0 & 0 \\ 0 & \cos \pi/4 & -\sin \pi/4 \\ 0 & \sin \pi/4 & \cos \pi/4 \end{bmatrix} . \tag{7}$$

The next rotation is about the vertical axis to provide a reference frame aligned with the mean flow direction in the horizontal plane:

$$R_2 = \begin{bmatrix} \cos\gamma & -\sin\gamma & 0 \\ \sin\gamma & \cos\gamma & 0 \\ 0 & 0 & 1 \end{bmatrix} . \tag{8}$$

The complete rotation of the variance-covariance tensor is accomplished by

$$\sigma' = (R_2 R_1)^T \sigma R_1 R_2 . \tag{9}$$

This tensor gives the Reynolds stress for vertical momentum flux or, equivalently, the friction velocity:

$$u_* = \sqrt{\sigma'_{13}} . \tag{10}$$

The same program obtains the turbulent flux vectors of heat and salinity,

$$H_f = \overline{H'u'} \tag{11}$$

and

$$S_f = \overline{S'u'} \tag{12}$$

The fluctuating component of sensible heat is obtained from the temperature fluctuations

$$H' = c_p T' \tag{13}$$

where c_p is the heat capacity of water. The fluctuating part of salinity was obtained by numerically differentiating the relationship given in "1978 Practical Salinity Scale Equations," IEEE Journal of Ocean Engineering, Vol. OE-5, No. 1, January, 1980. This algorithm was used to provide values of dS/dC at constant temperature, pressure and absolute conductivity, resulting in

$$S' = C' \left.\frac{dS}{dC}\right|_{C,T,P} . \tag{14}$$

H_f and S_f are vectors along the axes of the DLDV cluster reference frame. Rotation of these vectors to obtain vertical fluxes is accomplished with the same matrices used to rotate the variance-covariance tensor,

$$x' = R_2 R_1 x \tag{15}$$

The variance of the three components of motion as well as temperature and conductivity is also obtained. This program requires over 300 kilobytes of random access memory to accommodate the large data arrays. Processing time is about 10 minutes per cluster.

A program was also written to determine the wavenumber spectrum of each velocity component as well as temperature or conductivity. The time series of a given record is transformed into the spatial dimension by multiplying by the mean flow velocity. It is thus assumed that the turbulence is horizontally isotropic and that the statistics are stationary over the period of the record. This is known as the Taylor frozen turbulence hypothesis. Laser Doppler velocimeter data are characterized by time series of velocities obtained at random time intervals. This makes the spectral analysis using the standard FFT approach impossible because the FFT algorithm requires that the time series to be transformed must be obtained at regular intervals. An alternative technique was, therefore, used for the DLDV data. The spectrum is calculated using the Wiener-Khinchine theorem, which states that the spectral density is given by the Fourier transform of the autocovariance function. The autocovariance function is obtained from

$$R_{ij} = \overline{u(x_i)\ u(x_i+r)} \tag{16}$$

with

$$x_j \leq x_i + r < x_{j+1}$$

where r is the wavenumber offset analogous to a time lag in frequency space. This function can be estimated for time series that are spaced at random time intervals by dividing the time lag domain into discrete slots. The estimator is

$$R_r = \sum_{k=1}^{N} X_k X_{k+r} / H(r) \tag{17}$$

where H(r) is the number of lagged products obtained when the time lag lies within the time slot, r. The time slot for a given product is defined by

$$\left| \frac{t_{k+r} - t_k}{\Delta t} - r \right| \leq 0.5 \quad . \tag{18}$$

The averaging is done numerically using the slotted correlogram technique described by Bell (1983). Bell compared this technique with other approaches to spectral analysis of laser velocimetry and found it to be the best compromise between accuracy and efficiency. The spectrum is then calculated using the FFT. Spectral densities are normalized by the variance of the motion to allow direct intercomparison and averaging of spectra. Errors in the spectrum are related to the number of cross products, H, utilized in the average value at each offset value. The signal-to-noise ratio of the spectral density at wavenumber k is

$$SNR = \sqrt{12H/rk} \quad .$$

The program used to do this is called SPFAST. It requires a RAM of over 300 kilobytes and takes about an hour to provide one spectrum.

5. FIELD MEASUREMENTS AND RESULTS

To demonstrate the field deployability of the DLDVs, we built two experimental units and conducted a series of tests during MIZEX 84. Documentation of the MIZEX 84 tests is given in Section 5.1. From the results of MIZEX 84, which were very encouraging, we optimized the design of the DLDV modules and fabricated nine sets of prototype DLDV modules for use in three 3-axis high-resolution clusters. In addition to the three DLDVs, each cluster included a high-frequency thermistor and a conductivity probe. Each HRC was controlled by a processor that provided power to drive the sensors, preprocess the raw data and interface the sensor output to the host computer. The three HRCs were then deployed during AIWEX 85. Documentation of AIWEX 85 tests is given in Section 5.2.

5.1 MIZEX 84

Two field-deployable DLDVs were assembled and field tested during MIZEX 84. The objectives of our participation were twofold: (1) to determine the feasibility of the DLDV for use in the Arctic environment, which is the most severe test to the field deployability of this optical sensor, and (2) to gather design information for the prototype HRCs using the DLDVs as the primary velocity sensors, provided the feasibility was successfully demonstrated.

5.1.1 MIZEX 84 Site and Setup

The MIZEX field site was located well within the marginal ice zone at about 80° north latitude and 0° west longitude in the Fram Straits of the Greenland Sea. Living quarters and workshops were provided on-board the M/V Polar Queen. The DLDV tests were carried out on a 2- to 3-m-thick floe at a distance of about 250 m from the ship. The moderate-resolution turbulence measurement experiment carried out by Miles McPhee was set up at the same location.

A 1.2-m square hole was prepared in the ice for the DLDV frame. The ice at this point was 2.4 m thick. The electronic equipment was set up in a heated tent nearby. Two DLDV systems were deployed during the test. Power was provided by a 600-W gasoline-powered generator. The DLDV systems required two DC power supplies. Outputs from the photodetectors were filtered through two Krohn-Hite variable band-pass filters. The filtered Doppler signals were processed into analog signals proportional to the current by two systems, a Macrodyne Model 2096 Laser Doppler Signal Processor and a Thermal Systems Inc. (TSI) Model 1090 Laser Doppler Frequency Tracker, that used different processing schemes. The analog signal was sampled at a rate of 48 Hz and converted into a digital signal by a modified Sea-Bird Electronics Deck Unit. The digital data were recorded onto 3.5-inch floppy disks using a Hewlett-Packard 9816 microcomputer. Doppler signals were observed directly using a dual-channel, Tektronics storage scope.

The DLDV laser units were aligned at 0°C in a shack built on the ice. This is necessary to avoid thermal strains in the optics, which result in the beams no longer crossing and the Doppler signal being lost when the system is lowered into cold water. Only one of the systems was found to drift out of alignment when cooled from 25 to 0°C. This system also went out of alignment when brought to room temperature and returned to 0°C.

The laser units and photodetectors were then mounted on a rigid tubular frame and suspended just beneath the water surface for alignment with each other. Underwater alignment was necessary because the front surface of the focusing lens on the laser unit is nonplanar. Since the curvature of this lens was unknown, the relationship between the beam crossing angle in air and underwater was unknown. The beam crossing angle is used to determine the Doppler fringe spacing and, hence, the relationship between Doppler frequency and measured current speed. The beam crossing angles were observed to be the same as measured in the laboratory. The use of a lens with a planar front surface is recommended in the future because this allows the fringe spacing to be calculated from measurements in air and simplifies the locating of the crossing point (Doppler fringe volume) underwater.

A fiber optics rod 3 mm in diameter is used to transmit light from the measurement point to a photodetector diode. This rod must be located so that it transmits the light that is forward scattered by particles passing through the sampling volume. The alignment must be carried out in water at 0°C. This was done by suspending the DLDV frame just underneath the water in the hydro-hole. The experiment was carried out during the height of the Arctic summer, so it was not possible to observe the laser beams outdoors. A shack was therefore constructed over the hydro-hole to allow positioning of the photodetector fiber optic rod. The end of the rod was located 6 cm from the crossing point and centered between the two crossed laser beams. The laser units and photodetectors were mounted on adjustable mounts that allowed for a straight-forward alignment. Once the photodetector appeared to be properly aligned, a check was made to see if a Doppler signal could be obtained. This was done by stirring the water in the hole while observing the photodetector output on a storage oscilloscope. Better alignment could be made in a tank of ice water, so that the Doppler signal could be observed while the alignment was carried out. In the field, this would require a sizeable instrument shack capable of being darkened to allow observation of the laser light and having enough space for all the electronics. During the Arctic winter, an enclosed, heated space will be required for field alignment.

Once good Doppler signals were obtained from both DLDV systems, the systems were lowered beneath the ice. The ice thickness in the hole was 2.4 m, and the array was lowered 2 m below the bottom surface of the ice. This is a standard depth for under-ice measurements of current, and is generally well within the

boundary layer. One of the systems was oriented to observe the horizontal flow, while the other was oriented to observe the component of flow at 45° from the vertical. A tell-tale was used to orient the frame into the mean flow so that any turbulent fluctuations would be superimposed onto the mean. This is done to resolve the directional ambiguity in the observed current. The calibration constants and orientations of the two DLDVs are given in Table 2.

Table 2. Calibration Constants and Orientations of DLDVs

Laser	Orientation	Wavelength	Fringe Spacing
Hitachi	45°	793 nm	4.89 m
LDL	Horizontal	831 nm	4.58 m

The output power from a laser diode increases as the operating temperature is reduced. If the output power exceeds a critical level, the laser will be damaged. The Hitachi laser diode is equipped with a photodiode monitor that was used in a feedback loop to maintain constant laser power output regardless of temperature. The laser unit containing the Hitachi laser was aligned at room temperature and was found to maintain its alignment after transport to the field site and at freezing temperatures. No field adjustments were necessary to obtain a good Doppler signal from this unit. The LDL laser diode has no monitoring provision. The forward current on this laser diode was thus set at a constant value to give a power output of 5 mW at 0°C. The laser unit containing the LDL laser diode was found to be out of alignment after transportation to the field. This unit was found to be more sensitive to thermal strains so that it was not possible to align the unit at room temperature. Alignment was therefore carried out in the field shack at temperatures near freezing. Once this unit was aligned, a good Doppler signal was obtained. The strength of the signal obtained from the LDL system was never as good as that obtained from the Hitachi unit, and over a period of a week the Doppler signal from the LDL deteriorated significantly. This deterioration was apparently caused by a gradual creep in the glue joint of a broken glass plate holding the beam splitter cubes.

A total of 280 minutes of high-resolution turbulent flow data was recorded onto floppy disks. Of this total, 42 minutes were taken at times when the data rate was high enough to obtain both the horizontal and 45° components of the flow simultaneously. The DLDV units with the LDL and Hitachi diode lasers were used for the horizontal and 45° configurations, respectively. Up to two channels of DLDV data were recorded simultaneously. The Macrodyne counter was always used with channel 0, whereas the TSI tracker was always used with channel 1. In all of these records, a simultaneous recording was made of the output from Miles McPhee's MRC. This array was mounted 50 cm above the DLDV measurement volume. The magnitude and orientation of the mean horizontal flow was thus always measured. Data from the two types of current meters were used for comparison to assess their performance and the importance of turbulent motions on spatial scales of less than 2 cm.

For the most part, data collection was limited to one channel. Since the mean horizontal flow is required to resolve the vertical component of the 45° flow, it was usually not possible to obtain directly the vertical flow component. Back-to-back records of horizontal and 45° flows were taken to obtain a reasonable estimate of the mean horizontal flow for use in resolving the 45° component.

5.1.2 Results and Discussion

During MIZEX 84, a total of 18 DLDV data records was obtained at a depth of 2.5 m below the bottom of the ice floe and stored on floppy disks. Each record contains 14 minutes of data on two channels. Channel 0 is data output from the Macrodyne counter, and channel 1 is data from the TSI tracker. Data were sampled by the computer at a rate of 48 Hz for a total of 40,320 data points per channel. Much of the data is redundant because the Doppler burst rate was less than 48 Hz. A look at the raw data shows that alternate data points are slightly offset in time. This was apparently caused by our attempt to double the sampling rate available on the Sea-Bird A/D converter. To simplify processing and reduce the data files to a manageable size, only alternate data points were used in the analysis. The effective sampling rate for data analysis is thus 24 Hz. A number of runs were made simultaneously with ducted propeller meters on an MRC placed 50 cm above the DLDV cluster. Table 3 is a summary of the DLDV and MRC records.

Table 3. Summary of DLDV and MRC Records
(from McPhee, 1985b)

			Macrodyne (Channel 0)		TSI (Channel 1)	
Run	Date	Time	Sensor	Orientation	Sensor	Orientation
197.F	7/15	15:26	LDL	Hor.	---	---
197.F	7/15	15:46	Hitachi	45°	---	---
197.F	7/15	16:414	LDL	Hor.	Hitachi	45°
198.A	7/16	20:10	Hitachi	45°	---	---
198.B	7/16	20:34	LDL	Hor.	---	---
198.C	7/16	22:23	Hitachi	45°	---	---
198.D	7/16	22:45	LDL	Hor.	---	---
199.A	7/17	11:46	LDL	Hor.	---	---
199.B	7/17	12:07	Hitachi	45°	---	---
199.C	7/17	15:37	Hitachi	45°	Hitachi	45°
199.D	7/17	16:00	LDL	Hor.	Hitachi	45°
199.E	7/17	17:12	LDL	Hor.	Hitachi	45°
199.F	7/17	17:33	Hitachi	45°	Hitachi	45°
199.G	7/17	20:53	Hitachi	45°	Hitachi	45°
199.H	7/17	21:14	LDL	Hor.	Hitachi	45°

Doppler Burst Rate and Data Rate

Traces of the Doppler burst signals recorded on a storage scope, under a variety of conditions, were examined to understand the performance of the DLDVs in the Arctic environment. Doppler bursts from the photodetectors were band-pass filtered to remove the pedestal and high-frequency noise. For an optimally aligned DLDV, the typical signal-to-noise ratios (SNRs) are better than 20:1 after band-pass filtering. At times, we observed the presence of an intermittent 2 MHz noise thought to be associated with radio transmissions. The 0.5 MHz low-pass filter available on the Macrodyne counter reduced but did not eliminate the noise. For a misaligned DLDV with a poor SNR, this noise may overwhelm the Doppler signal. As a result, this noise never caused problems for the DLDV unit with the Hitachi laser diode but affected the signals measured by the DLDV unit with the LDL laser diode when the alignment deteriorated.

From the outputs of the Macrodyne counter and the TSI tracker, we estimated the Doppler burst rate. The most direct measure was made by recording the photodetector output signal using line triggering on the storage oscilloscope. The sweep rate was set at 2 ms/div, and a total of 3 seconds of signal was examined. Each sweep contained 20 ms of randomly sampled record. Doppler bursts are easily identified at this sweep rate. In 3 seconds, 26 bursts were identified for a burst rate of about 9 per second. Immediately afterwards, both the Macrodyne counter and the TSI frequency tracker were attached to the photodetector output, and 5 seconds of output was recorded. The threshold level of the Macrodyne counter and the gain on the TSI tracker were adjusted so that both systems responded to the same signal. This ensures that noise signals are not being interpreted as Doppler bursts. The data rate taken from this test was about 5 samples per second. The Macrodyne system was observed to not trigger on Doppler bursts that were identifiable as such but were too low in magnitude or had too few fringes. The data rate is thus substantially lower than the Doppler burst rate. The mean current during this test was about 7 cm/s, which gives a spatial resolution of 1.4 cm.

A 50-second record of Doppler period was analyzed. The data rate varies from 3 to 4 per second. The actual data rate is somewhat higher since the oscilloscope resolution is not fine enough to detect small changes in the output. The DLDV is oriented to measure the component of flow 45° from the vertical in the direction of the mean flow. The current during this time varied from 4 to 9 cm/s, with a mean of about 6 cm/s; the spatial resolution is thus about 1.7 cm.

It was not possible to get consistent tracking of the Doppler signal with the TSI processor at these low data rates. In two of the records, the same DLDV Doppler signal was fed into both signal processing systems. The output was converted into physical units to give a direct comparison of the two processing techniques. The TSI output is offset by about 1.5 to 2.5 cm/s from the Macrodyne signal and exhibits smaller variance. In the field tests, it was possible to directly verify that the voltage output from the Macrodyne frequency counter was proportional to the Doppler frequency observed on an oscilloscope trace. We thus have confidence that the Macrodyne output accurately reflects the current velocity. It was not possible to verify the TSI frequency tracker output in the field due to signal drift and noise. While the frequency tracker output occasionally appears to follow the

frequency counter output, it generally does not. This record confirms the field observation that the Doppler burst rate was not high enough to allow continual, accurate frequency tracking. Much of the observed signal is a result of the tracker locking onto noise signals. The origin of the velocity offset in the frequency tracker signal is probably associated with selection of the center frequency during the initial manual location of the Doppler signal. When a signal is not found, the TSI tracker tends to drift towards this frequency. In this record, the center frequency appears to correspond to a velocity of about 12 cm/s.

The Doppler burst rate or data rate was obtained by counting the number of times the Macrodyne output changed each second. This rate is quite variable, as shown in Figure 10 for record 199F. The mean data rate for this record was 10 Hz with a range of 4 to 18 Hz. The mean current velocity during this time was 14.4 cm/s, which gives a mean spatial resolution of 1.3 cm. The spatial resolution varies due to the random distribution of Doppler bursts. Given a record of the data rate, it is possible to select periods during which the data rate is relatively high if an analysis is desired of velocities with a smaller spatial resolution.

The LDL laser diode unit was not as well aligned as the Hitachi unit. The mean data rates obtained from this unit are therefore considerably lower. The maximum data rate obtained from this unit is just as high as that obtained from the Hitachi. This is because the Doppler burst rate should be about the same for both units. The LDL rate is lower because the signal strength was lower and more easily obscured by noise. When the noise level decreased, the LDL unit gave a data rate just as high as the Hitachi.

Comparison of DLDV and MRC Results

An extensive comparison of the velocity data measured simultaneously with the two experimental DLDV units and one of the MRCs was presented by McPhee (1985b). A few examples are excerpted here from that report to demonstrate the performance of the DLDV in the Arctic environment. Attempts are also made to interpret and correlate the velocity data measured by the two systems.

Figure 11 shows a comparison of the 1-second averaged time series (lower), the spectra (upper) and the squared coherency (middle) of the horizontal velocity component. Note that the MRC time series is shifted downward 4 cm/s to facilitate comparison. The DLDV unit for measuring this component was

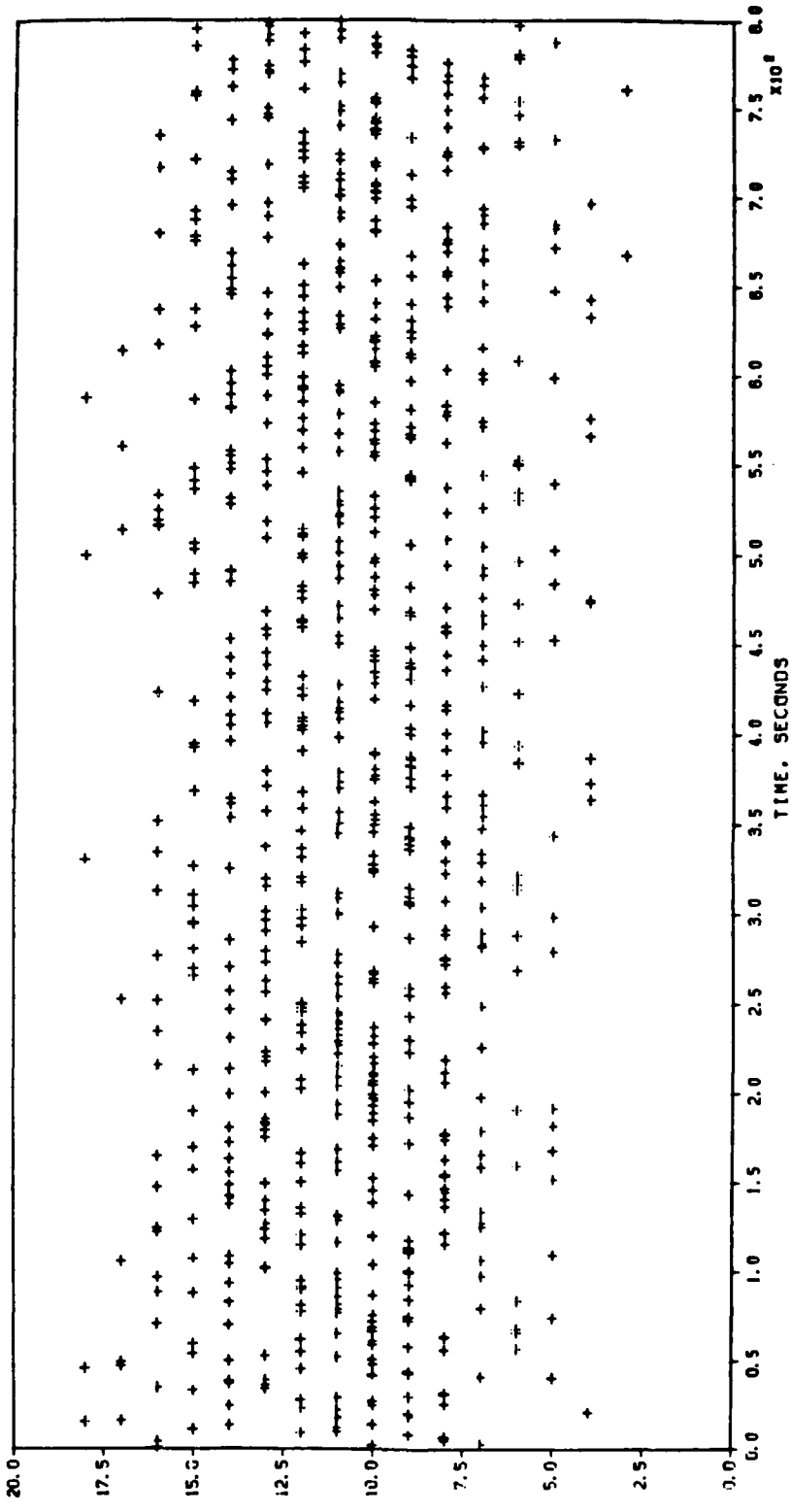

Figure 10. Data Rate at 1-second Intervals During Record 199F

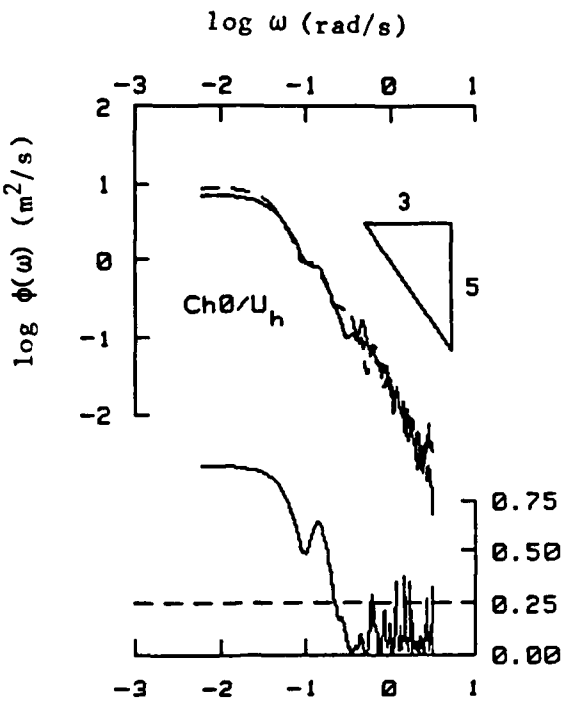

a. Autospectra of LDL-Ch0 (solid) and MRC UH (dashed) components for Run 197.E

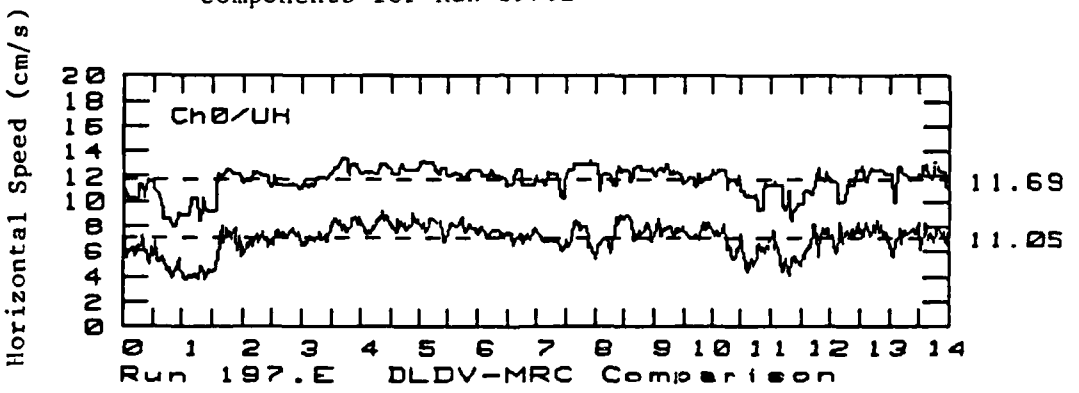

b. Comparison of 1-second-averaged time series; the MRC time series is displaced downward by 4 cm/s

Figure 11. Comparison of DLDV and MRC Measurements for the Horizontal Velocity Components (McPhee, 1985b)

equipped with the LDL diode laser, and the Macrodyne counter was used to process the Doppler signal. From the two time series, a high degree of similarity between the traces is noted, especially for the medium- to low-frequency components. As shown by McPhee (1985b), the horizontal velocity components of all the runs generally compare quite well. On the average, the mean and variance are about 2.4% higher and 5% lower for the DLDV data than for the MRC data (Tables 2 through 5, McPhee, 1985b). This is consistent with the fact that the MRC was 50 cm closer than the DLDV to the bottom of the ice floe within the oceanic boundary layer.

The time series of the DLDV data shows a "blocky" formation, which is caused by a slight misalignment of the two beams of the LDL unit as discussed in Section 5.1.1. The misalignment effectively reduces the data rate and, thus, the spatial resolution. As a result, the dynamic response of this DLDV unit is closer to that of the MRC. This is demonstrated by the reasonable match of the two spectra. Apparently, the "blocky" formation has little effect on the spectral density for the frequency range shown in the figure. At the high-frequency end, both velocity spectra tend to follow approximately an $f^{-5/3}$ power law.

Figure 12 shows the time series, spectra and squared coherency of the velocity component at 45° in the vertical plane of the horizontal component. For this configuration,the DLDV equipped with the Hitachi laser diode was used, and the output was fed to the Macrodyne counter (channel 0) and to the TSI tracker (channel 1). Here, we do not observe a "blocky" formation, as the DLDV with the Hitachi diode always stayed aligned during the experiment. In general, the time series from both channels 0 and 1 are highly similar; however, the magnitude of the velocity component measured with the TSI tracker is consistently about 20% lower than that measured with the Macrodyne counter. Part of the reason is the presence of a DC offset voltage that introduces a small error in the frequency-voltage conversion. It is inherent to the tracker that it would not work well for low burst rates, which is confirmed by the field results.

Let us now focus on the comparison of the results measured with the DLDV/Macrodyne (Channel 0) and the MRC. For the 45° configuration, the velocity component consists of both the vertical and horizontal components. Because the MRC was about 2 m and the DLDV 2.5 m below the bottom of the ice floe, the influence of the bottom topography would be more pronounced on the

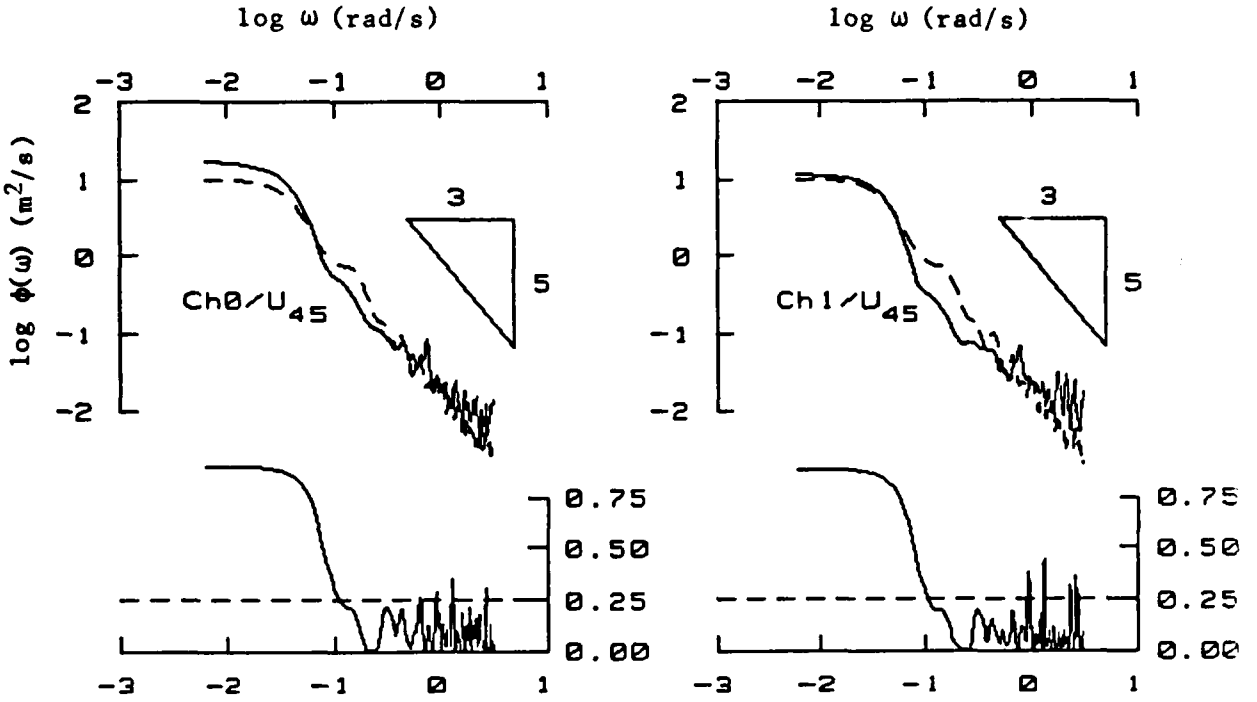

a. Macrodyne counter - Autospectra of Hitachi-Ch0 (solid) and MRC-U45 (dashed); lower trace is the square coherency.

b. TSI tracker - Autospectra of Hitachi-Ch1 (solid) and MRC-U45 (dashed); lower trace is the square coherency.

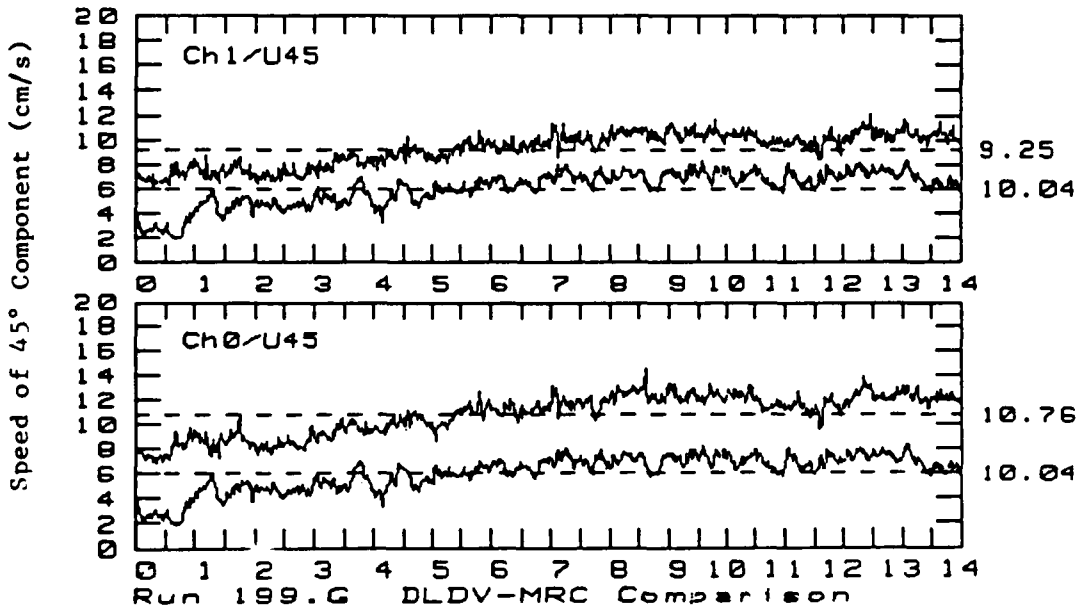

c. Comparison of 1-second-averaged time series.

Figure 12. Comparison of DLDV and MRC Measurements for the 45° Velocity Component (McPhee, 1985b)

vertical velocity component measured with the MRC than with the DLDV. This is reflected from the noticeably lower energy content in the medium- to low-frequency components measured with the DLDV than in those measured with the MRC, which is different from the comparison of the horizontal component (Figure 11). Comparison of the results of a similar configuration for other runs shows essentially the same trend (McPhee, 1985b). For all the runs with the DLDV set at the 45° configuration, the mean and variance are 10% higher and 8.4% lower for the DLDV data than for the MRC data, again consistent with the relative placement of the clusters in the boundary layer.

The above difference, resulting from the relative placement of the DLDV and MRC in the boundary layer, may also be identified from the spectra of the 45° velocity component. As shown in Figure 12, the spectrum estimated from the MRC data follows an approximate $f^{-5/3}$ power law, whereas that estimated from the DLDV data has a more gentle slope of about f^{-1}. A deficit in the spectral density at medium- to low-frequency components effectively reduces the slope of the spectrum estimated from the DLDV data. A similar trend is consistently observed for the velocity spectra for all the 45° configurations (McPhee, 1985b).

The method reported by Bell (1983), as described in Section 4.2, was then used to estimate the velocity spectrum of the DLDV data. In performing the spectral analysis of the DLDV data, only the data points that are updated (having values differ from those sampled at the previous time step) are used. Such a scheme results in a time series sampled at irregular time intervals that are multiples of the constant sampling time interval, which may lead to reduction in the spectral aliasing. As demonstrated by Masry et al. (1978), aliasing is avoided when the signal is sampled at random time intervals.

Figure 13 shows a spectrum estimated by the method of Bell (1983), with the cutoff (Nyquist) frequency extended to 12 Hz, corresponding to the time series of channel 0, record 199G. As can be seen in the figure, the spectrum displays an f^{-1} power law extending more than one decade from about 0.03 to 1 Hz. Beyond 1 Hz, the slope of the spectrum reduces to about $f^{-2/3}$. The method of Bell (1983) apparently reduces but does not remove entirely the aliasing, as the time series was sampled at irregular but not random time intervals. As a result, a slight flattening of the slope remains at the high-frequency end. Comparison of the spectra of the DLDV data shown in

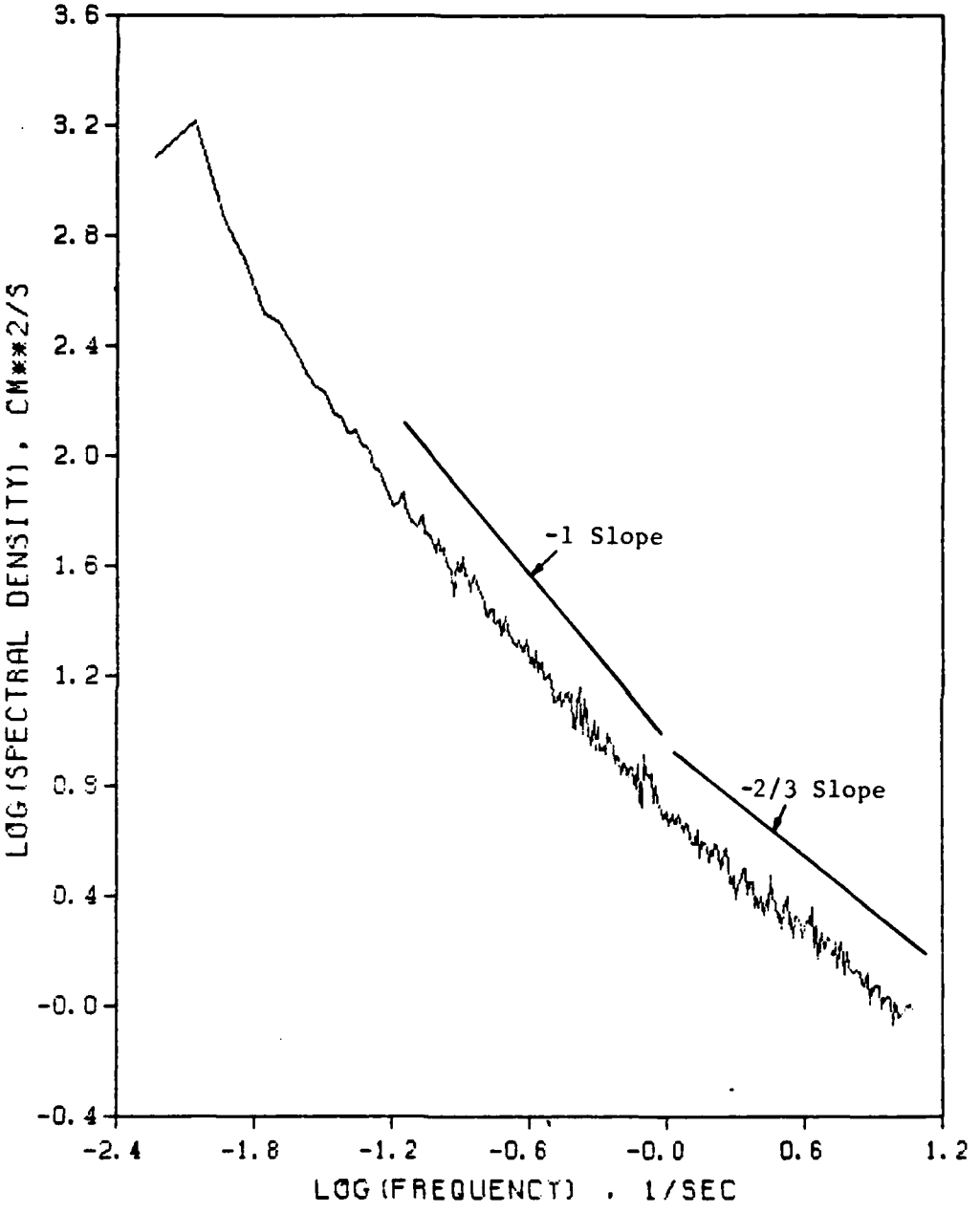

Figure 13. Velocity Spectra Estimated from the DLDV Data, Run 199G-ChO, Using the Method of Bell (1983)

Figures 12 and 13 shows that both display an f^{-1} regime at the high-frequency end. Additional work is required to resolve the question of the most appropriate prefiltering required to obtain representative spectra from the DLDV signal.

5.1.3 DLDV Performance in MIZ Environment

Two experimental DLDV systems were successfully deployed during MIZEX 84. Both systems were operative throughout the three-week deployment; the one equipped with the Hitachi laser diode outperformed the one equipped with the LDL laser diode. A total of several hours of high-resolution turbulent flow data was recorded under an ice floe. The DLDVs were calibrated against a set of ducted current meters placed in close proximity, and good agreement of the results was observed (see Section 5.1.2). Our assessment of the performance of the DLDV in the MIZ environment is given in this subsection.

The observed data rates were compatible with those observed in the open ocean with low particle densities [I]. However, the mean current in the MIZ oceanic boundary layer under an ice floe was usually below 10 cm/s. On the average, for a sampling rate of 48 Hz, a spatial resolution of between 1 to 2 cm for the DLDV data was obtained during these tests, representing an improvement in resolution of at least one order of magnitude over mechanical turbulence measurement techniques.

The feasibility of the development of a portable DLDV for deployment in the Arctic environment was successfully demonstrated during MIZEX 84. Our experience suggested several ways to improve the performance characteristics of the DLDV for applications in the Arctic environment, as listed below. A few of these improvements were incorporated into the design of the prototype units subsequently deployed during AIWEX 85.

(1) The laser power increases with decreasing temperature. It is essential to use a laser diode equipped with a photodiode monitor to maintain constant laser power regardless of temperature (e.g., Hitachi HL7801 series).

(2) Power levels used during these tests were conservative to minimize the chances of damage to the lasers. A laser power of 5 mW appears to be adequate, but higher power would enhance the scattered light intensity

and thus increase the burst rate or allow a larger separation between the tip of the fiberglass rod and the focal volume to minimize flow disturbance.

(3) The optical components should be treated with anti-reflective coatings to increase laser light transmission through the transmission optics and to reduce light reflection from optical surfaces. It is preferable to use a single-element beam splitter to maintain alignment of the optics induced by large temperature variations.

(4) The processors were designed for a relatively high burst rate and high-speed flows. Due to the low burst rate, it is necessary to use a counter rather than a frequency tracker for processing the Doppler signals. Improved filtering and Doppler burst discrimination could increase the data rate and, hence, improve the spatial resolution of the instrument by a factor of 2 or better.

5.2 AIWEX 85

Three prototype HRCs, each consisting of a three-axis DLDV system and a high-frequency temperature/conductivity probe pair, were deployed during AIWEX 85. The objectives were to test the system under field conditions and assess the system's reliability, robustness and performance in the Arctic and to measure the high-frequency turbulent fluxes of momentum, heat and salinity in the oceanic boundary layer under ice.

5.2.1 AIWEX 85 Site and Setup

Observations of the turbulent boundary layer beneath sea ice were made with the DLDV system during AIWEX 85, which was carried out during March and April at a camp in the Beaufort Sea approximately 200 miles northwest of Prudhoe Bay, Alaska. The DLDV clusters were deployed through first-year sea ice with a thickness of 165 cm. The deployment site was well over 100 m from any pressure ridge that could perturb the boundary layer structure. The DLDV deployment occurred during the period from March 26 to April 25. Air temperature during this time ranged from -30 to -17°C, while wind speeds were less than 5 m/s. The boundary layer under these conditions is well-mixed with a

layer of essentially constant-salinity, constant-temperature sea water in equilibrium, with the sea ice extending down to a depth of 20 to 30 meters.

The DLDV clusters were mounted on a rigid frame and lowered through a 100-cm-diameter hole drilled through the ice. The orientation of the frame was observed relative to local magnetic north.

Each DLDV cluster consists of three DLDV transmitter/receiver pairs. These are oriented to observe three orthogonal components of the flow field and thus obtain a complete description of the turbulence statistics. In addition, each three-axis cluster has a high-resolution temperature and conductivity probe mounted within 2 cm of the DLDV observation volume. Two clusters were deployed, one at 2 and one at 4 m beneath the lower surface of the ice.*

Each cluster included a temperature/conductivity probe pair. These probes were calibrated at the beginning and end of the experiment. Calibration of the conductivity probe was accomplished with a Beckman conductivity measurement cell. The conductivity of a sample of snowmelt and sea water measured on the Beckman instrument was used to calibrate the conductivity probe. The temperature calibration was carried out in two buckets of snow slush formed with fresh water and with sea water. The temperature of these baths was observed with a thermometer accurate to within 0.01°C. Calibration was done at a gain of 1, and the measurements were made at a gain of 100 (with the DC voltage offset). Note that the temperature/conductivity probes were designed to measure differentials, hence the fluxes but not the absolute values of sea water temperature and conductivity, and calibration was not conducted in a well-controlled environment in the field. Therefore, the absolute temperature and conductivity cannot be determined accurately. We may, however, infer the absolute temperature from the Sea-Bird temperature gauge deployed adjacent to the DLDV-T-C clusters. Since both the voltage outputs of the gauges are linearly proportional to the temperature and conductivity of the sea water within the measurement range of interest, the relative change of these physical quantities may be accurately measured at higher gains (with the sensitivity of the gauges determined at the gain of 1). At a gain of 100 and a 12-bit resolution (10 V full scale), the gain may resolve minute changes of 0.002°C and 2 μmho/cm.

---

*One of the processors was damaged due to a power surge at camp.

The mean flow direction beneath the ice was observed using a drifter such as a piece of gum or Tye-wrap. The two clusters were then oriented so that the cluster faced into the current at an angle of 30 to 45° to the left of the current. Both clusters were oriented in the same direction. An observation was then made of mean current, temperature and conductivity for a period of 60 seconds. The mean values of temperature and conductivity voltages were input as offset voltages. The variations from these reference values were then multiplied by a gain factor of 100 for output to the data file. The mean update was also used to orient the clusters, so that the velocity and the number of data points obtained from each cluster were similar, and to estimate the data rate to be expected.

The DLDV clusters were checked for alignment in air before deployment. Any variations from alignment were corrected, and the system was deployed just beneath the surface of the water. A squeeze bottle was then used to remove any air bubbles collecting around the lenses and receiver collimation tubes. The system was then checked for Doppler signals using an oscilloscope. Preliminary tests indicated that it was necessary to readjust the gain settings on each filter band of the system to match the processor amplifier to each DLDV pair. It was necessary to disable the two highest band-pass filters on the processor units to remove a high-amplitude radio signal from a radio beacon used in the camp. The lowest filter band was also disabled, as the processor was unable to filter out noise signals at frequencies in the range from 256 to 1000 Hz. Note that disabling the lowest frequency band increases the threshold speed to about 0.34 cm/s based on the calibration of 2960 Hz/(cm/s).

The sea water encountered was very clear; objects were visible to depths of 20 meters. This was reflected in a fairly low Doppler burst rate. While it was not possible to count directly the Doppler burst rate, it appeared to be in the range of 2 to 5 Hz. This is very similar to burst rates observed during MIZEX in the Greenland Sea in July of 1984. Observations were made at a variety of burst rates ranging from 2 Hz to 25 Hz. The spectra of turbulent motions observed by sampling at these two rates overlap, so the sampling rate was alternated from one sample to the next. First, a sample would be taken at 25 Hz for a period of 300 seconds, then a sample at 2 Hz for 3000 seconds. In this way the entire spectrum of turbulent motions was observed.

Data files were stored in 300-kilobyte files on a RAM disk. These files were transferred into 1 megabyte files on the COMPAQ plus computer hard disk memory using the MS-DOS pipeline utility. This process takes about 30 minutes for a typical file. Primary processing of the raw data was then performed using a program called CULL (See Section 4.2), and the results were stored on floppy disk.

5.2.2 Results and Discussion

A total of 28 records of velocity, temperature and conductivity was obtained at depths of 2 and 4 m beneath the bottom of the ice. The first 15 records were processed using faulty assumptions about the way in which the binary data file was stored and are thus of only minimal value. In addition, the filters on the processing system were not properly disabled until record 17. Table 4 lists the last ten records, 19 through 28, along with the sample rate, data rate and mean velocity. The AIWEX 85 data have been partially analyzed. Some of the results are presented and discussed in this subsection.

Table 4. *AIWEX 85 Data Summary*

Record	Date	Depth (m)	Rate (Hz)	Period (s)	Data Rates: U1, U2, U3 (Hz)			Speed (cm/s)	Heading (degrees)
19	4/17	2	5	1200	2.1	0.04	0.08	11.5	162
		4			0.4	0.4	0.7	12.0	175
20	4/17	2	2	3000	0.8	0.6	0.3	8.5	177
		4			0.6	0.8	0.9	9.5	185
21	4/18	2	25	240	3.7	1.5	0.6	9.0	200
		4			4.3	3.0	3.9	9.8	211
22	4/18	2	2	3000	1.3	0.4	0.4	7.5	195
		4			0.7	0.4	1.0	8.7	205
23	4/18	2	25	240	3.5	0.03	0.2	8.7	190
		4			1.5	0.4	1.5	9.8	205
24	4/20	2	25	300	4.4	2.1	0.6	11.0	56
		4			5.9	1.9	4.9	12.3	68
25	4/21	2	25	300	2.8	1.7	1.8	4.6	3
		4			4.3	1.9	2.9	4.7	31
26	4/21	2	2	3000	1.1	0.6	0.3	5.3	12
		4			0.8	0.9	1.2	5.8	36
27	4/23	2	25	300	1.9	3.3	1.7	8.1	149
		4			3.6	1.4	5.2	8.4	157
28	4/23	2	2	3000	1.1	1.1	0.5	9.1	162
		4			0.4	0.7	1.4	9.8	169

Time Series

The record length of the DLDV runs ranged from 240 to 3000 seconds. In only one of the observations in the boundary layer did the variation in temperature and conductivity exceed 0.01°C and 10 μmho/cm, indicating a well-mixed boundary layer for a time scale of up to one hour during AIWEX 85 (March and April 1985). Measurements by other AIWEX participants (McPhee, private communication) show essentially constant values of these quantities over periods comparable to that of the DLDV runs. However, they show noticeable long-term variations in these quantities. Figures 14 through 16 show the typical time series of temperature and conductivity variations and the U1 velocity component at the 2-m depth. The temperature time series is practically uneventful, whereas the conductivity time series shows only high-frequency fluctuations. Only the U1 velocity component shows noticeable temporal variations in both high- and low-frequency ranges.

Figures 17 through 19 are another set of time series of the same quantities. Figure 18 shows that the temperature time series at the 4-m depth displays a wave-like feature with a period of about 10 minutes and a wave height of 0.03°C. This sharp-crested wave-like feature of low amplitude is the only one observed among all the time series. A corresponding feature is not observed in the conductivity and velocity time series from the same run. Again, only high-frequency fluctuations are observed in the conductivity time series, whereas the velocity components show a relatively wide range of temporal variation.

Mean Current Speed and Heading

The mean current speed for the 10 records listed in Table 4 ranges from about 4 to 12 cm/s. The mean current speed at the 4-m depth is consistently higher than that at the 2-m depth, indicating that the DLDVs are within the boundary layer in which a vertical shear is present. For all ten records, the mean current shear, defined as $(U_{z=4m} - U_{z=2m})/U_{z=4m}$ in a dimensionless form where $U_{z=2m}$ and $U_{z=4m}$ are the mean current speeds at the 2- and 4-m depths, is 0.07. In addition, the mean headings of the current at the two depths also differ by about 14° with the current vector rotating in the clockwise direction as the depth increases. This turning of the current vector corresponds to the spiral structure in the Ekman layer (Ekman, 1905). The effect of the Ekman spiral was also observed by Hunkins (1975) during the

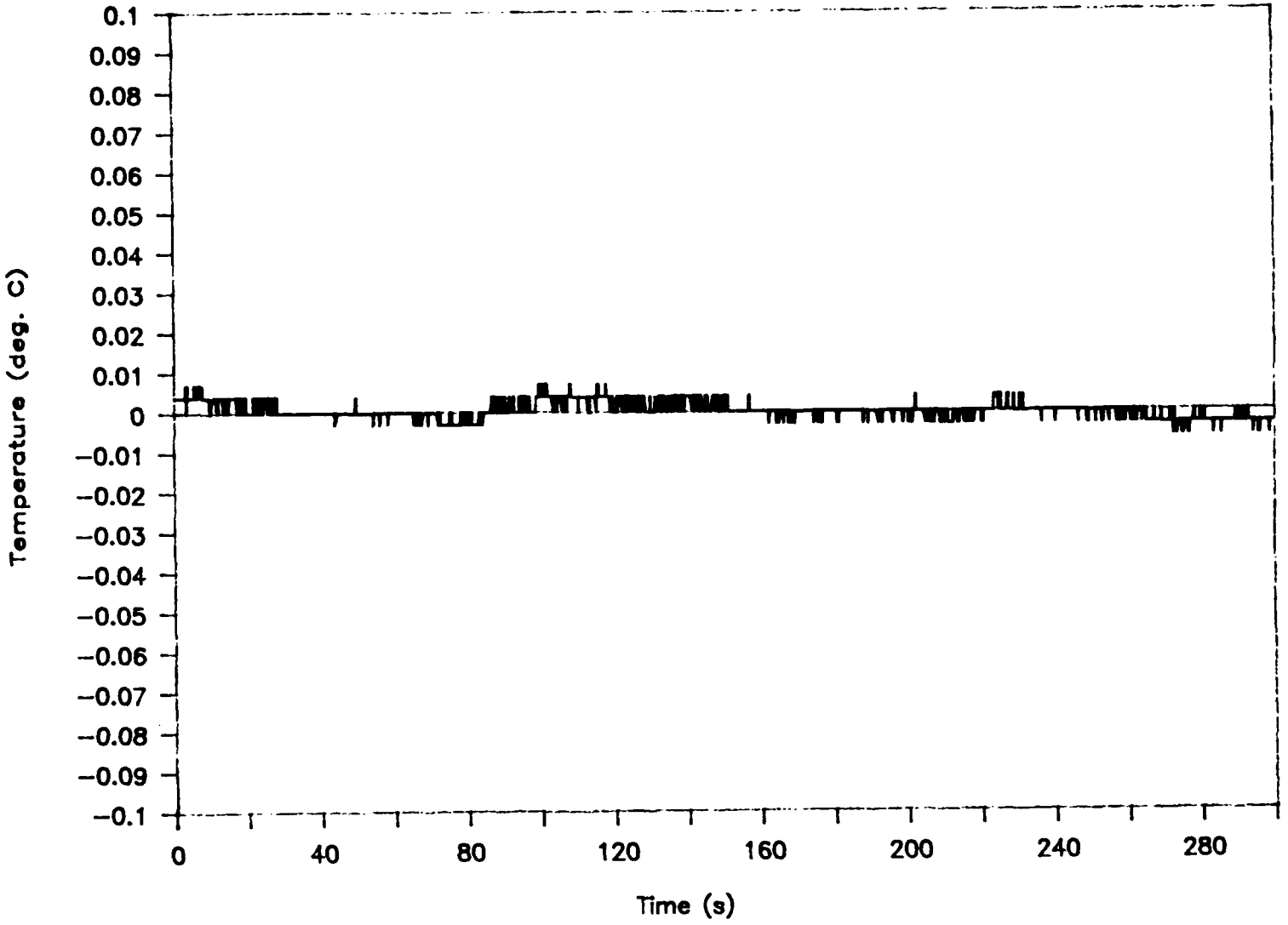

Figure 14. Temperature Variations Measured at 2-meter Depth

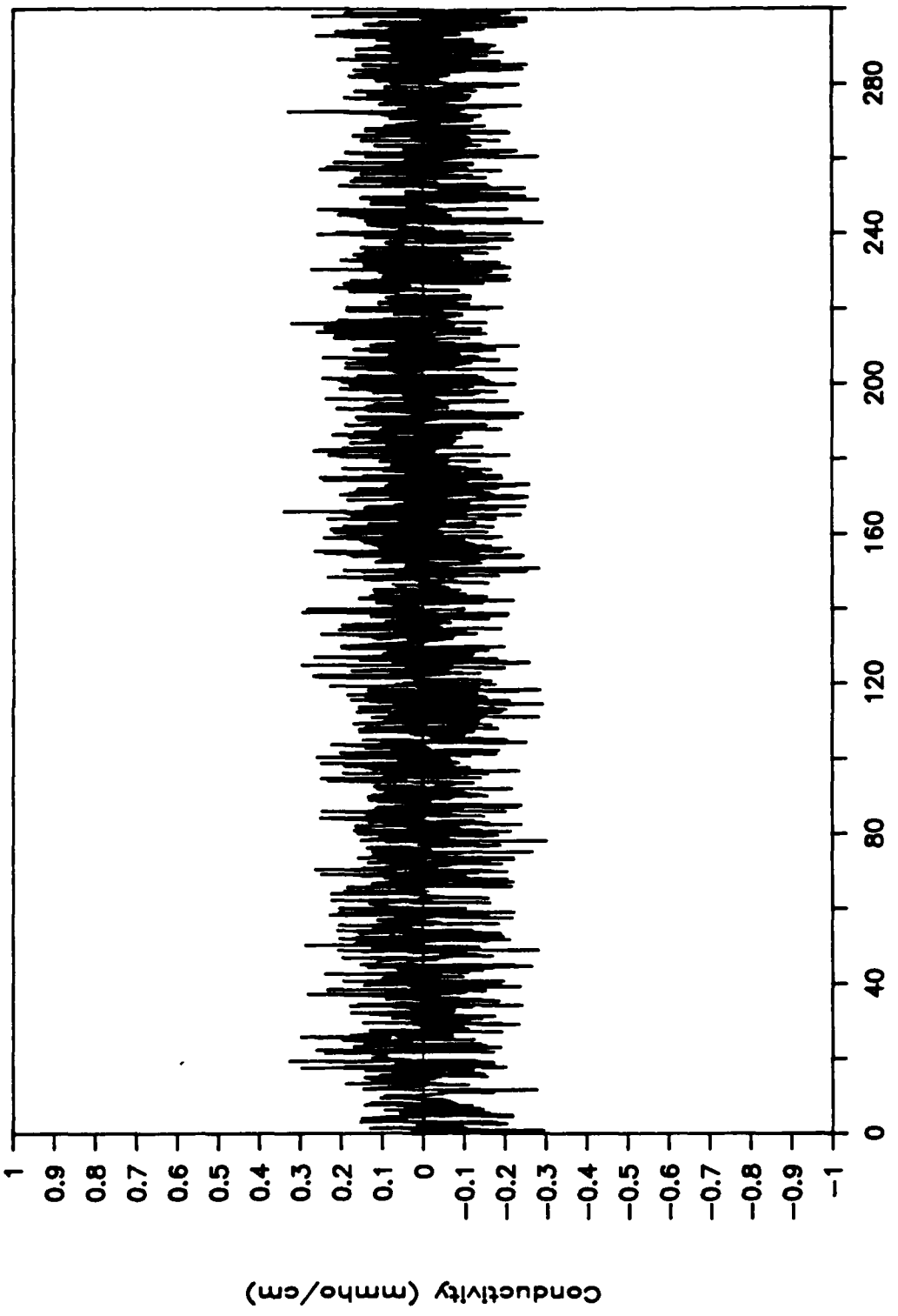

Figure 15. Conductivity Variations Measured at 2-meter Depth

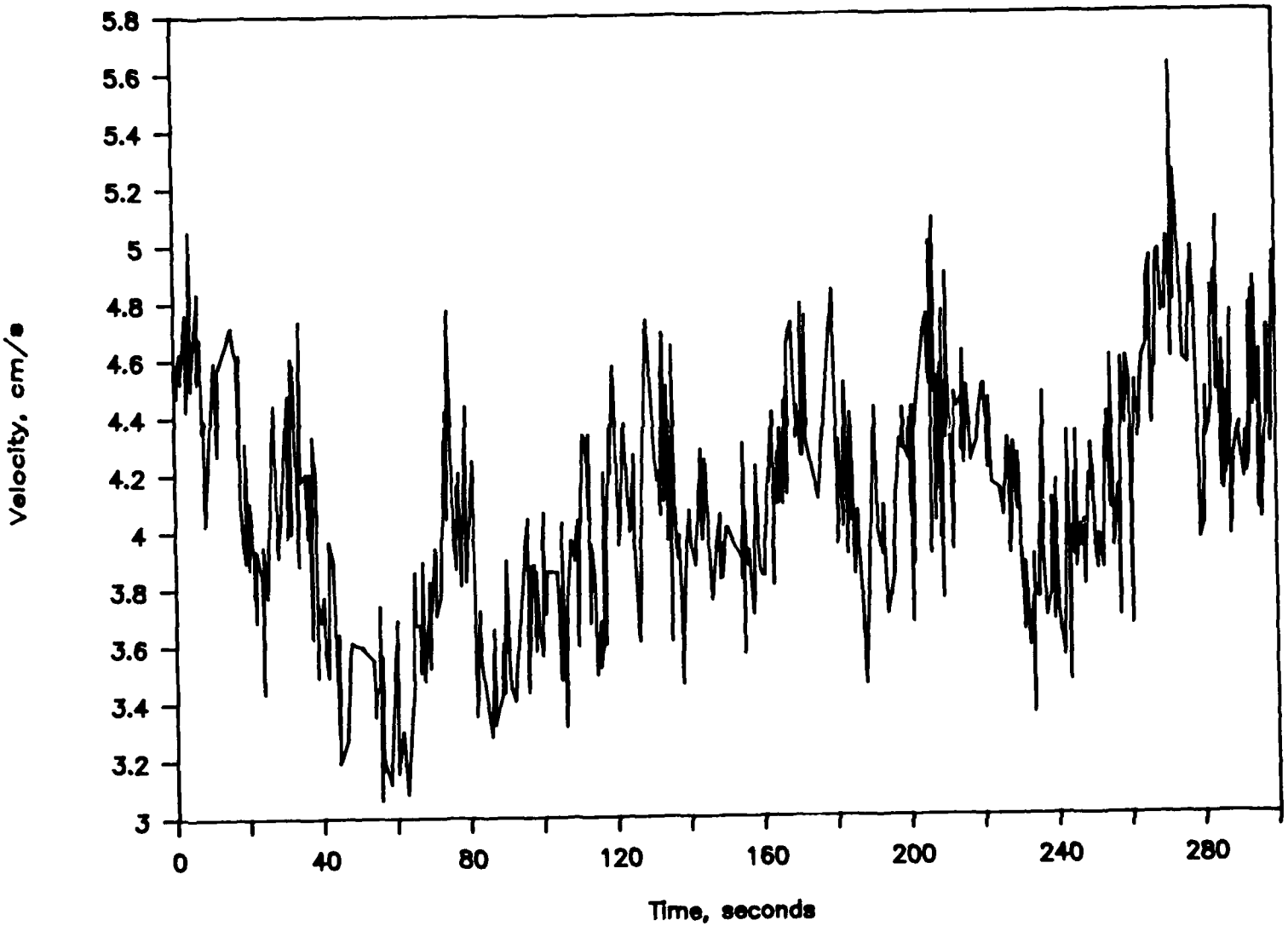

Figure 16. U1 Velocity Component Measured at 2-meter Depth

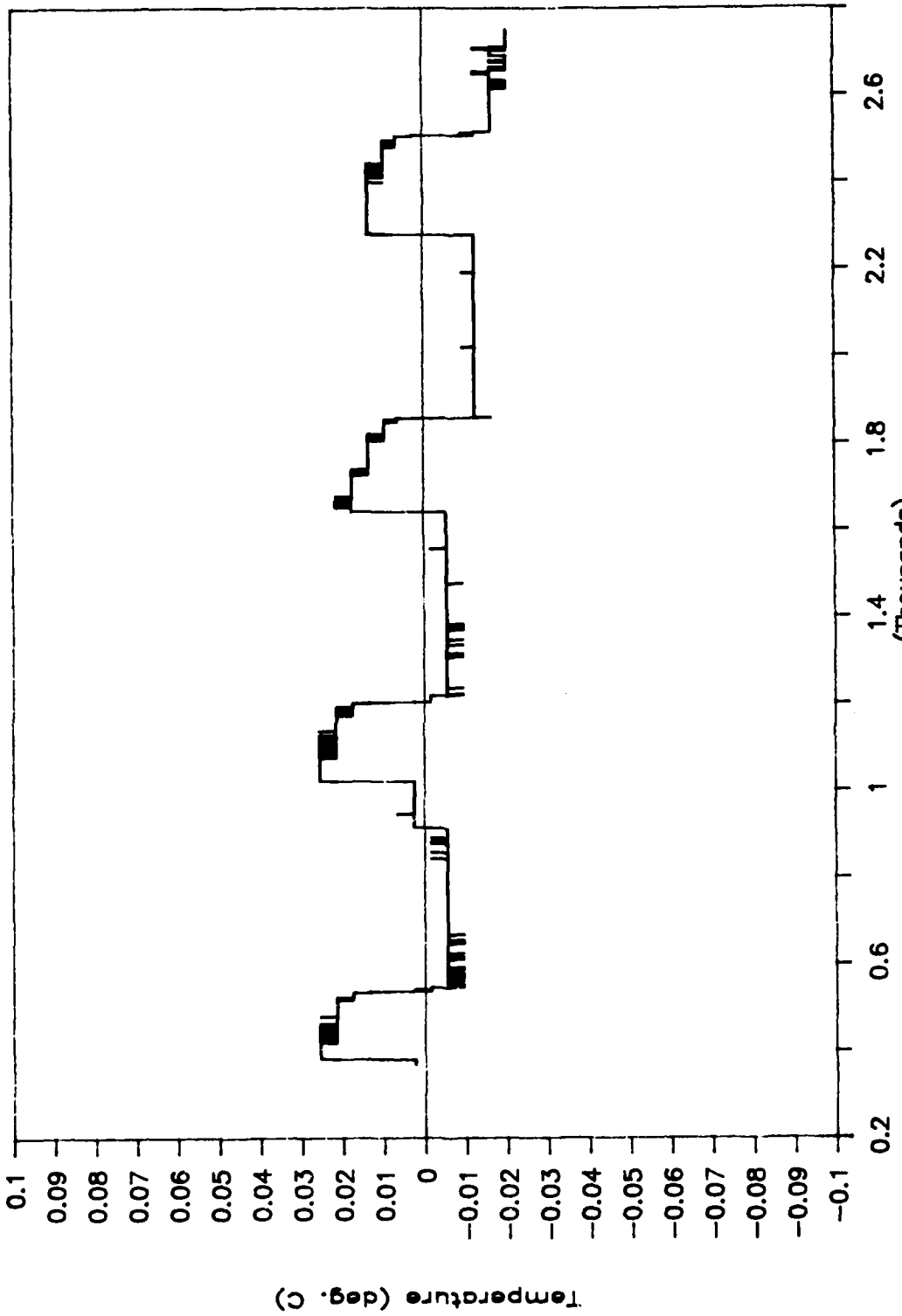

Figure 17. Temperature Variations Measured at 4-meter Depth

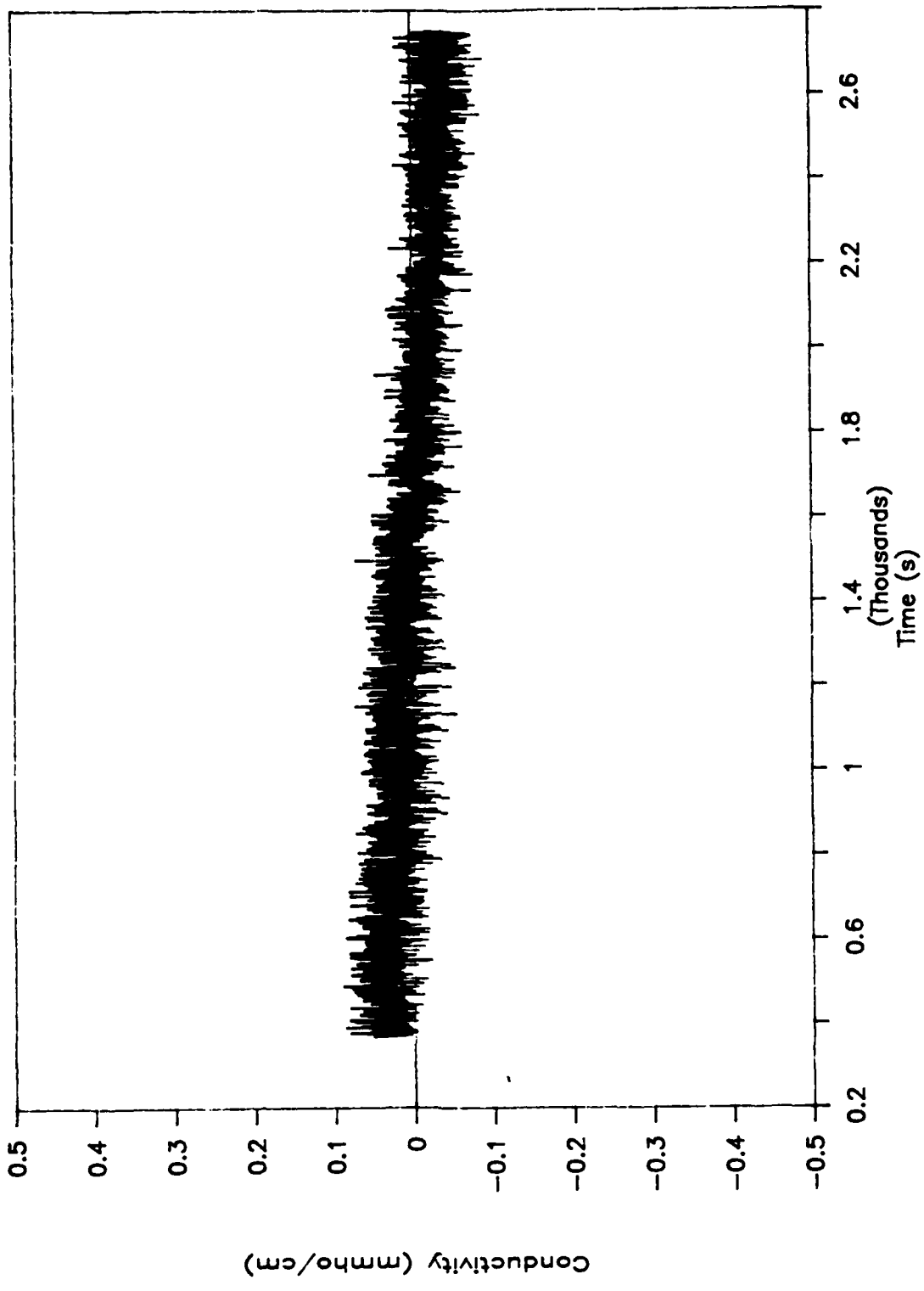

Figure 18. Conductivity Variations Measured at 2-meter Depth

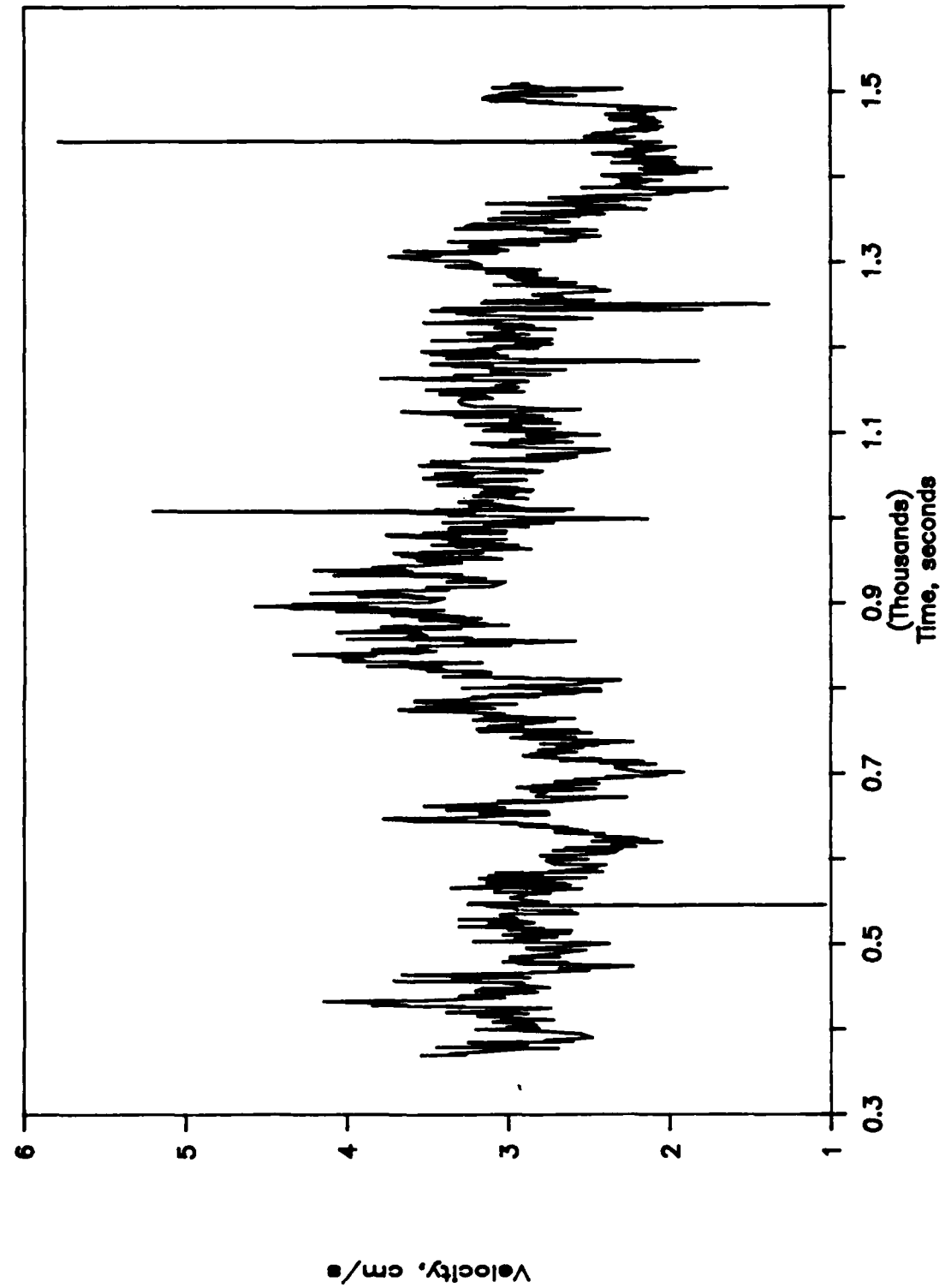

Figure 19. U1 Velocity Component Measured at 4-meter Depth

Arctic Ice Dynamics Joint Experiment pilot experiment. The angle of deflection between the two current vectors at the 2- and 4-m depths is generally larger for our measurements than those measured by Hunkins (1975). Furthermore, our results show that the angle of deflection tends to increase as the current speed decreases. For example, the angle of deflection for the run with the highest current speed (record 24, $U_{z=4m}$ = 12.3 cm/s) differs by 12°, whereas that for the lowest speed (record 25, $U_{z=4m}$ = 4.7 cm/s) differs by 28°. The same trend holds for the runs with the next highest and lowest current speeds.

Intuitively, the bottom topography of the ice floe, such as the presence of pressure keels, would have a relatively strong local influence on the headings of the current at these two depths.

Spatial Resolution

From the results given in Table 4, we estimate the spatial resolution, which is equal to the mean current speed divided by the mean data rate of the U1 velocity component (Figure 20). Also plotted in the figure is the spatial resolution estimated from the MIZEX 84 data. Figure 20 clearly demonstrates the trend of improving spatial resolution with increasing sampling rate. In an Arctic environment, a spatial resolution of 2 cm may be achieved for a sampling rate of 25 Hz and higher. Therefore, based on the above findings, at higher particle densities in water bodies other than the Arctic Ocean together with an increased sampling rate, a spatial resolution of the DLDV down to 1 mm is achievable.

The spatial resolution estimated from the AIWEX 85 data could be further reduced partly by optimizing the design of the counter electronics of the three-channel FLOW counter processor. As a trade-off to the multi-channel design, each of the three channels of the processor makes only one 5/8 comparison during each sampling cycle (See Section 2.3.1). After detecting a burst signal that does not pass the validation criterion, the processor would not look for another burst signal even if there is enough time to perform such comparison during the same cycle. For the single-channel Macrodyne processor used in MIZEX 84, however, the 5/8 comparison was made at a higher rate than the sampling rate. Therefore, a higher data rate or finer spatial resolution was attained with the Macrodyne processor than with the FLOW processor, as the spatial resolution is inversely proportional to the data rate. Software and

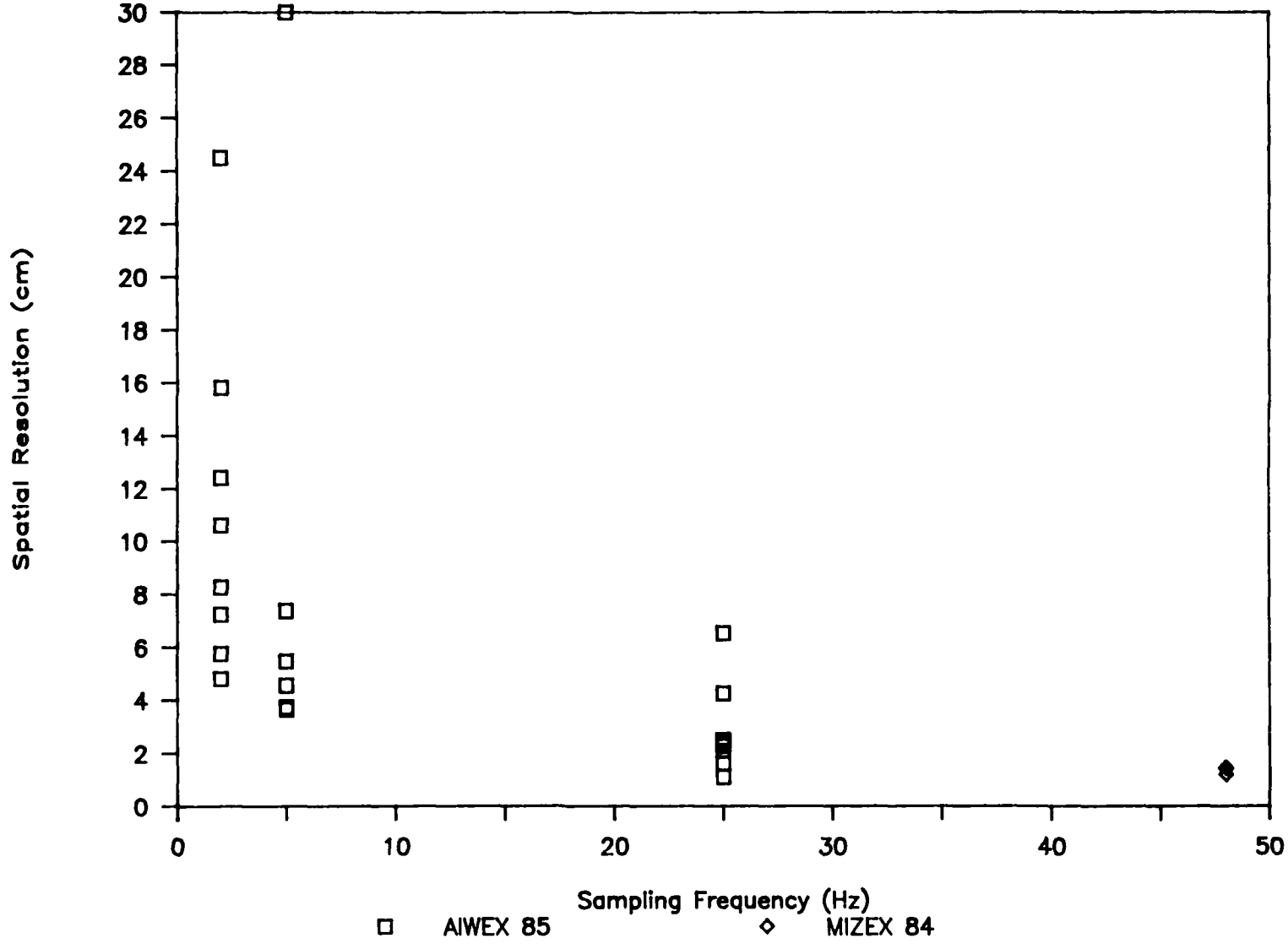

Figure 20. Estimated Spatial Resolution for the DLDV

hardware modifications may be incorporated into the FLOW processor to perform an essentially continuous 5/8 comparison to increase the data rate and, thus, to reduce the spatial resolution.

Wavenumber Spectra

The wavenumber spectra of the velocity components were estimated using the method of Bell (1983). Figure 21 is a composite wavenumber spectrum of the U1 component measured at 2- and 4-m depths for Run No. AIWEX 24. The abscissa and ordinate are the wavenumber k in cm^{-1} and the normalized velocity spectrum. Because the individual spectra are essentially the same, the composite spectrum is presented to improve the accuracy of the spectrum. The corresponding wavenumber spectrum for the U3 component is shown in Figure 22. Both spectra tend to show a $k^{-5/3}$ trend for almost one decade at wavenumbers beyond the first spectral peak. The spectral density at higher wavenumbers has a more gentle slope and eventually levels off.

The leveling off of the spectrum is mainly due to the presence of infrequent spikes, which contaminate the signals, and to limitations in preprocess filtering, which tend to enhance high-frequency spectral power. As described in Section 5.2.1, one of the sources of the spikes was a high-amplitude radio signal from a radio beacon used in the camp. It was discovered that the three-channel FLOW counter processor that uses the filter band concept (Section 2.3.1) had not been optimized for noise isolation or filtering. Band-pass filtering of the signals to remove noise outside the frequency bands of interest would definitely improve the performance of the FLOW processor. In reducing the raw data, the large spikes were removes through a persistence check described in Section 5.2.1. Only those spikes that have amplitudes less than 2 to 3 times the variance of the velocity were not removed. Although the energy content of these spikes is insignificant compared with the total kinetic energy, the spikes do mask the low-level spectral components at the high-wavenumber end, especially when the flow is not strongly turbulent as was encountered during AIWEX 85. A better spike removal algorithm will be required to discriminate the relatively small spikes from the signals. For future field experiments, however, emphasis should be made to improve the capability of the processor in noise isolation and suppression. Several recommendations are given in Section 7 for further system improvements of the DLDV sensors and processor for field deployment under hostile environmental conditions.

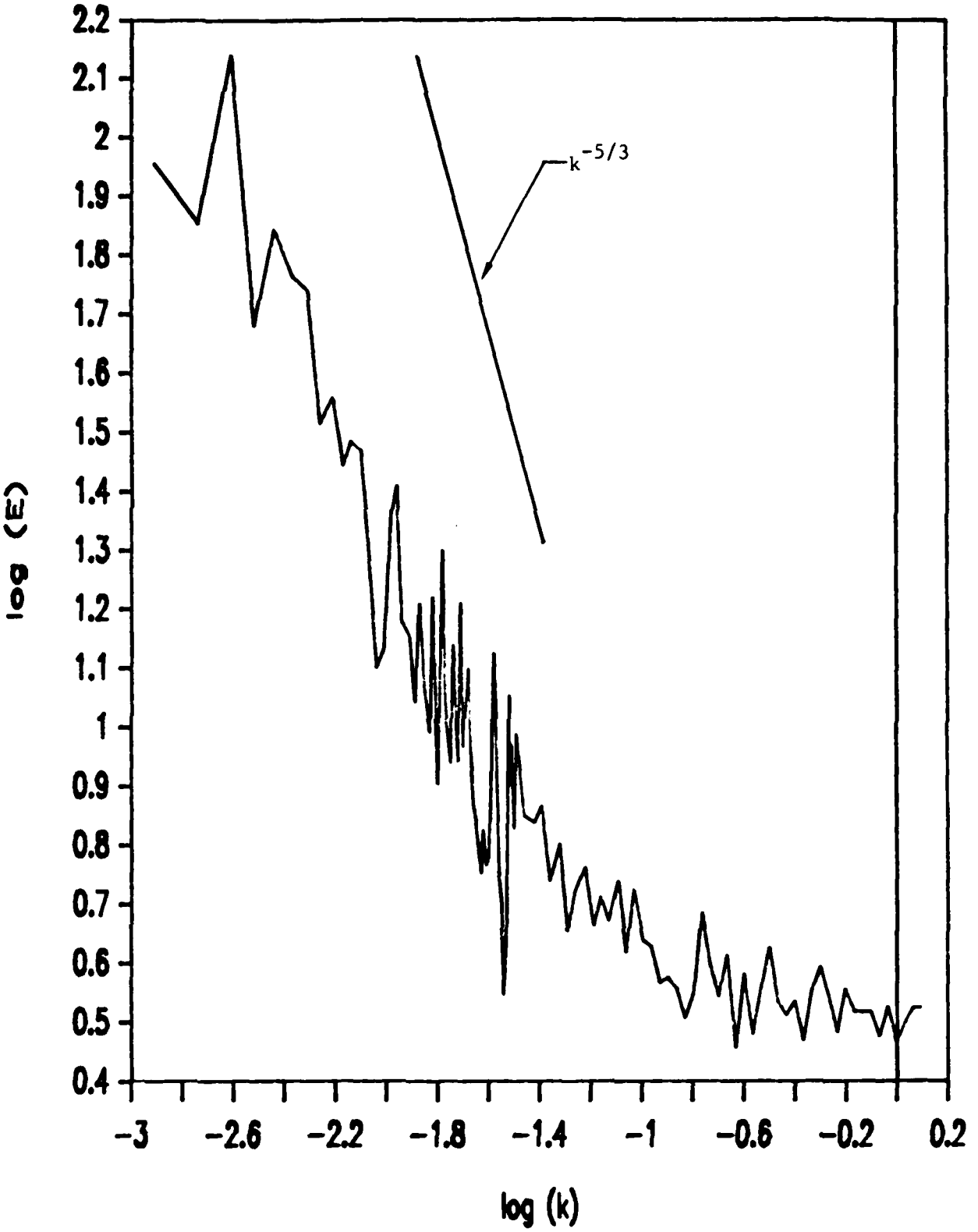

Figure 21. Composite Wavenumber Spectrum of the U1 Component at 2- and 4-meter Depths

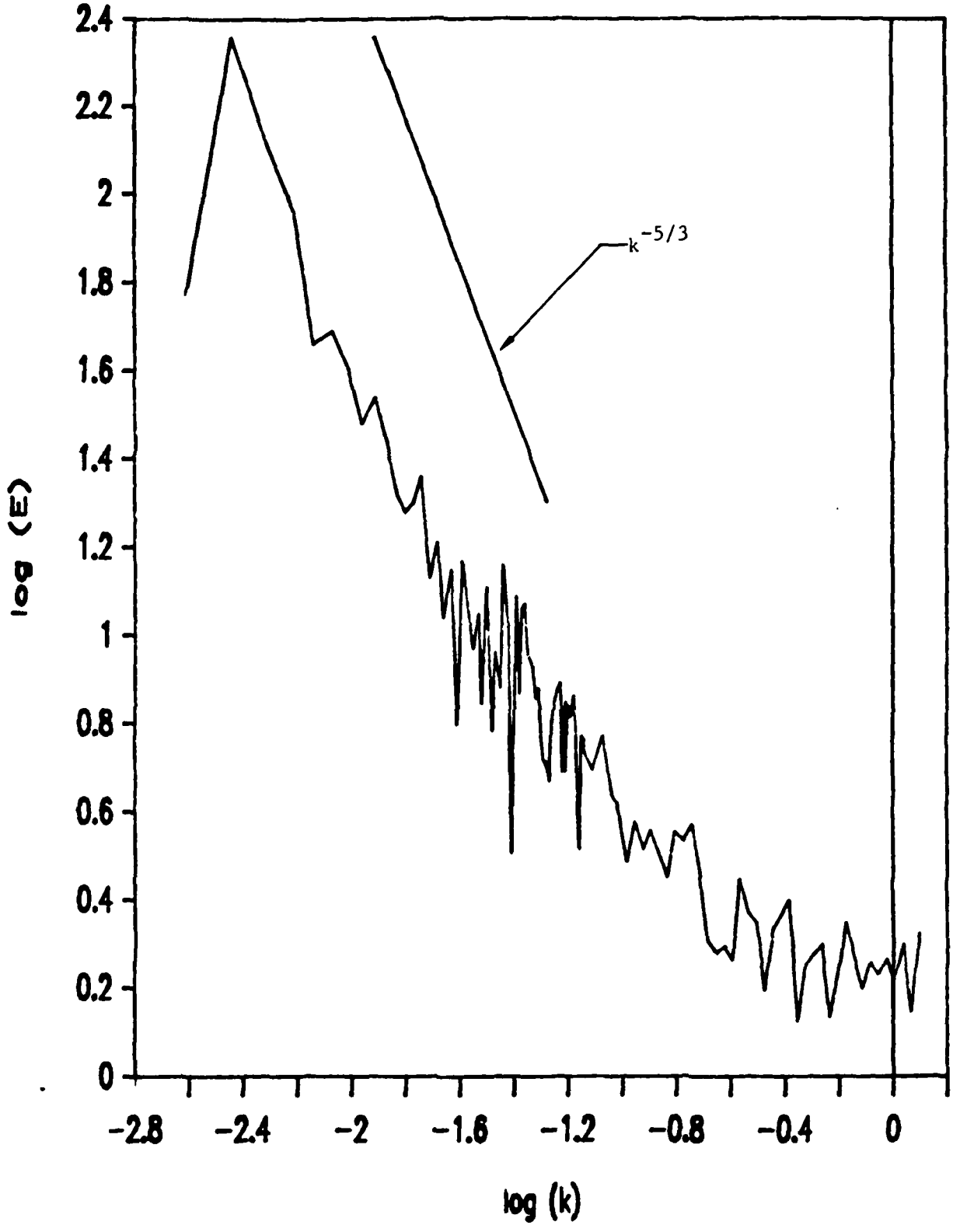

Figure 22. Wavenumber Spectrum of U3 Component at 4-meter Depth

6. SUMMARY

During the first 12 months of the Phase II research and development effort, we participated in two Arctic field experiments, using two experimental models of DLDVs during MIZEX 84 and three prototype HRCs of velocity-temperature-conductivity (V-T-C) sensors during AIWEX 85 for turbulence measurements under ice floes. The experimental DLDV units and the sensors and processors of the prototype HRCs were successfully developed, fabricated, tested and calibrated prior to deployment. The results from MIZEX 84 were also used to revise the design of the prototype HRC units before their deployment during AIWEX 85.

In essence, we have demonstrated even in an Arctic environment that the DLDV is a viable oceanographic instrument for high-frequency and high-resolution turbulence velocity measurements. The field-proven DLDV transmitter and receiver have high potential to be developed into a commercial product without major modifications. At present, we have partially analyzed the AIWEX 85 data. Based on our experience gained from the field deployment and the analysis performed so far, we summarize several of our important findings:

(1) The field worthiness of the prototype DLDV unit, including the transmitter and receiver, has been proven in terms of its portability, robustness and performance. The DLDV units were not only trouble-free during the field deployment, but they also performed satisfactorily as projected and survived the shipping/handling and the deployment in the hostile Arctic environment. The DLDV unit in its current configuration (extendable to 20 mW of laser power) may readily replace a gas laser of the same power rating and the associated optics and photodetector used in commercial LDV processors (counters or frequency trackers) for laboratory and field measurements, thus achieving one of the main goals set for the project. The main advantages of the DLDV over a conventional LDV using a gas laser and an assembly of optical and electronic components are:

- o Compactness, portability and robustness for laboratory and field deployment.
- o Integrated transmitting and receiving modules to simplify the test procedure.

o Low power requirement for field deployment in remote locations.

Six months after AIWEX 85, we turned on two transmitters selected at random to learn that they were still in good working order with no realignment required. According to the manufacturer, Hitachi Corporation, the lifetime of the laser diode is 10^6 hours at 25°C. One of the units is now under life testing to determine its longevity under normal operating conditions.

(2) Simultaneous measurements of the current velocity components using the ducted current meters on the medium-resolution cluster (MRC) and the DLDV units (McPhee, 1985b) placed in close proximity (50 cm vertical separation) were conducted during MIZEX 84. Comparison of the results shows generally good agreement between the time series and frequency spectra, especially for the horizontal velocity component. For the 45° velocity component, there is a deficit in the spectral density of the DLDV spectrum at medium to low frequencies. The deficit is apparently due to the more pronounced influence of the ice bottom topography on the vertical velocity component measured with the MRC than with the DLDV, as the MRC is 0.5 m closer to the ice bottom than the DLDV. The capability of measuring high-frequency velocity components ($f > 0.5$ Hz) using the DLDV is demonstrated.

(3) From the results of MIZEX 84 and the experience gained during that field experiment, we have successfully demonstrated that the DLDV is a viable instrument deployable in the Arctic environment. Our assessment of its performance during MIZEX 84 indicates several achievable improvements (see Section 5.1.3) that were subsequently incorporated into the design of the prototype units (Section 2) deployed during AIWEX 85.

(4) The time series measured during AIWEX 85 at 2- and 4-m depths below the bottom of an ice floe shows that the variations in temperature and conductivity generally do not exceed 0.01°C (except in one case) and 10 μmho/cm for a time scale up to an hour or so, indicating a

well-mixed boundary layer during April and May of 1985. This is consistent with measurements by other participants over time periods comparable to that of the DLDV runs, although noticeable long-term variations were reported.

(5) In both locations where the two field experiments were conducted, there were adequate scatterers in the Arctic Ocean water to achieve the target spatial resolution of 2 cm or better for velocity measurement. Our results show that the spatial resolution improves with the data rate. A 2-cm spatial resolution was achieved with a sampling rate of about 25 Hz or higher. In other oceans and water bodies where natural scatterers are plentiful, a spatial resolution of the order of 1 mm is achievable when off-axis detection is employed at similar or higher sampling rates.

(6) The wavenumber spectra of the velocity components estimated from the AIWEX 85 data tend to show the presence of an $f^{-5/3}$ regime. However, the spectral densities at high frequencies were contaminated by the presence of infrequent noise spikes induced by a radio beacon. As a result, the spectrum at the high-frequency end levels off, as opposed to a slight flattening of the slope of the spectrum of the MIZEX 84 data. Optimization of the FLOW counter processor for better noise isolation/filtering would be required to reject most of the noise spikes.

(7) As a potential oceanographic instrument for velocity measurements, the DLDV has several advantages over mechanical sensors:

- o High-frequency response limited only by the number density of scatterers.
- o Small sampling volume and high spatial resolution (down to millimeters).
- o Linear and absolute calibration (no drift).

- o Very low threshold speed (< 0.3 cm/s).

- o Minimal disturbance to the flow field (no physical probe at the sampling volume).

7. RECOMMENDATIONS

Based on the results of this two-phase investigation, we have concluded that the DLDV has a high market potential to become a commercial velocity sensor for field, laboratory and engineering applications. To further enhance its performance for a wide range of applications, we recommend several improvements to be incorporated into the design of the DLDV and the processor. In addition, suggestions for software development for post analysis of the DLDV data obtained in MIZEX 84 and AIWEX 85 are given to enhance the SNR so that we may obtain accurate estimates of the high-order statistics from the data whose high-frequency components are contaminated with infrequent noise spikes.

(1) For the current 3-axis DLDV system, we have avoided the directional ambiguity inherent to laser velocimetry by orienting the three DLDV units in a special geometrical configuration (Section 3.1). This avoidance scheme only works in a flow field with a prevailing current. For general applications, it is preferable to have a truly directional sensing capability. Several techniques are available for removal of directional ambiguity, but none is compatible with the compactness and portability of the DLDV for field deployment (Durst and Zare, 1974). During Phase II, we looked into several innovative alternatives. Among these, the technique of imaging the focal volume onto a position-sensitive or lateral-effect photodiode seemed most promising. The lateral-effect photodiode has two back contacts at opposite ends of a single-axis model. The current output at each of the contacts increases with the proximity of a light spot imaged onto the active strip of the diode. By imaging the focal volume of the DLDV onto the diode, with the plane of the beam intersection aligned with the axis of the diode, we may discriminate whether a particle is entering from one end or the opposite end of the focal volume, as

detected from the differential output of the two contacts of the diode, which senses the direction of the light scattered from the moving particle. From the sum of the two outputs, we reconstruct the Doppler signals for sensing the speed of the particle. Currently, we are testing this technique and assessing the feasibility of its implementation to the current DLDV design under the sponsorship of DOE. If successful, we will have the option to increase the laser power and to operate the DLDV in a back-scattering mode by combining two separate modules into a single one, greatly simplifying the deployment of the instrument.

(2) As described in Section 5.2.2, the counter logic in the three-channel FLOW processor does not have the provision to look for more then one Doppler burst, whether it is validated or not, during each sampling cycle. This effectively reduces the data rate. This provision should be incorporated through hardware/software design so that the processor continuously searches for and validates Doppler bursts detected by the photosensor until a validated burst is encountered and updated during each sampling cycle.

(3) During AIWEX 85, we experienced interference of the DLDV signals from a radio beacon. As a result, we had to manually disable the highest frequency band (> 64 kHz) of the DLDV. The lowest band (256 to 1000 Hz corresponding to a current speed of less than 0.34 cm/s) was also disabled to avoid noise contamination in this frequency range. After this correction, we still found infrequent noise spikes that contaminated the high-frequency components of the spectra. To improve the performance of the DLDV for deployment in a "noisy" environment, better noise isolation/filtering through careful shielding of the cable and instrument will be required. Furthermore, provisions for switching off individual filter bands should be implemented so that the optimum selection of the filter bands for noise rejection may be made under various flow conditions.

(4) A parallel effort to design a decontamination algorithm to recognize and remove the infrequent spikes that contaminate the DLDV signals would help to recover the high-frequency information. A similar algorithm has been used successfully by Dugan and Okawa (1982) to remove spikes contaminated by the conductivity signals due to particulates passing through the sensing volume.

(5) A part of the results derived from AIWEX 85 and presented in this report has shown some interesting features in the high-frequency and small-scale regimes that cannot be attained with conventional sensors. This unique set of data definitely deserves careful examination in an attempt to characterize the turbulence processes taking place in the Arctic Ocean boundary layer under ice. We recommend a detailed data analysis, including the development/adaptation of a spike decontamination algorithm and refinement of the statistical and spectral analysis, to derive statistical and spectral parameters of the HRC data.

REFERENCES

Bell, W. A. (1983) "Spectral Analysis Algorithms for the Laser Velocimeter: A Comparative Study," AIAA J., Vol. 21, No. 5, pp. 414-719.

Dantzler, H. L. Jr. (1974) "Dynamic Salinity Calibrations of Continuous Salinity/Temperature/Depth Data," Deep Sea Res., Vol. 21, pp. 675-682.

Dugan, J. P. and Okawa, B. (1982) "Indirect Technique for Small Scale Temperature and Salinity Measurements," Proceedings of the Marine Tech. Society Intl. STD Conference, La Jolla, CA, pp. E1-E7.

Durst, F., and Zare, M. (1974) "Removal of Pedestals and Directional Ambiguity of Optical Anemometer Signals," Appl. Optics, Vol. 13, No. 11, November.

Ekman, V. W. (1905) "On the Influence of the Earth's Rotation on Ocean Currents," Ark. Mat. Astron. Fys., Vol. 2, No. 11, pp. 1-52.

Gregg, M., and Meagher, A. (1980) "The Dynamic Response of Glass Rod Thermistors," J. Geophys. Res., Vol. 85, No. C5, pp. 2779-2786.

Gregg, M., Meagher, A., Pederson, A., and Aagaard, E. (1978) "Low Noise Temperature Microstructure Measurements with Thermistors," Deep Sea Res., Vol. 25, pp. 843-856.

Hunkins, K. (1975) "The Oceanic Boundary Layer and Stress Beneath a Drifting Ice Floe," J. Geophys. Res., Vol. 80, No. 24, pp. 3425-3433.

Krumholz, D. B., and Murphy, R. J. (1974) "Design Considerations for a Counter Based LV," Proceedings of the Second International Workshop on Laser Velocimetry, Purdue University, Vol. 1, pp. 224-234.

Liu, H.-T., Kollé, J. J., Schedvin, J. C., and McPhee, M. G. (1985) "Development of a Diode Laser Doppler Velocimeter for Measurements in the Oceanic Boundary Layer Under Ice," (Abstract only), EOS, Vol. 66, No. 18, April 30, p. 280.

Lueck, R. G., Hertzman, O., and Osborn, T. R. (1978) "The Spectral Response of Thermistors," Deep Sea Res., Vol. 24, pp. 951-970.

Lumley, J. L., and Panofsky, H. A. (1964) The Structure of Atmospheric Turbulence, Monographs and Texts in Physics and Astronomy, Vol. XII, Interscience, New York.

Masry, E., Klamer, D., and Mirabile, C. (1978) "Spectral Estimation of Continuous-Time Processes: Performance Comparison Between Periodic and Poisson Sampling Schemes," IEEE Transactions on Automatic Control, Vol. AC-23, No. 4, pp. 679-685.

McPhee, M. G. (1984) "MIZEX 84 Upper Ocean Turbulence Experiment," EOS, Transactions of the American Geophysical Union, Vol. 65. p. 935.

McPhee, M. G. (1985a) "Medium Resolution Turbulence Cluster for Upper Ocean Measurements under Sea Ice," Third Working Conference on Current Measurement, January 22-24, 1986, Airlie, VA.

McPhee, M. G. (1985b) "Comparison of Diode-Laser-Doppler Velocimeter and Medium Resolution Turbulence Cluster Measurements in MIZEX 84," Technical Report 85-1, McPhee Research Company, Yakima, Washington.

McPhee, M. G., and Smith, J. D. (1976) "Measurements of the Turbulent Boundary Layer under Pack Ice," J. Phys. Ocean., Vol. 6, No. 5, pp. 711-969.

Meagher, T. B., Pederson, A. M., and Gregg, M. C. (1982) "A Low-Noise Conductivity Microstructure Instrument," Proceedings Ocean '82 IEEE-MTS Conference, Washington, D.C., September 20-22.

Roden, G. I., and Irish, J. D. (1975) "Electronic Digitization and Sensor Response Effects on Salinity Computation from CTD Field Measurements," J. Phys. Oceanogr., Vol. 5, pp. 195-199.

Schedvin, J. C., and Liu, H.-T. (1984) "The Development of a Diode Laser Doppler Velocimeter for Boundary Layer Measurements Under Ice: A Feasibility Investigation," Technical Report No. 290, Flow Industries, Kent, Washington, April.

APPENDIX A

DLDV OPERATING INSTRUCTIONS

Software Version 1.2

November 8, 1985

Flow Industries Inc.
Automation, Instrumentation & Controls Division

David R. Schmidt

I. CONNECTIONS BETWEEN CLUSTERS AND PERSONAL COMPUTER

All control and data signals are passed over the GPIB cable, which connects the personal computer (PC) with the cluster units. The cables themselves just connect all of the connectors on all of the devices in parallel, although some practices should be followed:

1. The units should be connected in a linear fashion.

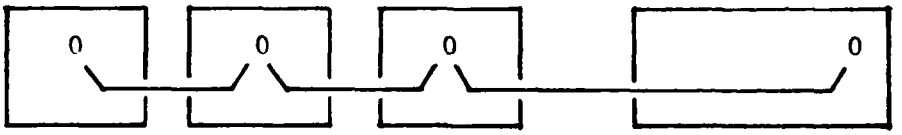

   If the PC had been connected in the middle of the string of other devices, it may have worked most of the time, but reflections on the cable could cause an increased error rate.

2. Don't over tighten the thumbscrews that hold the GPIB connectors. They are only there to keep the cable from torquing the connector loose. If they are tightened too much, the threaded sockets on the chassis can come loose or break.

3. The GPIB cables are expensive and hard to fix: beware.

II. ERROR RECOVERY

Due to the nature of the GPIB, there are times when all of the cluster units will need to be reset to escape from an error condition. Generally, when the program is 'hung up' in some undesired state, reset all of the cluster units and, if necessary, reboot the PC. A reset push button is located inside the front door of the cluster unit on the left side of the card cage. Cycling the power off for 10 seconds should perform a reset, but at times it may be necessary to press the reset button as well. It appears that some of the purchased boards in the cluster units do not reset correctly from the reset button and need to be reset by turning off the power.

III. RUNNING THE DLDV PROGRAMS

The simplest way to run the software that makes the system work is to boot the PC from the 'DLDV BOOT DISK.' This diskette will set up the device drivers for the GPIB interface, create a ram-based simulated disk, copy the latest version of the operating program to the ram disk and perform a few dos initializations. There are several files of interest:

1. c:\DLDV\DLDV.exe - the main operating program
2. c:\DLDV\showdldv.exe - inspect data and status files
3. c:\DLDV\svb.exe - special version of showdldv
4. c:\DLDV\DLDV.sav - boot-up version of DLDV setup
5. b:DLDV.sav - current version of DLDV setup

IV. DETAILS OF EACH PROGRAM

A. DLDV

1. ex

Exit from DLDV. Saves status of the program for later loading with the 'rp' command or inspection with showdldv or sbv.

2. rp

On exit from the DLDV program, most of the status information is saved in the file 'DLDV.sav'. This means that it is possible to escape from DLDV and restore your place later by using the 'rp' command.

3. on cluster_number (enable cluster)

4. of cluster_number (disable cluster)

5. id cluster_number (set GPIB address for cluster)

Each cluster has two numbers associated with it. One is the cluster number, which determines the column that a cluster's information is displayed in on the screen. The leftmost column is always cluster number 1. The other number is set by the hardware on the GPIB board in the cluster unit itself. This allows a particular hardware unit to be addressed by the PC. The 'GPIB address' line on the DLDV status display shows which cluster number maps to which of the three cluster boxes. It is recommended that the GPIB address values be left as 1, 2, and 3 and that they match the cluster numbers. This may reduce confusion. Internally to the DLDV program, each of the clusters may be enabled or disabled. A disabled cluster is never read or written to. An attempt to read or write to a cluster that is either not connected or turned off will cause the system to hang up.

6. rt time
(set run time for mu and td)

7. fs freq
(set sampling frequency for mu and td)

8. %
(set 5/8 ratio check error bandwidth)

These commands set the sampling parameters for the data collection. The rt command is followed by the runtime in seconds. Fs command frequencies are limited to 2, 4, 5, 10, 20, and 25 hertz. Exit saves the runtime and sampling frequency, but not the error bandwidth specified by the % command. In doing the 5/8 ratio check, it is not always desired to require an exact 5/8 ratio and the percentage allowed is specified with the % command. THE PERCENTAGE IS NOT SAVED ON EX NOR LOADED WITH RP.

9. mu (update means for all on-line clusters)

This command performs two functions. It allows the operator to get a quick check on the average Doppler frequencies from all of the on-line clusters without having to collect data to disk. It also sets up the temperature and conductance board for normal operation.

10. td filename (collect data to disk)

This is the real workhorse function. It will save the data collected from all on-line clusters into the file specified. The file should be on the b: ram disk since the delays caused by a mechanical disk are too long. The filename should be a simple name with no paths (no backslash characters allowed). No screen updates are done during the collection, as the computer is very busy transferring the data and no time is left to run the display. At the end of the sample period, the elapsed time is displayed and the system prompt appears.

11. gt cluster_number

12. gc cluster_number

13. ct cluster_number

14. cc cluster_number

Adjust the temperature and conductivity calibrations for the various clusters. Gains are specified with the single digits 0, 1, 2, or 3, which correspond to physical gains of 1, 10, 100, and 1000 respectively.

15. lo placename

The placename is up to 16 characters long and is saved with the data and status files. It is not used by the program, so it may contain any kind of identifying information desired. The placename may also be set from the dos command line. For example the dos command

```
DLDV kent wa 001
```

would run DLDV and set the placename to 'kent wa 001'.

16. ud

This is useful for verifying that the GPIB connection works. It merely transfers some data to the on-line units.

17. cz cluster_number

Clears the cluster specified. Not especially useful except during software debugging.

18. end

Causes an immediate exit from the DLDV program. DOES NOT SAVE STATUS. Useful if the disk fills up or you don't want to save the current status for some reason.

V. MISCELLANEOUS NOTES

1. If its on the ram disk (b:) and you want to keep it, copy it to the hard disk (c:) or to a floppy (a:) before turning the machine off.

2. You won't get any sympathy for not doing backups of both your floppies and hard disk.

3. The system clock must be set from dos.

APPENDIX B

DIAGRAMS FOR THE DLDV CIRCUIT BOARD AND SIGNAL CONDITIONER

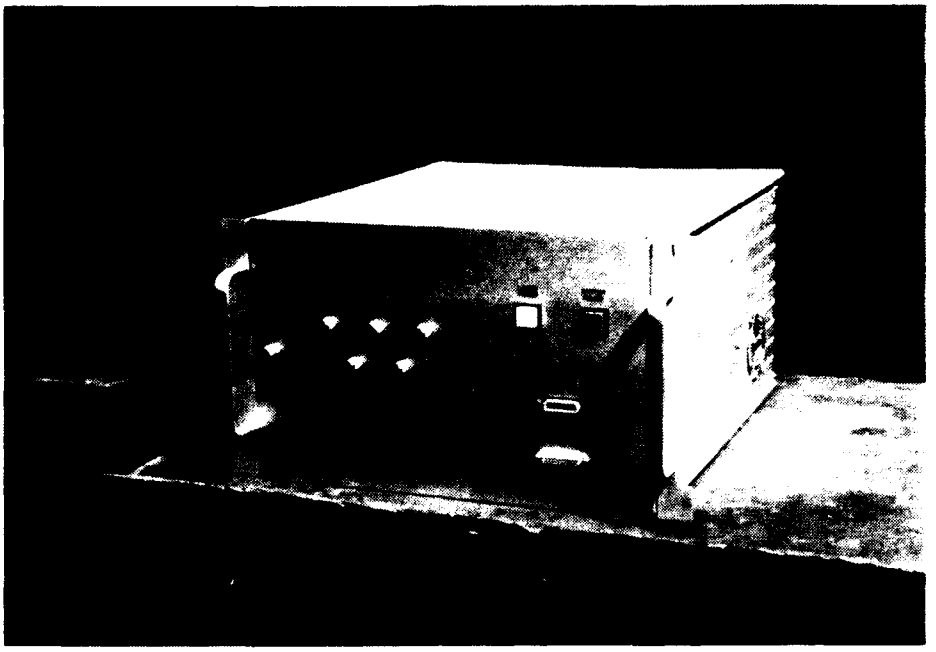

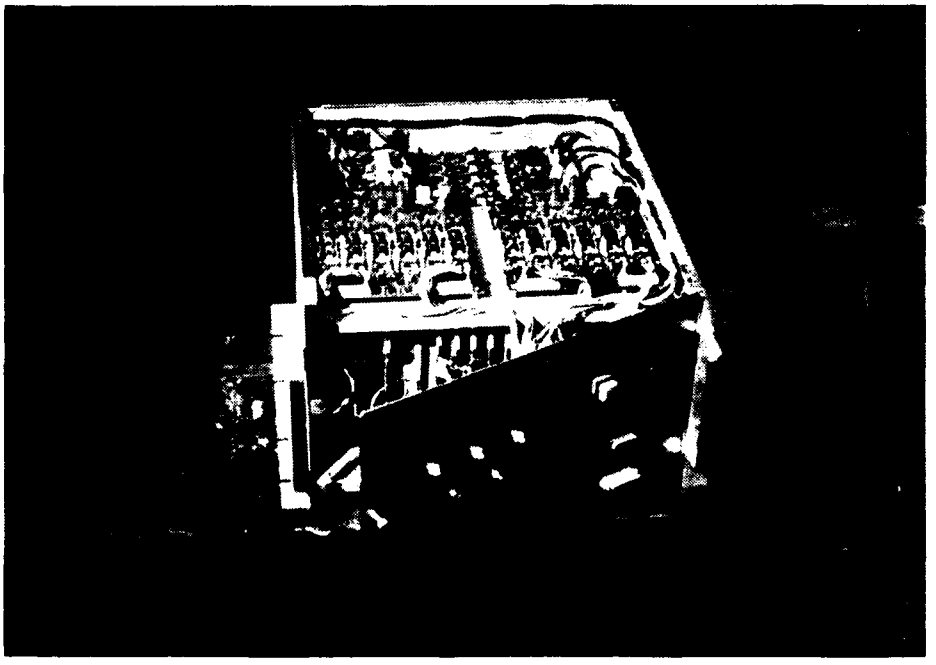

Figure B1. Photographs of DLDV Signal Conditioner

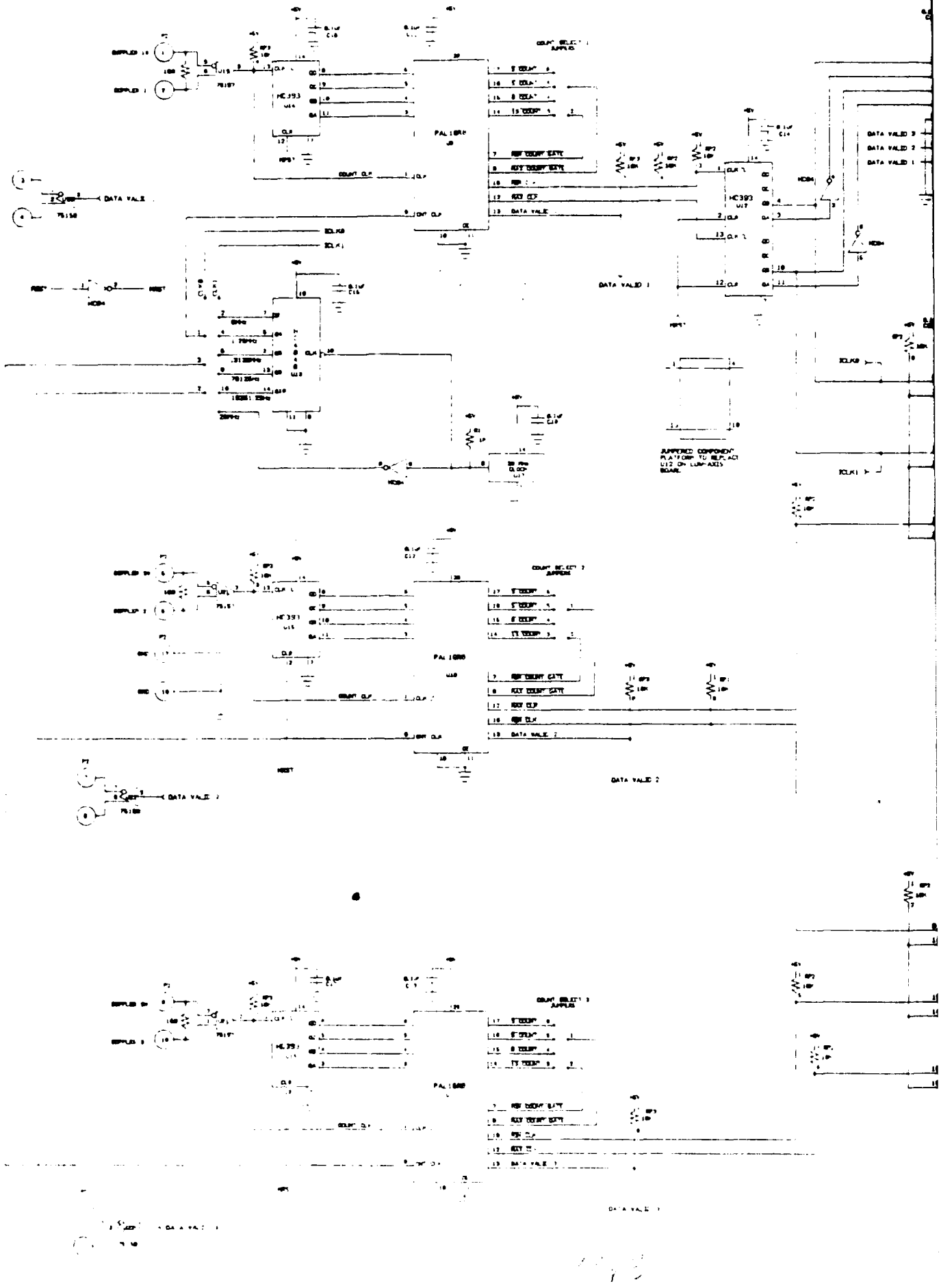

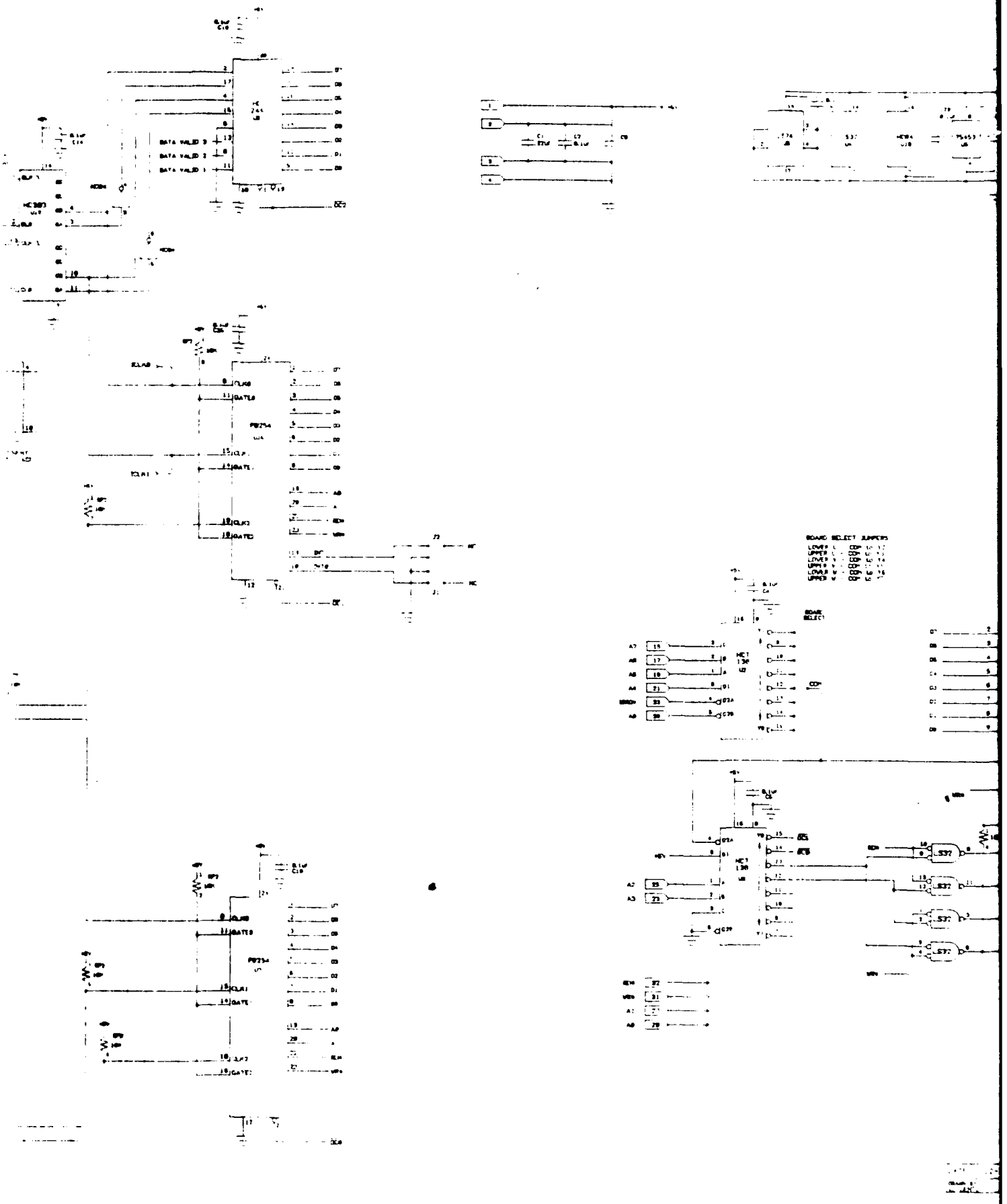

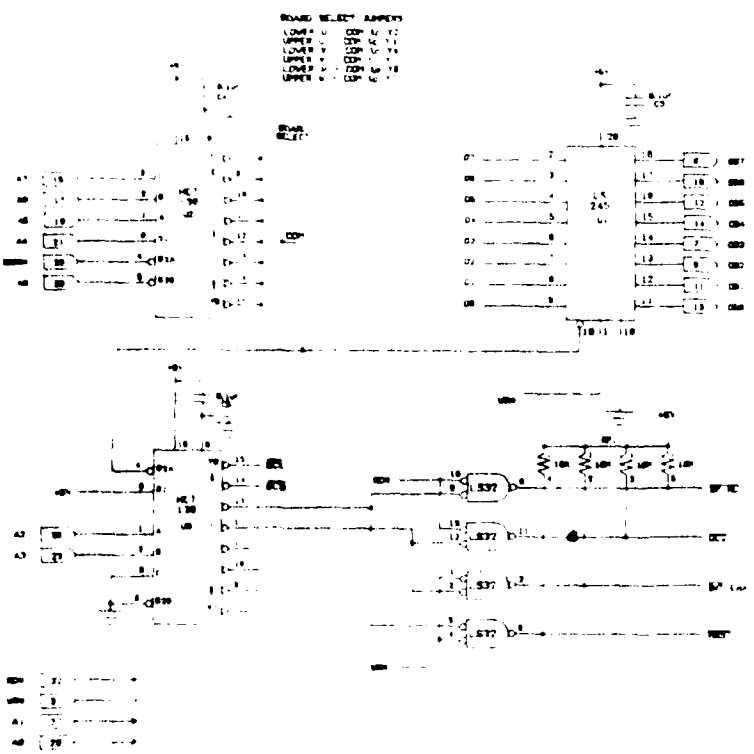

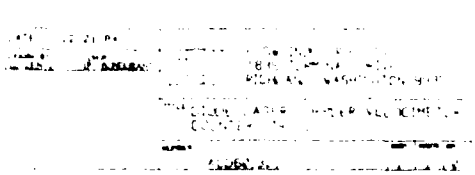

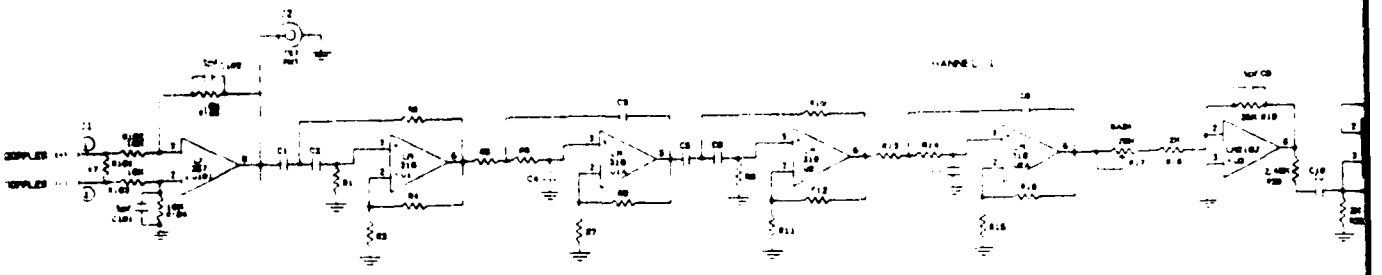

CHANNEL 2

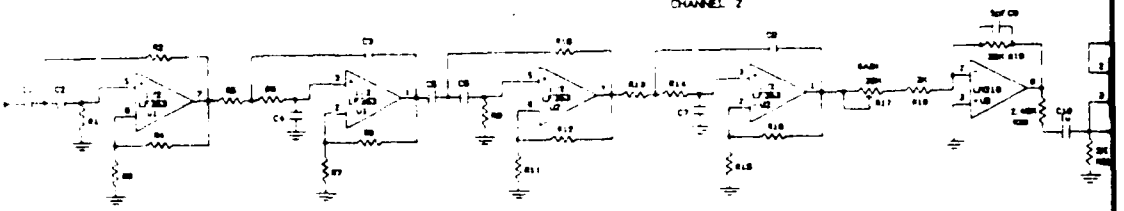

CHANNEL 3

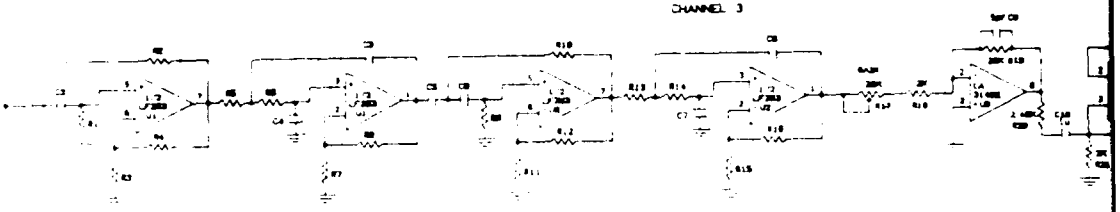

CHANNEL 4

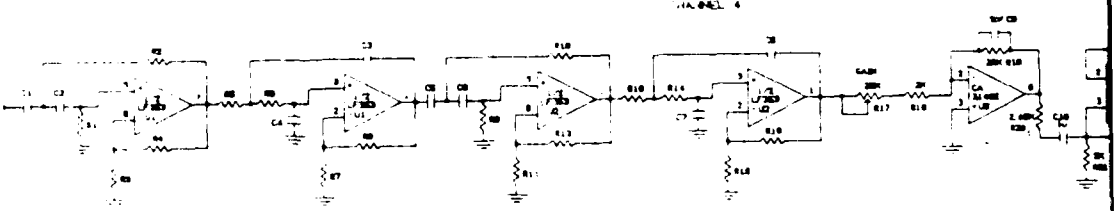

CHANNEL 5

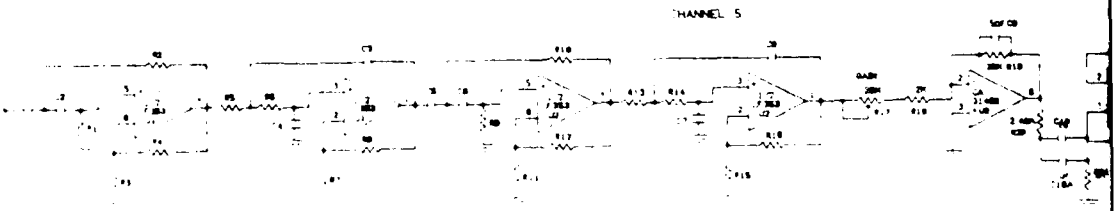

CHANNEL 6

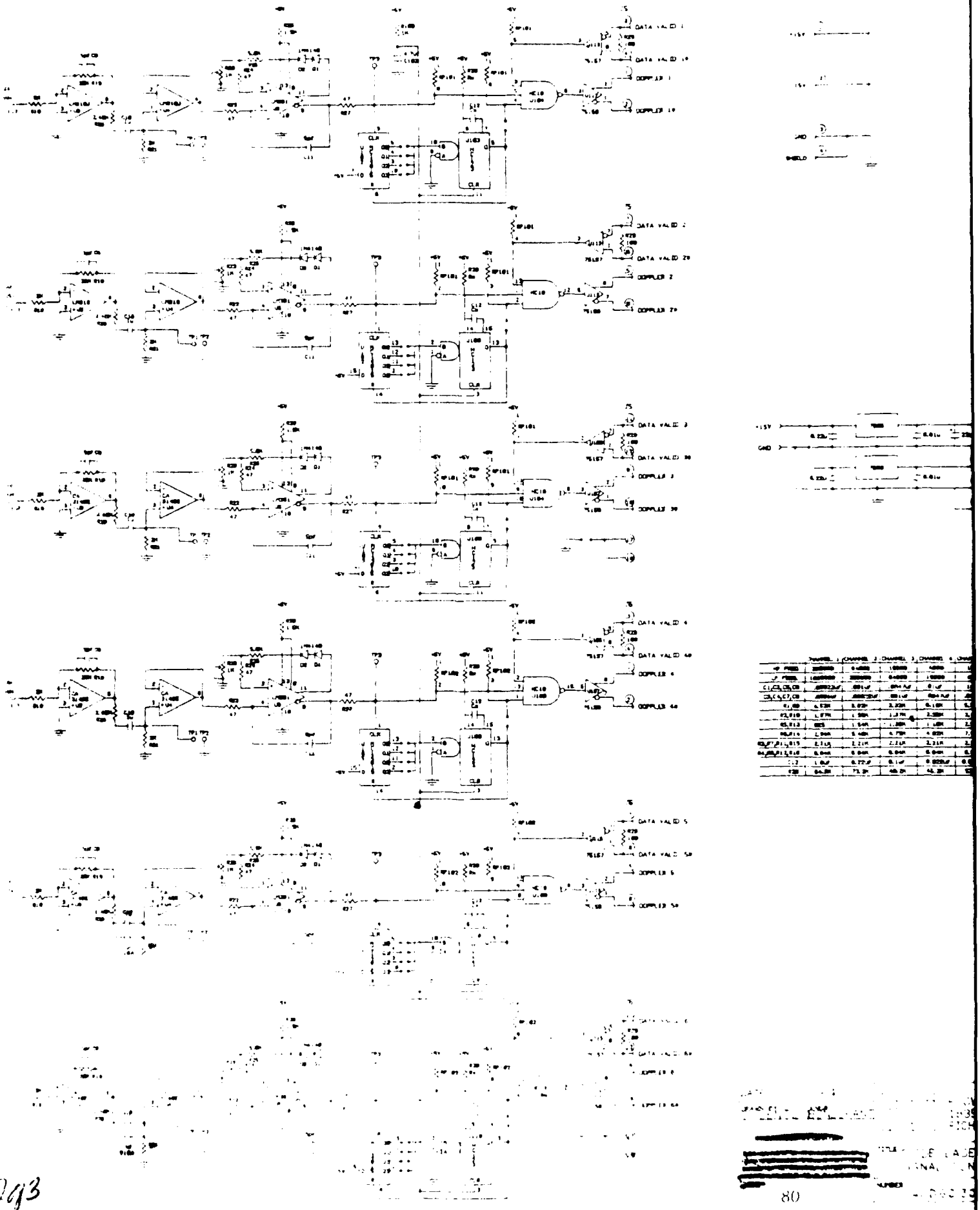

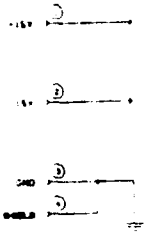

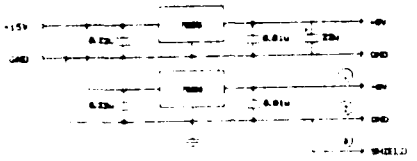

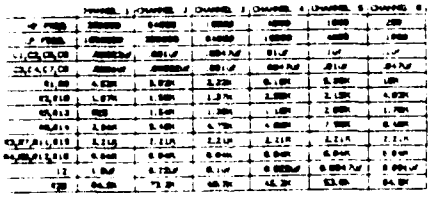

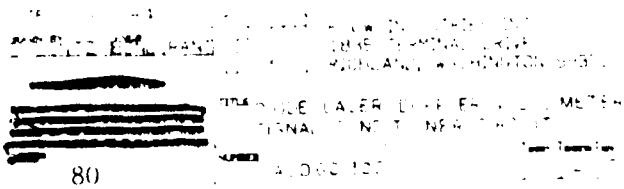

APPENDIX C

DESIGN INFORMATION FOR THE TEMPERATURE/CONDUCTIVITY CIRCUITRY

PTC-1

Programmable
TEMPERATURE
CONDUCTANCE

by

Paul Stockton

Datacon Electronics
Albany, Oregon

OCT 30,84

TEMPERATURE - CONDUCTANCE

CIRCUIT DESCRIPTION:

The unit is a single circuit board designed to be physically and electronically compatible with an industry standard computer internal buss structure known as the Standard Buss (STD-BUS).
The prototype board performs three basic functions.

1.) To convert temperature to a voltage acceptable to the analog interface board.
2.) To convert the conductance of saltwater to a voltage acceptable to the analog interface board.
3.) Provide programmable control of both temp & cond to enable computer control of gain and offset for both temp & cond. This capability provides very high resolution over a wide dynamic range.

TEMPERATURE; The temp. circuit is a simple resistance divider where one resistor is the temperature sensitive element (fast probe model FP-07) and a precision load resistor (R1). Voltage to this divider is provided by a precision voltage reference source. The value of R1 has been choosen to provide maximum sensitivity at the anticipated temperature range of -4 degC to +15 degC. A very low noise low drift precision amplifier is the voltage follower/buffer for the signal from the thermister. The signal is then Low Pass filtered at either 25Hz, 50Hz or 100Hz selectable. The signal is now a voltage representing temperature and is controllable by the computer through a selectable gain amplifier and offsettable by a sixteen bit digital to voltage converter. The possible gains are X1, X10, X100, and X1000. Prior to the gain control, the signal is offsettable from 0VDC to +10.0000VDC in incremants of 0.000153VDC.

CONDUCTANCE; Conductance is determined by RMS value of an AC current (Isig) flowing through the sample solution being tested. The conductance is equal to the probe voltage (Vsig) divided by the probe current (Isig). The circuit measures both Isig and Vsig, divides; Isig/Vsig to obtain a voltage proportional to conductance independent of fluctuations in Vsig (within limits). This voltage is then processed through exactly the circuitry as the temperature so control circuitry has matched freq. response and phase shift. Again, the programmable gain and offset provide very large dynamic range and resolution.

NOTE:The RMS-->DC converters in the conductance circuit, may produce a small coorelation error of the temp vs cond. They also limit freq response. These can be eliminated with further development. Post processing of the raw data can remove this phase shift difference if objectionable.

TERMINOLOGY OCT 31,84

Alp : LP gain of LP filters.
Abp : Bandpass gain of the LP filters.

B : One of two equations, "A" & "B" for filters.

Cave : Averaging capacitor for the RMS-->DC converter.
*Note: Will determine the freq res of the RMS-->DC conv.
[CIRCUIT TRADE-OFFS: 1.) Keep the freq of the sine wave oscillator as high as possible to keep Cave as small as possible to keep the response of the conv. high.
2.) The freq is limited by the input amps high freq response If the input amps gain changes with signal strength, non-linearity will occur.
Cext : External capacitor for the LP filters UAF14.
Cfo : The frequency determining capacitor of the sine wave osc.

Dout : DC voltage at output of conductance divider.

fo or fc : -3db point at freq. fo of LP filters. (UAF41)
Freq or Fco : Frequency of Sinewave Oscillator.

IRa : Charging current in sine wave osc. Vcc/(5*Ra)
Isine : The maximum current out of the sine wave oscillator.

Q : 'Q' for filter eq.
Qp : 'Q' product for multiple stage filters.

Ra,Rb : Charge & discharge current determining resistors
: on the sine wave oscillator.
Radj : Divider resistor for sine wave osc output.
Rdiv : Thermistor series divider resistor.
Rf1 & Rf2 : Feedback resistors for the LP filters UAF41.
Rfb : Feedback resistor of conductance 1st amplifier.
: Determines the range of the circuit.
Rg : Gain resistor for the LP filter UAF41.
Rin : RMS voltage at input of RMS-->DC converter in conductance
Rl : Sine wave osc load resistor or Thermistor divider resistor
Rout : DC voltage at output of RMS-->DC converter in conductance
Rpb : Probe resistance (Conductance).
Rq : 'Q' determining resistor for the LP filters.
Rthm : Temperature probe resistance.

sp.gr. : Specific gravity

Temp : Temperature of Environment.

Vin : RMS voltage at input of RMS-->DC converter in conductance
VOmax : Maximum desired sine wave voltage at input to 1st amplifie
VOmin : Minimum desired sine wave voltage at input to 1st amplifie
VOrange : VOmin-VOmax
Vout : DC voltage at output of RMS-->DC converter in conductance
Vsig : RMS voltage measured at the conductance probe.
Vsine : The RMS voltage output of the sine wave oscillator.

Dec 27,84

HOW TO MAKE IT WORK

INITIAL PROGRAMMING SETUP: GAIN=1 OFFSET=0
REMEMBER!
For straight binary offset (0-10VDC), INVERT MSBit
From factory address decoding = 80H = Jumper #1

1.) ZERO TEMPERATURE DAC

A.) Zero MSByte	1000 0000	1000 0100
B.) Activate WR. (Pin 3)		
C.) Zero LSByte	0000 0000	1000 0101
D.) Activate WR. (Pin 2)		
E.) Xfer data to DAC output	XXXX XXXX	1000 0110
F.) Activate WR. (Pin 1)		

2.) SET COND. PROG. GAIN=1

A.) Set Gain of Cond Amp.	XXXX XX00	1000 0011
B.) Activate WR.		

3.) ZERO CONDUCTANCE DAC

	Db 7654 3210	Ad 7654 3210
A.) Zero MSByte	1000 0000	1000 0000
B.) Activate WR. (Pin 3)		
C.) Zero LSByte	0000 0000	1000 0001
D.) Activate WR. (Pin 2)		
E.) Xfer data to DAC output	XXXX XXXX	1000 0010
F.) Activate WR. (Pin 1)		

4.) SET TEMP PROG. GAIN=1

A.) Set Gain of Temp. Amp.	XXXX XX00	1000 0111
B.) Activate WR.		

EXAMPLE: ASSUME TEMP=1.25 volts
SET OFFSET TO ZERO, INCREASE GAIN TO 10
Assumed address decoding of 80H

1.) Set MSByte OF Temp DAC to 1.25V
LSByte will remain same.

	Db 7654 3210	Ad 7654 3210
A.) Set DAC to 1.25V	1010 0000	1000 0100
B.) Activate WR.		

2.) Set Temp Amp Gain to 10

A.) Set Gain X10= 01	XXXX XX01	1000 0111
B.) Activate WR.		

TABLE 1 OCT 23,84
ADDRESS SELECT

Switch	A7	A6	A5	A4	A3	A2	A1	A0	
1	1	0	0	0	0	X	X	X	$80+X
2	1	0	0	0	1	X	X	X	$88+X
3	1	0	0	1	0	X	X	X	$90+X
4	1	0	0	1	1	X	X	X	$98+X
5	1	0	1	0	0	X	X	X	$A0+X
6	1	0	1	0	1	X	X	X	$A8+X
7	1	0	1	1	0	X	X	X	$B0+X
8	1	0	1	1	1	X	X	X	$B8+X

TABLE 2
DAC/GAIN SELECT

	A2	A1	A0	
Sel Cond DAC MS Byte	0	0	0	
Sel Cond DAC LS Byte	0	0	1	
Output Cond Dac	0	1	0	Note 1
Cond Amplifier Gain	0	1	1	See Table 3
Sel Cond DAC MS Byte	1	0	0	
Sel Cond DAC LS Byte	1	0	1	
Output Cond Dac	1	1	0	Note 1
Cond Amplifier Gain	1	1	1	See Table 3

TABLE 3
AMPLIFIER GAIN

Av	D1	D0
1	0	0
10	0	1
100	1	0
1000	1	1

Note 1
Data written to this register is ignored. The effect o write to this address is to transfer the LSByte and MS a 16 bit register within the DAC. A change in the outp only occurs after a write to this register.

FIG 5A BALANCED DIVIDER CIRCUIT
NOV 6,84 TABLE OF TERMISTOR RESISTANCES VS TEMPERATURE
TEMPERATURE RANGE: -5.0 —> +25.0 Degrees C

Ref. THERMOMETRICS T.C. Manual 181-D page A-2
R25: Zero power res. of T.C. at calibrated temp 25 deg.C+273.15Kelvin
RT: Zero power res. of T.C. at temp. t(C)+273.15 Kelvin
RTo: Zero power resistance at temp. To;To=t(C)+273.15
T: Absolute temperature T;T=t(C)+273.15
B: Beta of T.C. ... Function of T.C material.
R25/R125: Ratio of RT @ 25Deg to RT @ 125Deg
RD1,RD2: Divider resistors for balanced input divider network.

FOR:
10000 RTo=R25=10K Ohms
10000 RD1 THM divider res... positive side
10000 RD2 THM divider res... negative side
3540 B=Beta is Kelvin temp. const. for material "A"
19.8 R25/R125=19.8
273.15 Kelvin ref.
298.15 To=25+273.15

$RT = RTo \exp\{B(1/T - 1/To)\}$

2.5 =es; Thermistor divider source voltage
eo(T) =eo; eo(T)=es/[1+(RT/R)]
0.6 =s; Choosen from best linearity curve for material "A" @ 0 Deg C
15000 =RD1+RD2=R25/s; Resistance needed for best
0.002442 = Data System Resolution for 12b Conv

Degrees C	RT(C) K Ohms	dRT K Ohms	Rd1 Vlow 2.5	Rd2 Vhigh	Rthm Voltage Drop
-6	39.55				
-5	37.65	1.903	0.43367	2.06633	1.633
-4	35.85	1.798	0.44764	2.05236	1.605
-3	34.15	1.700	0.46169	2.03831	1.577
-2	32.54	1.608	0.47582	2.02418	1.548
-1	31.02	1.521	0.49001	2.00999	1.520
0	29.58	1.440	0.50424	1.99576	1.492
1	28.22	1.363	0.51849	1.98151	1.463
2	26.93	1.291	0.53276	1.96724	1.434
3	25.70	1.223	0.54702	1.95298	1.405
4	24.54	1.159	0.56126	1.93874	1.377
5	23.44	1.099	0.57546	1.92454	1.349
6	22.40	1.043	0.58961	1.91039	1.321
7	21.41	0.989	0.60370	1.89630	1.293
8	20.47	0.939	0.61771	1.88229	1.265
9	19.58	0.892	0.63163	1.86837	1.237
10	18.73	0.847	0.64544	1.85456	1.209
11	17.93	0.805	0.65913	1.84087	1.182
12	17.16	0.765	0.67270	1.82730	1.155
13	16.44	0.727	0.68613	1.81387	1.128
14	15.74	0.692	0.69941	1.80059	1.101
15	15.09	0.658	0.71252	1.78748	1.075
16	14.46	0.626	0.72547	1.77453	1.049
17	13.86	0.596	0.73825	1.76175	1.024
18	13.30	0.568	0.75084	1.74916	0.998
19	12.76	0.541	0.76324	1.73676	0.974
20	12.24	0.515	0.77544	1.72456	0.949

21	11.75	0.491	0.78744	1.71256	0.925
22	11.28	0.468	0.79923	1.70077	0.902
23	10.83	0.447	0.81082	1.68918	0.878
24	10.41	0.426	0.82218	1.67782	0.856
25	10.00	0.407	0.83333	1.66667	0.833

FIG 5A NOV 6,84

DATA SYSTEM
RESOLUTION v.s. TEMPERATURE
@ OP AMP GAINS:
BASED ON 10VDC F.S. / 4095

Degrees C	Gain X1 millideg C	Gain X10 mC	Gain X100 uC	Gain X1000 uC
-5	11.4376	1.1438	114.3756	11.4376
-4	11.5111	1.1511	115.1109	11.5111
-3	11.5716	1.1572	115.7163	11.5716
-2	11.6191	1.1619	116.1910	11.6191
-1	11.6535	1.1653	116.5348	11.6535
0	11.6748	1.1675	116.7480	11.6748
1	11.6832	1.1683	116.8316	11.6832
2	11.6787	1.1679	116.7872	11.6787
3	11.6617	1.1662	116.6167	11.6617
4	11.6323	1.1632	116.3228	11.6323
5	11.5908	1.1591	115.9083	11.5908
6	11.5377	1.1538	115.3769	11.5377
7	11.4732	1.1473	114.7322	11.4732
8	11.3979	1.1398	113.9786	11.3979
9	11.3121	1.1312	113.1206	11.3121
10	11.2163	1.1216	112.1629	11.2163
11	11.1111	1.1111	111.1107	11.1111
12	10.9969	1.0997	109.9691	10.9969
13	10.8744	1.0874	108.7436	10.8744
14	10.7440	1.0744	107.4397	10.7440
15	10.6063	1.0606	106.0630	10.6063
16	10.4619	1.0462	104.6191	10.4619
17	10.3114	1.0311	103.1137	10.3114
18	10.1552	1.0155	101.5524	10.1552
19	9.9941	0.9994	99.9407	9.9941
20	9.8284	0.9828	98.2841	9.8284
21	9.6588	0.9659	96.5879	9.6588
22	9.4857	0.9486	94.8574	9.4857
23	9.3098	0.9310	93.0976	9.3098
24	9.1313	0.9131	91.3134	9.1313
25				

TEMPERATURE RESOLUTION

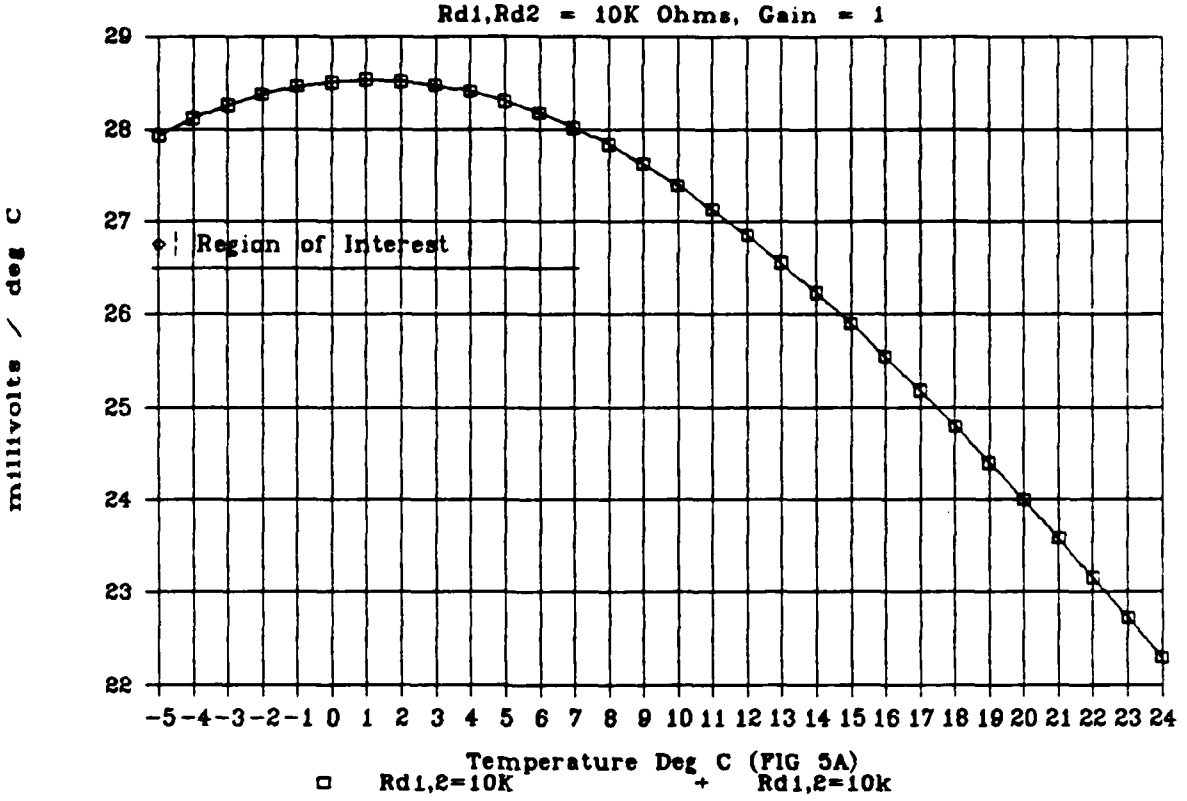

DATA SYSTEM TEMP RESOLTUION

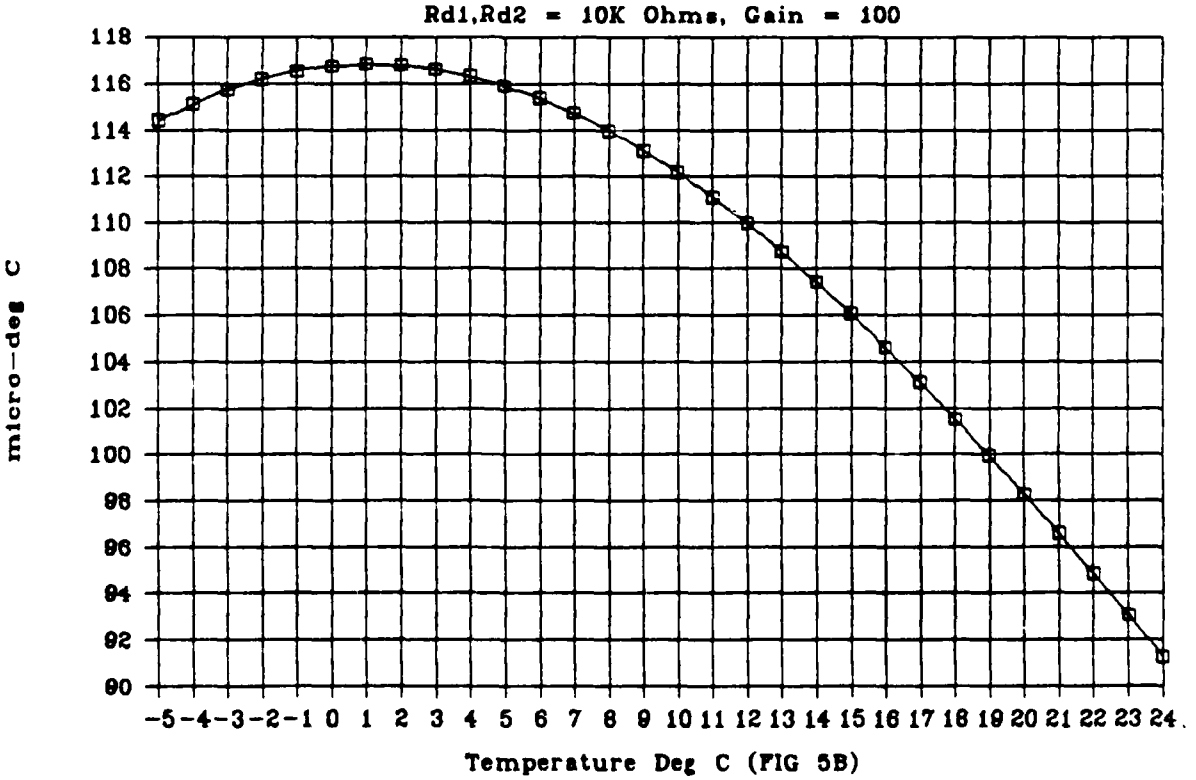

OCT 31,84
DESIGN CALCULATIONS FOR BURR-BROWN UAF41 FILTER
FUNCTION = 2 POLE BUTTERWORTH L.P.

INVERTING

2 = # of poles.
1 = fn
0.70711 = Q
0.70711 = Qp = Q for fo*Q products
less than 1E5 Hz
25 = fo(1)
50 = fo(2)
100 = fo(3)
B = Equation for fo<8KHz
Rf1=Rf2: Feedback Resistors
Rf1=Rf2 = 5.033E7/(fo)
Alp: Low-Pass Gain
1 = Alp
Abp: Bandpass Gain
0.223768 = Abp = (Qp/3.16)*Alp
Rg: Gain Resistor
49928 = Rg = (1.58E4*Qp)/Abp
Rq: Q Resistor
29682.19 = Rq = 5E4/[(3.48*Qp)+Abp-1]
Radd: Added Res. needed for Eq"B"
5490 = Radd (Res added: pins 12&13)
Cext: Added Cap to lower Rf values
1.00E-07 = Cext (.1ufd)
Rf(new): New Rf1 & Rf2 due to
the addition of Cext.
Rf(new)=Rf(old)*[1E-9/(1E-9+Cext)]

fo Hz	Rf1,Rf2 Ohms	Cext Farads	Rf(new) Ohms		Rg Ohms	Rq Ohms
25	2013200	1.00E-07	19932.67	INV	49928	29682.19 Ohms
50	1006600	1.00E-07	9966.336			
100	503300	1.00E-07	4983.168			

Same Rf values
INV & NON-INV

OCT 31,84
DESIGN CALCULATIONS FOR BURR-BROWN UAF41 FILTER
FUNCTION = 2 POLE BUTTERWORTH L.P.

NON-INVERTING

2 = # of poles.
1 = fn
0.70711 = Q
0.70711 = Qp = Q for fo*Q products
less than 1E5 Hz
25 = fo(1)
50 = fo(2)
100 = fo(3)
B = Equation for fo<8KHz
Rf1=Rf2: Feedback Resistors
Rf1=Rf2 = 5.033E7/(fo)
Alp: Low-Pass Gain
1 = Alp
Abp: Bandpass Gain
0.223768 = Abp = (Q/3.16)*Alp
Rg: Gain Resistor
223444.7 = Rg = (5E4*Q)/(Abp*Qp)
Rq: Q Resistor
40421.22 = Rq = 5E4/[3.48*Qp-((Abp*Qp)/Q)-1]
Radd: Added Res. needed for Eq"B"
5490 = Radd (Res added: pins 12&13)
Cext: Added Cap to lower Rf values
1.00E-07 = Cext (.1ufd)
Rf(new): New Rf1 & Rf2 due to
the addition of Cext.
Rf(new)=Rf(old)*[1E-9/(1E-9+Cext)]

fo Hz	Rf1,Rf2 Ohms	Cext Farads	Rf(new) Ohms		Rg Ohms	Rq Ohms
25	2013200	1.00E-07	19932.67	NON-INV	223444.7	40421.22 Ohms
50	1006600	1.00E-07	9966.336			
100	503300	1.00E-07	4983.168			

Same Rf values
INV & NON-INV

TEMPERATURE - CONDUCTANCE

Nov 12,84

J1 Data Translation DT2745 20pin Interconnect

	J1		
CONDUCTANCE SIG CH 0	1	2	CONDUCTANCE SIG GND
TEMPERATURE SIG CH 1	3	4	TEMPERATURE SIG GND
FROM (J2-P1) CH 2 HI	5	6	FROM (J2-P2) CH 2 LO
FROM (J2-P3) CH 3 HI	7	8	FROM (J2-P4) CH 3 LO
(N/C) Ch 4 HI INPUT	9	10	Ch 4 LO INPUT (N/C)
(N/C) Ch 5 HI INPUT	11	12	Ch 5 LO INPUT (N/C)
(N/C) Ch 6 HI INPUT	13	41	Ch 6 LO INPUT (N/C)
(N/C) Ch 7 HI INPUT	15	16	Ch 7 LO INPUT (N/C)
(N/C) ANA COMMON	17	18	AMP COMMON (N/C)
FROM (J2-P9) EX TRG	19	20	DIGITAL GND (N/C)

J2 Sensor I/O 10pin Connector

	J2		
Ch2 HI INPUT (J1-P7)	1	2	Ch2 LO INPUT (J1-P8)
Ch3 HI INPUT (J1-P7)	3	4	Ch3 LO INPUT (J1-P6)
Conductance Pb ->	5	6	<- Conductance GND
Thm Pos. Input ->	7	8	<- Thm Neg. Input
EXT TRIG (J1-P19)	9	10	-> ANALOG GND

AD-A165 250 A HIGH-RESOLUTION CLUSTER OF OCEANOGRAPHIC INSTRUMENTS FOR BOUNDARY LAYER MEASUREMENTS UNDER ICE(U) FLOW INDUSTRIES INC KENT WA H LIU ET AL. NOV 85 2/2

UNCLASSIFIED TR-352/11-85 N00014-83-C-0764 F/G 8/10 NL

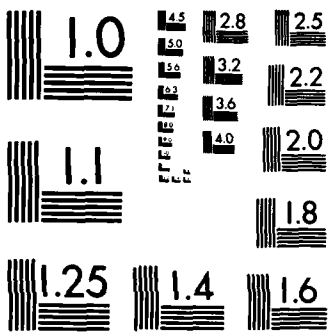

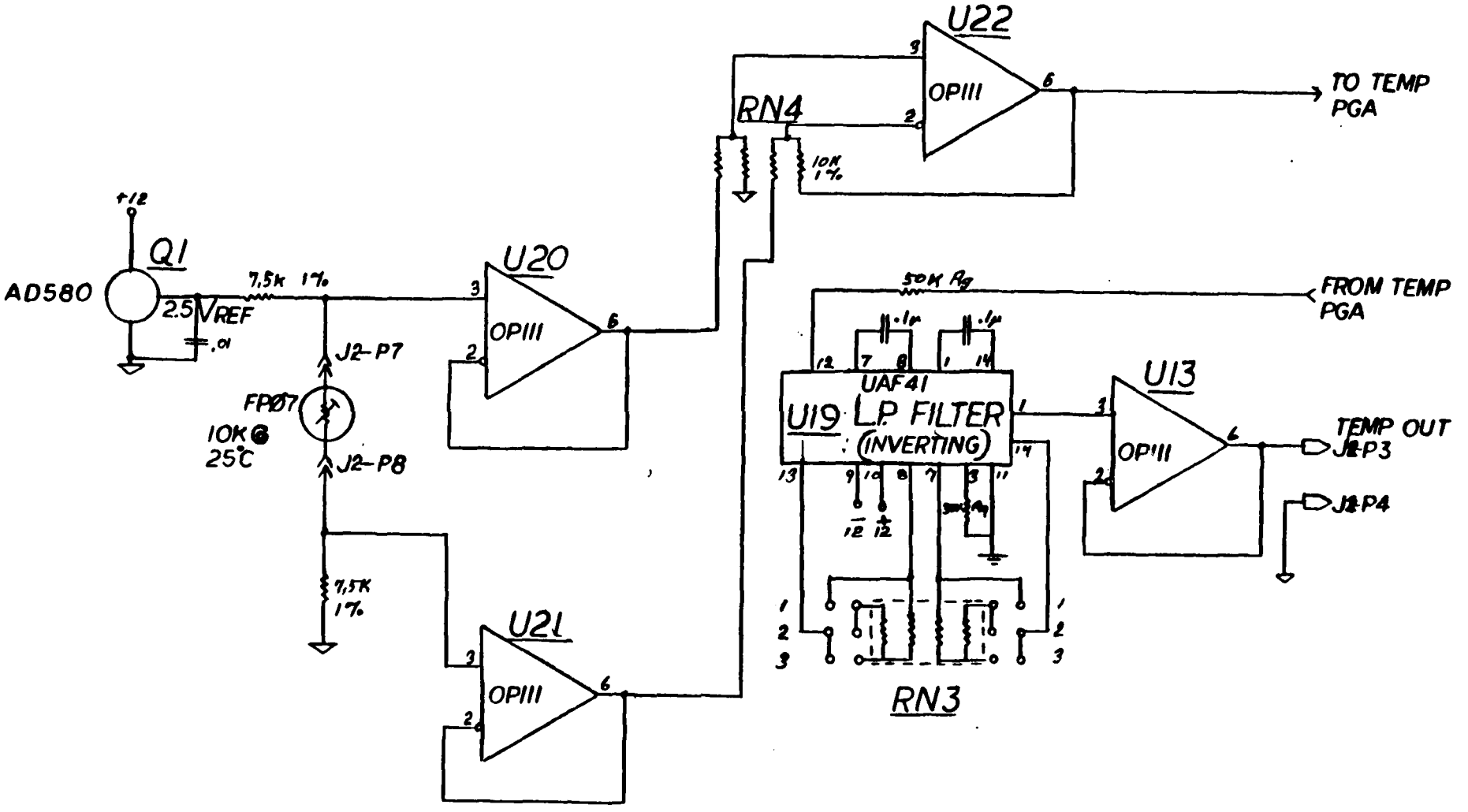

92

TEMPERATURE→ VOLTAGE

PTC-1

NOV 12, 84

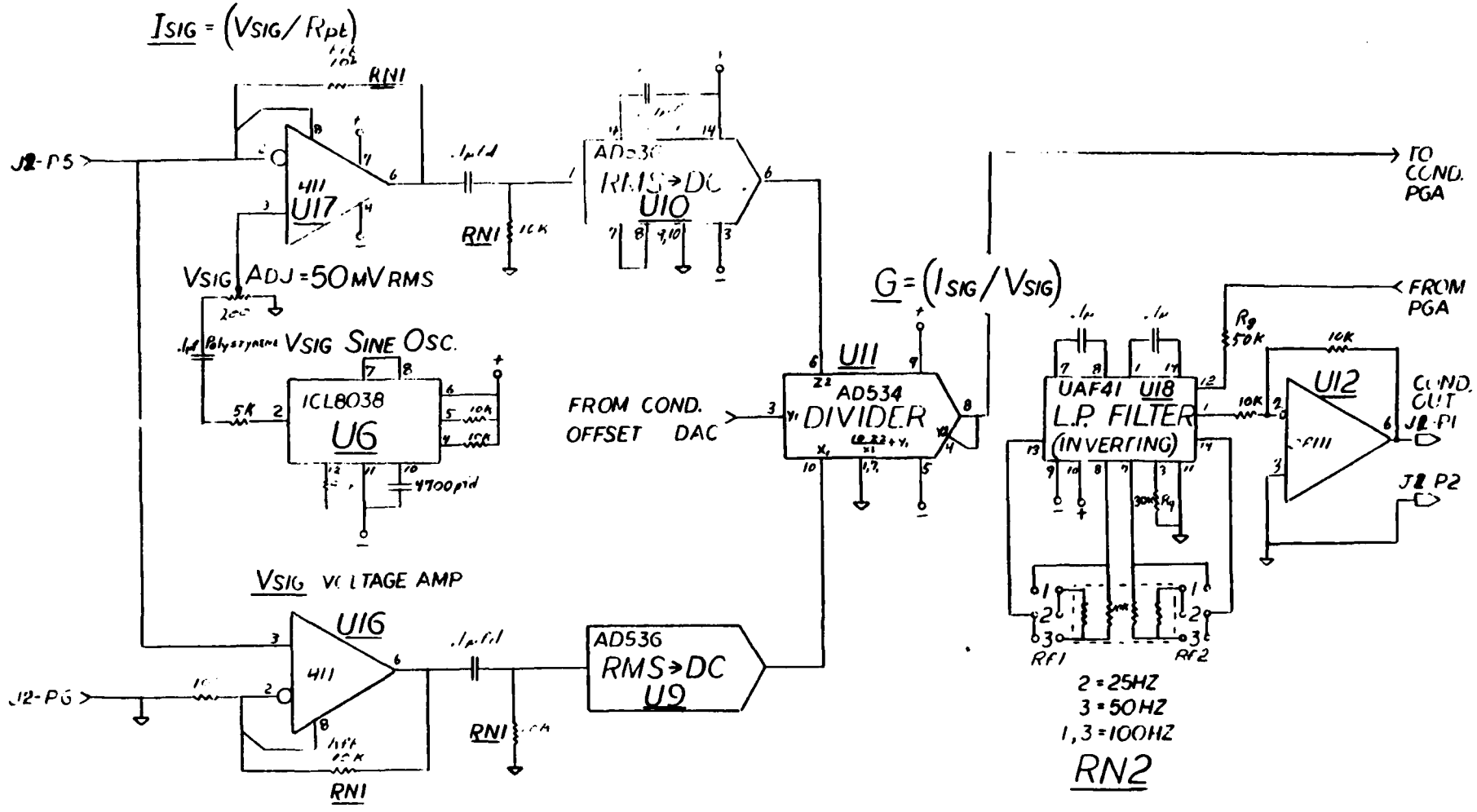

CONDUCTANCE → VOLTAGE

PTC-1
NOV 11, 81

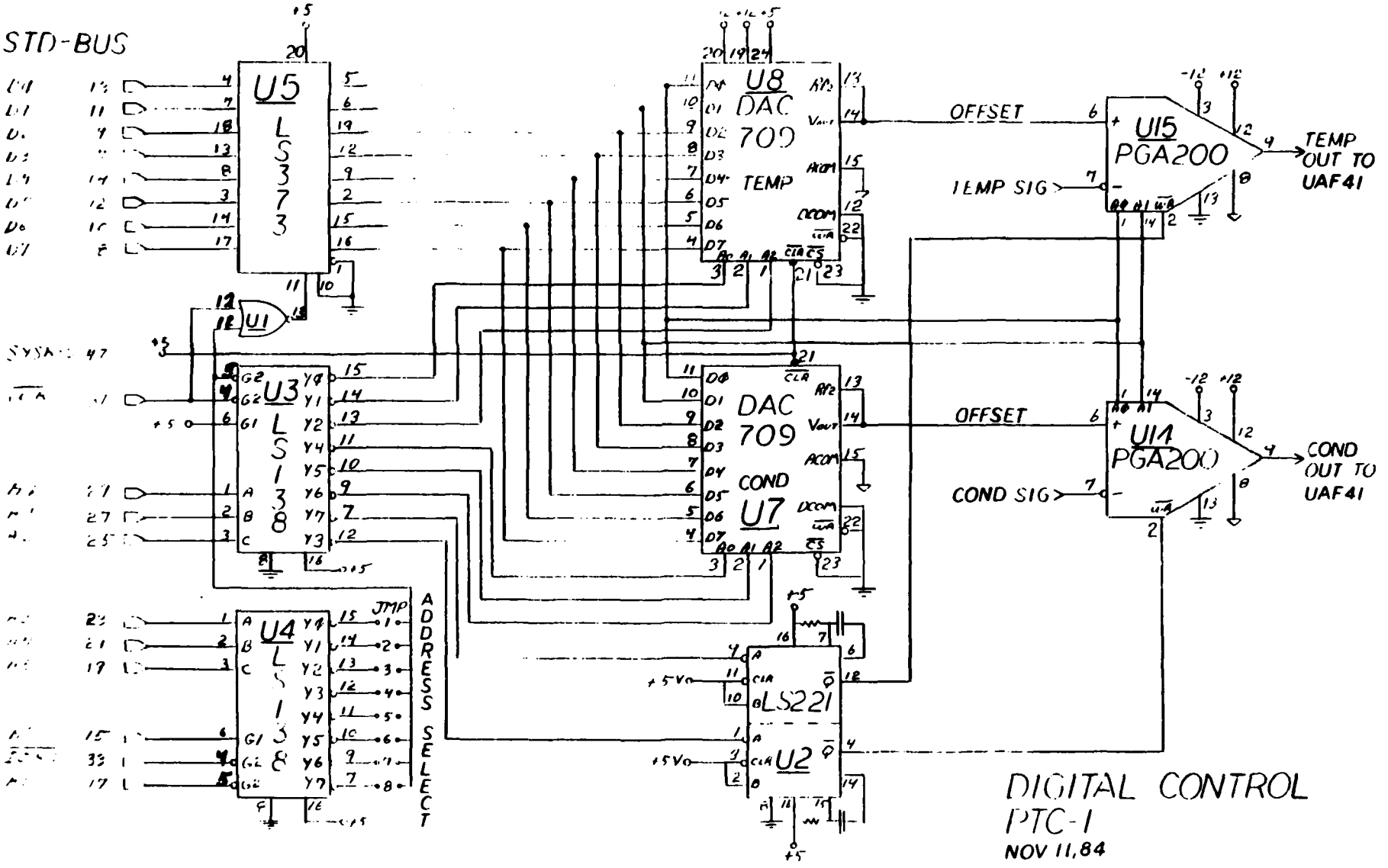
STD-BUS
U5
LS373
U1
U3
LS138
U4
LS138
JMP
ADDRESS SELECT
U8
DAC 709
TEMP
U7
DAC 709
COND
LS221
U2
OFFSET
TEMP SIG
U15
PGA200
TEMP OUT TO UAF41
OFFSET
COND SIG
U14
PGA200
COND OUT TO UAF41
DIGITAL CONTROL
PTC-1
NOV 11,84

R1,R2	10K 1%	MK132	C1,C4	.1 Monocap
R3	50K 1%			
R4	30K 1%		C2,3,5,6,7,8,13,14,15,16	
R5	100 1%			.1 Poly
R6	200 Bourns pot Model 3059P			
R7	5K 1%		C5,9,10,17,18	
R8	30K 1%			.1 Mono
R9	50K 1%			
R10,R11	10K 1%		C11,C12	.01 Poly
R12,R13	10K Carbon 5%		C19,C20	68pfd Mica
R14	82K 1%			
R15,R16	10K 1%		C21,22,23,24	
RN1,2,3,4	10K 1%			10 @ 35V
	694-3-R10K-F 8PIN DIP			
Q1	AD580	Vref. 2.5VDC	C25	4700pf

U1	74LS02	NOR GATE, LATCH DB WHEN ADDR & WR ARE TRUE
U2	74LS221	WR PULSE STRETCHER MONO FOR PGA'S
U3,U4	74LS138	ADDRESS DECODING
U5	74LS373	DB LATCH
U6	ICL8038	PREC. SINE WAVE GENERATOR
U7,U8	DAC709BG	16 BIT D/A, OFFSETS
U9,U10	AD536	RMS —> DC CONVERTERS
U11	AD534	DIVIDER, Isig/Vref=G (conductance)
U12,13,20,21,22	OPA111	PREC OP AMP
U14,U15	PGA200BG	PROG GAIN AMPS. X1,X10,X100,X1000
U16,U17	LF411CN	MED SPEED OP AMPS
U18,U19	UAF41	L.P. FILTERS

J1	20 PIN HEADER CONNECTOR, MALE. TO DT2745 A/D BD
J2	10 PIN HEADER CONNECTOR, MALE. INPUTS

NOV 12,84 PTC-1 CIRCUIT BD

5 : Minimum # of boards needed.
450 : Total # of holes.
±0.003 : Hole tolerance, all holes.
29.25 : Board area (sq. in.)
0.062 : Board thickness.

SPECIAL INSTRUCTIONS:

BRIGHT ACID TIN TRACES.
GOLD PLATED FINGERS.
SOLDER MASK.
LEGEND.

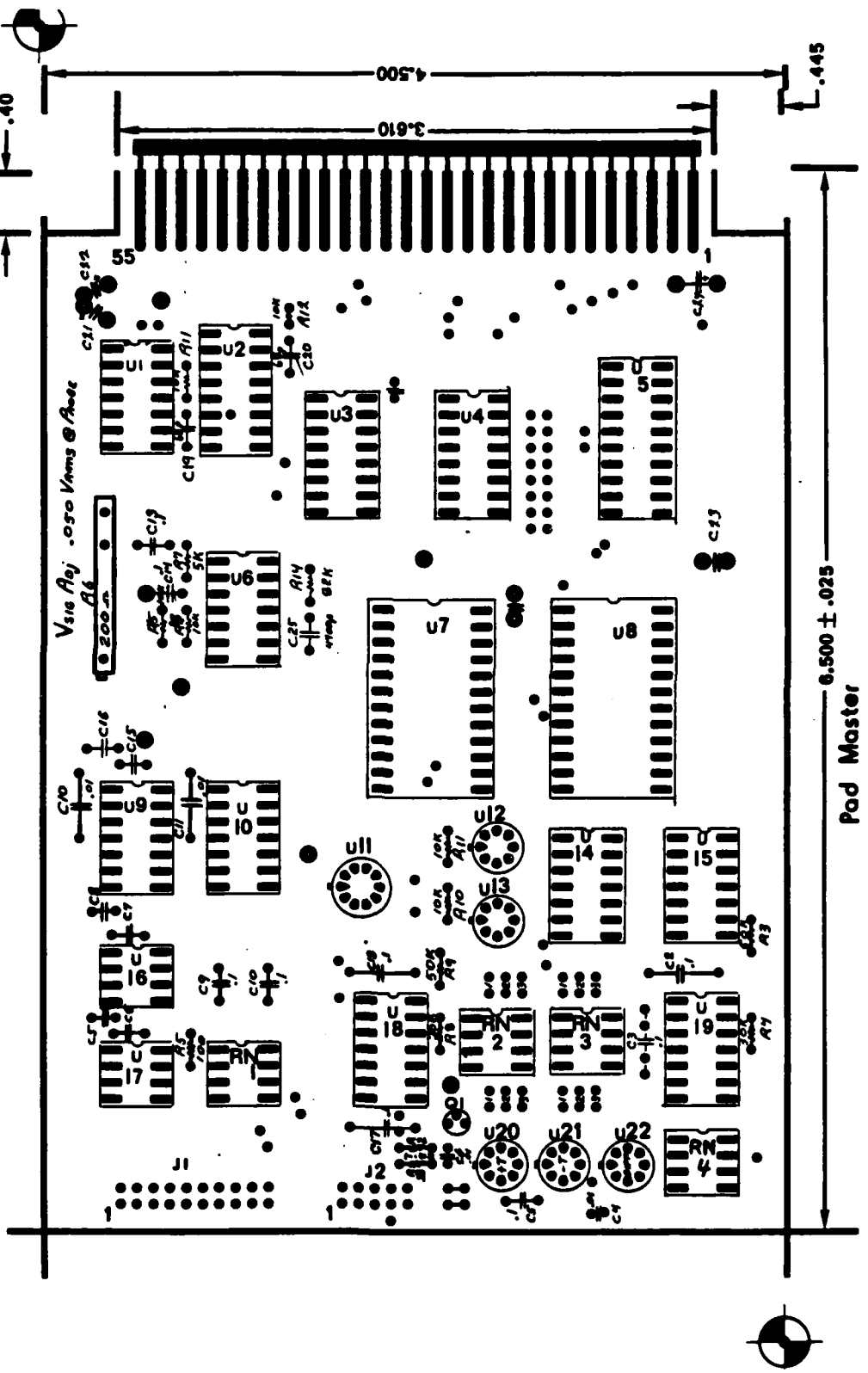
4.500
3.610
.445
.40
55
1
0.500 ± .025
Pad Master
J1
J2
U1
U2
U3
U4
U5
U6
U7
U8
U9
U10
U11
U12
U13
U14
U15
U16
U17
U18
U19
U20
U21
U22
RN1
RN2
RN3
RN4

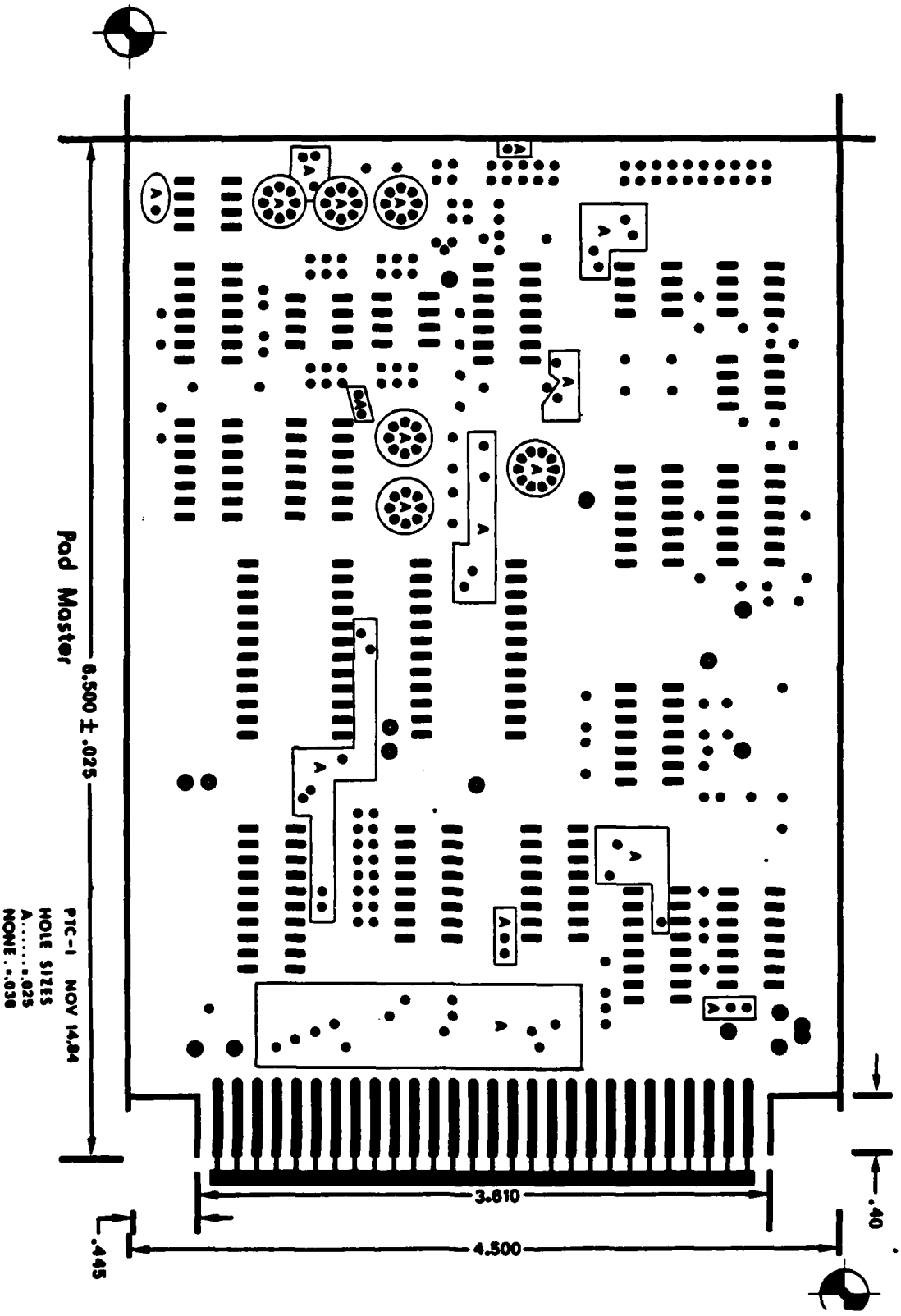
Pod Master
6.500 ± .025
PTC-1 NOV 14,84
HOLE SIZES
A.....025
NONE..038
3.610
4.500
.445
.40

DTIC

FILMED

4-86

END